UNIVERSITY OF CALGARY

Physiological and molecular mechanisms contribute to altered smooth muscle contractility during dextran sodium sulfate-induced colitis in mice

by

Alexandra Valderrama Bonilla

A THESIS

SUBMITTED TO THE FACULTY OF GRADUATE STUDIES

IN PARTIAL FULFILMENT OF THE REQUIREMENTS FOR THE

DEGREE OF MASTER OF SCIENCE

DEPARTMENT OF BIOCHEMISTRY & MOLECULAR BIOLOGY

CALGARY, ALBERTA

SEPTEMBER 2008

UNIVERSITY OF
CALGARY

Abstract

Gastrointestinal tract inflammation evokes alteration of intestinal smooth muscle contractility. The aims of this study were to determine whether colonic smooth muscle responds abnormally during acute inflammation and if these alterations are correlated with changes of myosin isoform composition. Inflammation was induced in female C57BL/6 mice by the addition of 2.5% dextran sodium sulphate (DSS) to the drinking water for 7 days. Mouse circular colonic smooth muscle strips from normal and DSS-inflamed mice were prepared to evaluate contractile responses. Whereas non-receptor stimulation was diminished (1.7-fold), carbachol-induced contraction was enhanced (4.3-fold) in DSS-treated mice during acute inflammation. Ca^{2+}- sensitization of contractile elements induced by carbachol was not different between DSS-treated and control mice. In addition, the Ca^{2+} sensitivity was decreased for Ca^{2+} concentrations lower than 320 nM and increased for concentrations higher than 355 nM. Real-time PCR experiments showed a slight increase for all the myosin isoforms in DSS-inflamed mice. The greatest change of expression was found for the LC17b myosin isoform (3.5-fold). Western blot analysis showed no differences in the protein expression for all the myosin isoforms. These data suggest that abnormal colonic contractility is not related to changes in myosin isoform content, but may be associated with alterations in the Ca^{2+} sensitivity of the contractile elements.

Acknowledgements

I would like to thank my supervisor, Dr Justin MacDonald for allowing me to be a part of his research laboratory, his support and guidance. I would also like to extend my gratitude to MacDonald laboratory's members, in particular to Dr Eikichi Ihara for his priceless collaboration, guidance and teachings on the physiologic studies.

I would like to thank my committee members for their time and advice throughout my degree.

I am grateful to Dr Michael Walsh (University of Calgary) and Dr Robert Adelstein (National Institutes of Health, Bethesda, MA) for the antibodies kindly provided to me for western blot experiments of this thesis.

Thank you to Dr Paul Beck fo r the figures generously given to me for completion of this thesis, for his time and valuable suggestions for this project.

To all the members of the Smooth Muscle Research Group (SMRG) and Gastrointestinal Research Group (GIRG), I thank you for providing a learning environment.

I also would like to express my thanks to Dr Andrew Braun for his time and kind advice.

I extend my gratefulness to Ana Colina, Alma Rosales, Soleil Hurst, and Claudia Silva for their scientific support and their friendship.

Dedication

To Luis for his love, support, and friendship

To my Lord for your support even in the most difficult time

Table of Contents

List of Tables

List of Figures and Illustrations

List of Symbols, Abbreviations and Nomenclature

Symbol	Definition
ACh	Acetylcholine
CaM	Calmodulin
CCh	Carbachol
CD	Crohn's disease
CPI-17	PKC-potentiated inhibitory protein of MLCP of 17 kDa
C_T	Cycle number at which the fluorescence generated within a reaction crosses the threshold
DSS	Dextran sodium sulfate
D85	MHC invariant reference sequence
ED_{50}	Concentration of agonist needed to produce a 50% maximal response
ENS	Enteric nervous system
GMC	Giant migrating contractions
IBD	Inflammatory bowel disease
ICC	Interstitial cells of Cajal
ICC-IM	Intramuscular ICC
ILK	Integrin-linked kinase
KES	118 mM K^+ extracellular solution
LC17a/b	Myosin light chain isoforms 17 kDa
LC20	Myosin light chain 20 kDa
LPS	Lipopolysaccharide
MHC	Myosin heavy chain
MLC	Myosin light chain
MLCK	Myosin light chain kinase
MLCP	Myosin light chain phosphatase
MPO	Myeloperoxidase
MYPT1	Regulatory targeting subunit of myosin phosphatase

NES	Normal extracellular solution
NM	MLC invariant reference sequence
PKC	Protein kinase C
PMN	Polymorphonuclear cells, neutrophils
ROK	Rho-associated kinase
RPC	Rhythmic phasic contractions
SM1/SM2	Myosin heavy chain isoforms 1/2
SMA/SMB	Myosin heavy chain isoforms A/B
TC	Tonic contractions
ZIPK	Zipper-interacting protein kinase

1 INTRODUCTION

1.1 Colonic structure and motility

The colon wall is composed of four layers that have morphological and functional differences. The four layers (listed in the adluminal to abluminal direction) are the mucosa, the submucosa, the muscularis propia and the serosa (Figure 1). The muscularis propia consists of an outer longitudinal smooth muscle layer and an inner circular smooth muscle layer. Human longitudinal muscle does not form a continuous layer over the whole surface of the large intestine; instead, the muscle fibers are arranged in three flat, longitudinal bands (*taenia coli*). The circular muscle fibers form a thin layer over the ceacum and colon, but in the anal canal they become numerous and constitute the internal anal sphincter (Standring, 2004).

Colonic motility is a complex activity that guarantees extensive mixing of the luminal contents to enable optimal absorption of water and electrolytes. The smooth muscle cells of the circular muscle layer are subject to tonic and phasic rhythmic contractions. Tonic contractions are sustained over hours and appear to play a role in mixing. Rhythmic phasic contractions can completely occlude the lumen to turn-over and/or propel the luminal contents through the intestine. Contractions of the longitudinal muscle can produce bulging of the colonic wall between the *taenia coli*, without any effect on mixing or propulsive function. The importance of this action remains poorly understood.

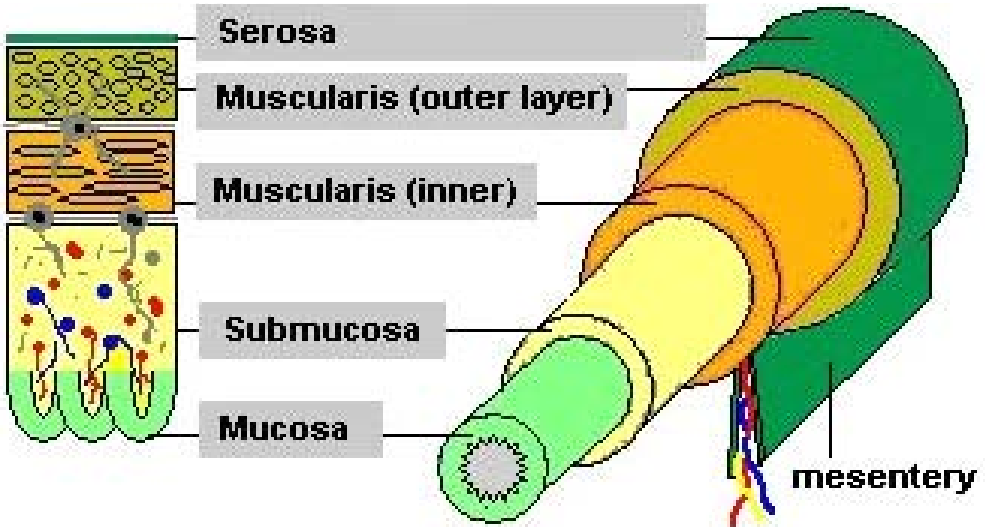

Figure 1. Diagram of the four major layers of the large intestine.

Taken from http://arbl.cvmbs.colostate.edu/hbooks/pathphys/digestion/basics/gi_ microanatomy.html

1.1.1 Myogenic and neurogenic regulation of smooth muscle contractility

The contractile function of the colonic circular smooth muscle layer is regulated by a complex interaction between myogenic and neurogenic mechanisms.

1.1.1.1 Myogenic mechanisms

The smooth muscle of the gastrointestinal (GI) tract is classified as unitary-type smooth muscle, where the fibers contract in unison (syncytial). The GI smooth muscle contracts spontaneously both in the absence of neural or endocrine influence and in response to stretch. Three different types of contractions have been distinguished in colonic smooth muscle: rhythmic phasic contractions (RPCs), giant migrating contractions (GMCs) and tonic contractions (TCs) (Sarna, 1991).

The RPCs generally do not occlude the lumen, and they can only propagate over very short distances of the colon. There are two types of RPCs: short-duration RPCs and long-duration RPCs. The short-duration RPCs, known also as slow waves, occur frequently depolarizing the smooth muscle cell membranes without generating a contraction of significant amplitude. However, this depolarization is accompanied by Ca^{2+} influx that produces the initial phosphorylation of myosin light chain (LC20) which is then increased by ligand-induced pharmacomechanical coupling. On the other hand, the long-duration RPCs occur in bursts of variable durations usually lasting a few minutes. They are produced by the spontaneous and intermittent high-amplitude depolarizations of the colonic smooth muscle cellular membrane. Since these depolarizations are highly frequent, the spike bursts are nearly fused, generating a long-duration contraction. Although the cell

signalling for these RPCs has yet to be investigated, it is known that they help the mixing and slow propulsion of feces as it solidify (Sarna & Shi, 2006; Bywater *et al*., 1998).

The origin of the slow waves intrigued investigators for several decades. The present consensus is that the electrical potentials are originated by specialized cells, the interstitial cells of Cajal (ICC), that act as electrical pacemakers. The ICCs are found at the circular muscle/submucosa plexus border and produce spontaneous electrical slow waves (Serio *et al*., 1991; Langton *et al*., 1989; Sanders, 1996). Slow waves depolarize the smooth muscle cells to induce the opening of voltage-dependent L-type Ca^{2+} channels. The electrical activity of slow waves is propagated through networks of ICCs and conducted passively to smooth muscle cells through gap junctions. These low-resistance connections between ICCs and smooth muscle cells facilitate the propagation of electrical events from one cell to another.

The amplitudes of slow waves and contractile force are regulated by the enteric nervous system. An excitatory neural input can increase the amplitudes of slow waves, increasing Ca^{2+} entry and enhancing the force of contraction. On the other hand, an inhibitory neural input can activate K^{+} channels and suppress inward current conductances in smooth muscle cells, reducing the amplitude of slow waves and suppressing contractile force. Major neural stimulation is mediated through the intramuscular ICC (ICC-IM). The ICC-IM is a type of ICC which is intermingled within bundles of smooth muscle cells. In fact, morphologic descriptions of ICC-IM have indicated that these cells are closely associated with neuronal processes (Faussone *et al*., 1977; Rogers & Burnstock, 1966). Physically, the ICC-IM are interposed between nerve terminals and smooth muscle cells, receiving and transducing neuronal signals, and then transmitting stimuli to the smooth

muscle cells. As well, the slow waves are conditioned by other substances such as hormones, paracrine substances, and inflammatory mediators. It is not clear yet if these substances have sites of action on ICC-IM (Sanders *et al*., 2006).

The GMCs, originally known as peristaltic contractions, are large-amplitude contractions that propagate over longer distances to produce mass movements of lumenal contents. The GMC is not initiated by slow wave depolarization; instead, GMCs are stimulated by pharmacomechanical coupling triggered by the large and prolonged release of acetylcholine (ACh) at the neuroeffector junction. The ACh stimulates $Ca_v1.2$ channel (voltage-dependent L-type Ca^{2+} channel) opening to cause influx of Ca^{2+}. The enhancement of cytosolic Ca^{2+} concentration ($[Ca^{2+}]_i$) is enough to evoke spikes on each depolarization (Murthy, 2006).

Colonic TCs are increased after ingestion of a meal. The narrowing of the lumen produced by colonic TCs makes the RPCs more effective in propulsion and mixing because phasic contractions of smaller amplitude may occlude the lumen more adequately. Stimulation of small monomeric GTPase, Gαq/11, and further activation of Ca^{2+} independent kinases, such as Rho kinase and PKC, elicit the phosphorylation of the regulatory targeting subunit of myosin phosphatase (MYPT1), under low Ca^{2+} concentrations. The phosphorylation of MYPT1 inactives myosin phosphatase activity and generates a sustained increase in muscle tone that is not regulated by slow wave activity (Figure 2) (Sarna & Shi, 2006; Murthy, 2006).

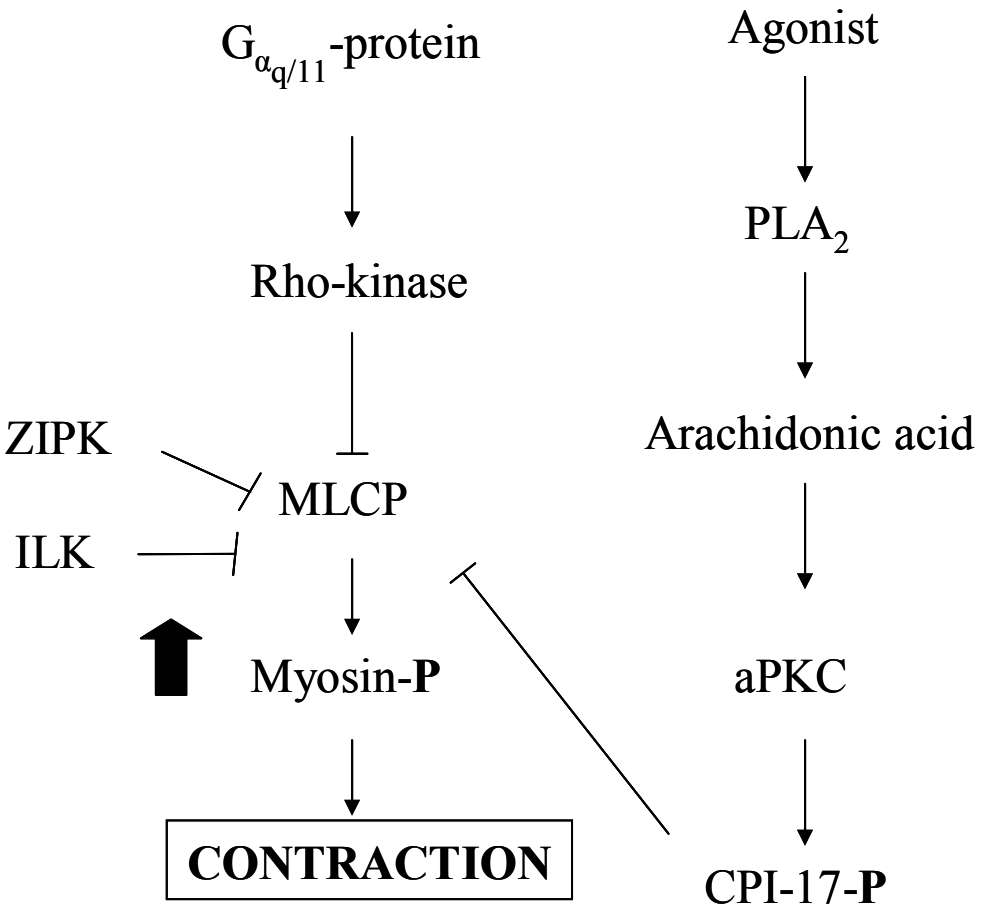

Figure 2. Mechanisms of Ca^{2+} sensitization of smooth muscle contraction.

Inhibition due to MLCP phosphorylation, PKC-phosphorylated CPI-17, or arachidonic acid-induced dissociation leads to an increase in LC20 phosphorylation and force in the absence of changes in $[Ca^{2+}]_i$. ROK, Rho-associated kinase; MLCP, myosin light chain phosphatase; MLCK, myosin light chain kinase; PLA_2, phospholipase A_2; aPKC, PKCζ, atypical protein kinase C isoenzymes; CPI-17, PKC-potentiated inhibitory protein of MLCP of 17 kDa; ZIPK, zipper-interacting protein kinase; ILK, integrin-linked kinase. Adapted from Kargacin & Walsh, 2001.

1.1.1.2 Neurogenic mechanisms

The neural regulation of colonic motility is provided by three divisions of the autonomic nervous system (ANS). The first division, the enteric nervous system (ENS), is formed by a network of neurons located entirely within the GI wall. The ENS mediates gastrocolic and duodenocolic reflexes and senses the environment within the lumen, regulating gastrointestinal blood flow and controlling epithelial cell function (Furness *et al*., 1995). The neurons of the ENS are collected into two types of ganglia: the myenteric (Auerbach's) and submucosal (Meissner's) plexuses. Myenteric plexi is located between the inner and outer layers of the muscularis propia, while submucosal plexi is located in the submucosa (Yamada *et al*. 2003). The second division of the ANS is composed of neurons of the prevertebral ganglia (Szurszewski & King, 1989) that control peristaltic reflexes by coordinating the activity of widely separated intestinal regions. The third division of nervous coordination is performed by the central nervous system (CNS) via neural connections contained within the extrinsic parasympathetic and sympathetic nerves (Venkova *et al*., 2002).

The neural excitatory and inhibitory inputs to the smooth muscle occur by neurotransmitter release. Efferent fibres of the CNS provide cholinergic input to excitatory motorneurons in ganglia of the pelvic and myenteric plexus, which in turn induce smooth muscle contractions through the release of acetylcholine (ACh) and/or excitatory non-adrenergic, non-cholinergic (NANC) neurotransmitter(s). In addition, efferent parasympathetic nerves may synapse with inhibitory motorneurons inducing muscle relaxation via the release of nitric oxide and/or inhibitory neurotransmitters such as vasoactive intestinal peptide and ATP (Venkova *et al*., 2002).

1.2 Evidence that inflammation alters intestinal motility

Motility dysfunction in patients with IBD has been documented since the 1950s (Kern *et al*., 1951, Reddy *et al*., 1991). Motility disorders of the gastrointestinal tract are clinically important since they can contribute to systemic disease. The mechanisms underlying intestinal motility dysfunction have been the subject of numerous investigations, both in animal models of colitis (Kiyosue *et al*., 2006; Ohama *et al*., 2007) and human disease (Vermillion *et al*., 1993; Akiho *et al*., 2005). Some studies have shown evidence of decreased contractile activity (Annese *et al*., 1997; Sato *et al*., 2007), whereas others have shown evidence of increased contractile activity (Grossi *et al*., 1993; Ihara *et al*, *in progress*). The inflamed intestinal wall is characterized by a myriad of diverse neurotransmitters and other potential contractile agonists that make more complex the understanding of altered motility.

A great deal of investigation has focused on the contractile responses to ACh (or carbachol) as the primary neurotransmitter of the gastrointestinal tract, as well as on the contractile responses elicited by other contractile agonists (e.g., serotonin, histamine and neurokinin). As previously mentioned, some researchers have described reduced contractile responses with intestinal inflammation. In a trinitrobenzene sulphonic acid (TNBS) rat model of colitis, Wells and Blennerhassett (2004) observed a decrease in the contractile response of colonic smooth muscle cells both to carbachol (CCh) and serotonin (5-HT) but without significant changes in the response to histamine. Similarly, suppressed contractile responses to ACh in canine colonic smooth muscle cells were detected in an ethanol and acetic acid colitis model of intestinal inflammation (Shi *et al*. 2003). In contrast, Hosseini

and colleagues (1999) detected increased contractile responses to substance P and ACh but decreased responses to neurokinin in rat circular colonic smooth muscle strips from the TNBS-acute inflammation model.

Furthermore, both *in vivo* and *in vitro* investigations have established that intestinal inflammation impairs agonist-induced contraction of the intestinal smooth muscle (Vermillion *et al*., 1993; Reddy *et al*., 1991). Decreased segmenting colonic motility and increased numbers of propagating contractions have been reported in ulcerative colitis (UC) patients. These motility dysfunctions allow for rapid anterograde movement of luminal contents that may contribute to symptoms such as diarrhea (Reddy *et al*., 1991). Also, Snape and colleagues (1991) observed a reduction in bethanechol-induced contractions of colonic circular smooth muscle strips from patients with ulcerative colitis. In summary, investigations of human disease and animal models of colitis have indicated that mucosal inflammation elicits colonic dysfunction which may involve changes in smooth muscle contractility.

1.3 Smooth muscle myosin isoforms

Myosin II is the molecular motor of skeletal, cardiac, and smooth muscle tissues. The velocity of muscle contraction is determined by the ATPase activity of myosin when it interacts with actin (Barany, 1967). Smooth muscle myosin is composed of a pair of myosin heavy chains (MHCs) and two pairs of myosin light chains (MLCs). The MHCs wrap around each other to form a α-helical carboxyl-terminal tail and two amino-terminal globular heads (Figure 3). Each head is composed of a globular motor domain and a long

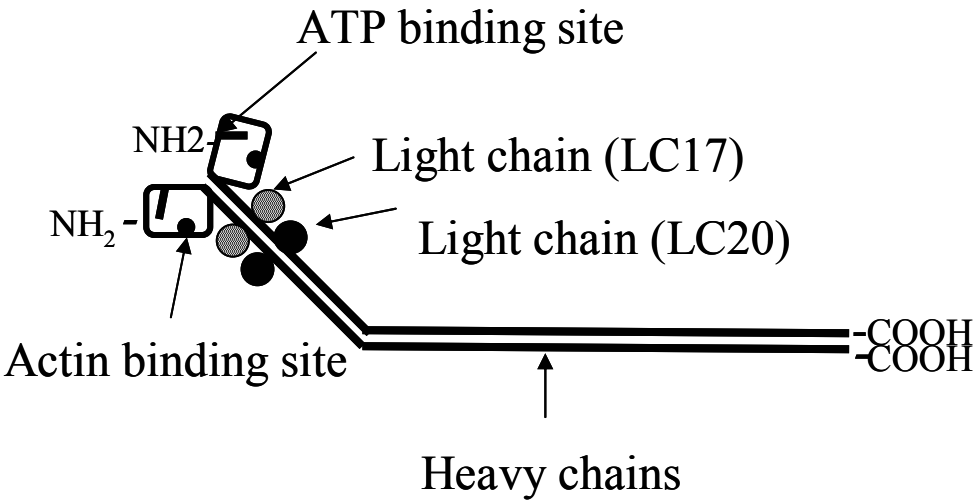

Figure 3. Schematic representation of smooth muscle myosin showing the two globular heads and the α-helical coiled-coil tail.

Motor domains contain the ATPase and actin–binding sites. One pair of LC17 and one pair of LC20 are bound to the neck region of the heads. Adapted from Kargacin & Walsh, 2001.

neck that is stabilized by association with MLCs. Located in the head region are the actin binding site and an active site for ATP hydrolysis. Both are needed to drive the myosin head along the actin filament to produce force (Adelstein & Eisenberg, 1980). Myosin contains two different pairs of MLCs, a pair of non-phosphorylatable essential MLCs (LC17) and a pair of phosphorylatable regulatory MLCs (LC20).

Alternative RNA processing of a single gene generates four isoforms of MHC. SM1 and SM2 differ in the carboxyl-terminal, and SMA and SMB differ in the amino-terminal head region of the molecule (Hamada *et al*., 1990; White *et al*., 1993). SM1 and SM2 are approximately 204 and 200 kDa, respectively. The transcripts are identical over the first 1424 nucleotides (Nagai *et al*., 1989; Babij & Periasamy, 1989); however, the mRNA for SM1 encodes 43 amino acids after the point of divergence from SM2 mRNA, whereas SM2 has an extra sequence of 39 nucleotides that encodes 9 amino acids (Figure 4A, 4B). The SMA and SMB isoforms differ at the amino terminus of the MHC, in the globular head region, by the presence or absence of a seven amino acid insertion. The splice site is located 20 amino acids downstream of the actin-activated Mg^{2+}-ATPase region (White *et al*., 1993). It has been proposed that the presence of the seven amino acid insert does not affect the ability of myosin to generate molecular force but rather alters the rate at which myosin transitions through the cross-bridge cycle. The insert increases both the rate of Mg^{2+}ATP binding and Mg^{2+}ADP release from the active site (Lauzon *et al*., 1998). The seven amino acids found in the SMB isoform are highly conserved among mouse, rat, rabbit (Babu *et al*., 2000), and human (Leguillette *et al*., 2005). The SMB isoform is predominantly expressed in small muscular arteries, bladder, intestine and stomach (DiSanto *et al*., 1997; White *et al*., 1993) (Figure 4A, 4B).

Two different isoforms of the 17-kDa light chain are generated by alternative splicing from a single gene (Lenz *et al*., 1987). The two LC17 isoforms have the same molecular weight but different isoelectric points, one more acidic, LC17a and the other one more basic, LC17b (Helper *et al*., 1988). An analysis of the amino acid sequence of the two LC17 isoforms from mammalian smooth muscle reveals that both consist of 151 amino acid residues (Hasegawa *et al*., 1992). The nucleotide sequence of the LC17 isoforms indicates that they are identical except in 5 of the 9 COOH-terminal amino acid residues (Nabeshima *et al*., 1987) (Figure 4C).

1.4 Myosin isoforms in physiological and pathological conditions

Phasic smooth muscle, like that found in the gastrointestinal tract, can undergo rhythmic rapid shortening and re-lengthening cycles. Tonic smooth muscles such as those found in blood vessels have slower shortening velocities and assist in blood pressure regulation by their ability to maintain prolonged contractions with little energy expenditure. Studies have reported that the heterogeneity in the contractile properties among smooth muscles of diverse organs was related to the relative content of various smooth muscle myosin isoforms (Babu *et al*.,2000; Kelley *et al*., 1993). The expression of the SMA and SMB isoforms is tissue specific and related to the function of the smooth muscle bed. Whereas SMA (the non-inserted isoform) is found mainly in tonic muscle (e.g., aorta), SMB (with seven amino acids insert) is found predominantly in phasic muscle (e.g., urinary bladder and intestine). In intestine, the increased expression of SMB correlated with a higher velocity of movement of actin filaments *in vitro* and higher actin-activated Mg^{2+}-ATPase activity compared with vascular myosin (Kelley *et al*. 1993).

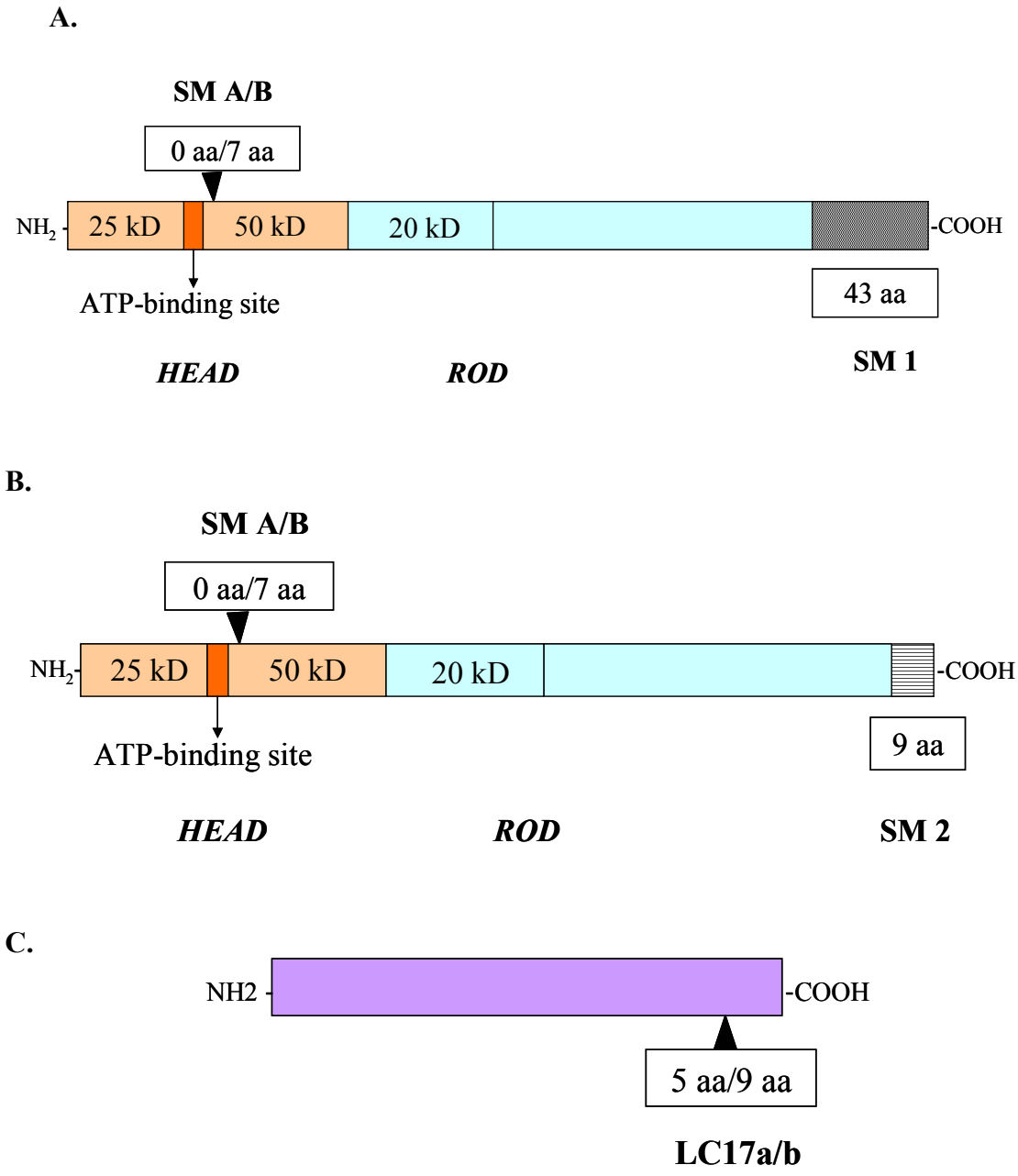

Figure 4. Schematic representation of myosin isoforms.

A, B, Four isoforms of myosin heavy chain. C, Two isoforms of myosin essential light chains. Adapted from White *et al*., 1993.

Although it has been suggested that SM1 and SM2 modulate smooth muscle contractile function this has yet to be defined a positive correlation between SM1 myosin content and maximal velocity of muscle shortening (V_{max}) was detected in rat uterine smooth muscle (Hewett *et al*., 1993; Sparrow *et al*., 1988). However, Kelley *et al* (1992) using an *in vitro* motility assay did not detect any significant difference in velocity between SM1 and SM2 myosin. Similarly, while the expression of SM1 and SM2 was not altered, changes in the contractility of mouse smooth muscle were found (Martin *et al*., 2007).

The LC17a/LC17b isoform composition may be related to the tonic nature of smooth muscle since the ratio of LC17b to LC17a is greater in tonic-like muscles (e.g., aorta) than in more phasic muscles (e.g., intestine). However, contradictory data have been reported concerning the influence of the composition of these two isoforms on the smooth muscle contractile force. An increase in the amount of LC17b in aortic myosin decreases the actin-activated ATPase activity (Hasegawa & Morita, 1992). Likewise, replacement of the predominant LC17a isoform in the urinary bladder with the LC17b isoform resulted in a significant decrease in the unloaded shortening velocity of nonphosphorylated myosin, i.e., slowly cycling cross bridges (Matthew *et al*., 1998). Nevertheless, the velocity of movement of actin filaments measured with an *in vitro* motility assay was the same for aortic myosin regardless of the LC17a and LC17b content (Kelley *et al*., 1993). Indeed, keeping the LC17 isoform composition constant but altering the SMA/SMB content generated increased myosin ATPase activity (Sweeney *et al*. 1998). Furthermore, SMB knockout mice showed no changes in LC17 isoform composition but a decrease in the velocity of shortening, indicating a functional role for the SMA/SMB composition that was independent of LC17 content (Babu *et al*., 2001).

The expression of myosin isoforms is altered in different human and animal model studies under pathological conditions. Increased expression of SM1 in patients with congenital uteropelvic junction obstruction may be related to increases in the contractile nature of the muscle (Hosgor *et al*., 2005). Significantly, a positive correlation has been found between the maximum velocity of shortening and the expression of SMB and LC17a in hypertrophied detrusor smooth muscle in a rabbit model of partial urinary bladder outlet obstruction (DiSanto *et al*., 2003). The expression of myosin isoforms has been found to be altered in other pathologic states, including megacolon in Hirschprung's disease (Siegman *et al*., 1997) and following spinal cord injury in mice (Wilson, *et al*., 2005). However, focused studies on the expression of myosin isoforms following intestinal inflammation have not yet been completed.

1.5 Mechanism and regulation of smooth muscle contraction

The main function of gastrointestinal smooth muscle is to mix and propel intraluminal contents to enable efficient digestion of food, progressive absorption of nutrients, and evacuation of wastes. These functions are enabled by intrinsic electrical and mechanical properties of smooth muscle, such as the ability to maintain tone or undergo phasic contraction. The contraction of smooth muscle occurs at the expense of ATP hydrolysis which induces shortening as a result of the sliding of overlapping, interdigitating thin and thick filaments (crossbridge cycling model). The contractile apparatus of smooth muscle consists of the contractile proteins (actin/tropomyosin and myosin, which are arranged into the thin and thick filaments, respectively) and associated regulatory proteins

such as: myosin light chain kinase (MLCK), calmodulin (CaM), myosin light chain phosphatase (MLCP), caldesmon and calponin.

Stimulation of the smooth muscle cell by neurotransmitters, hormones, growth factors, or membrane depolarization induces a rise in the concentration of intracellular free calcium ($[Ca^{2+}]_i$), which is the major trigger for the contraction of smooth muscle. The elevation of $[Ca^{2+}]_i$ leads to CaM-dependent activation of MLCK which phosphorylates the 20-kDa light chains of myosin (LC20). Phosphorylated myosin can interact with actin and hydrolyze ATP, which provides the energy for rapid crossbridge cycling and shortening of the muscle. Removal of Ca^{2+} leads to the dissociation of the Ca^{2+}-CaM-MLCK complex and permits dephosphorylation of LC20 by MLC phosphatase (MLCP) and relaxation of the smooth muscle (Bitar, 2003; Kargacin & Walsh, 2001) (Figure 5).

The phosphorylation and dephosphorylation of smooth muscle myosin by MLCK and MLCP, respectively, plays a central role in the regulation of smooth muscle contraction. However, muscle force can be generated in the absence of changes in $[Ca^{2+}]_i$. The phenomenon of Ca^{2+} sensitization describes the effects of various agonists that increase Ca^{2+} sensitivity by inducing LC20 phosphorylation and force without a change in $[Ca^{2+}]_I$. Ca^{2+} sensitization is believed to be a result of MLCP inhibition, not activation of MLCK. Inhibition of MLCP activity is mediated by an agonist-induced, G protein coupled process. MLCP can be inhibited both by phoshorylation of myosin-target-subunit of MLCP (MYPT1) (Trinkle-Mulcahy *et al*., 1995) and by the phosphorylation by protein kinase C (PKC) by the PKC-potentiated phosphatase inhibitor protein-17 (CPI-17), an endogenous inhibitor of MLCP (Li *et al*., 1998) (Figure 2).

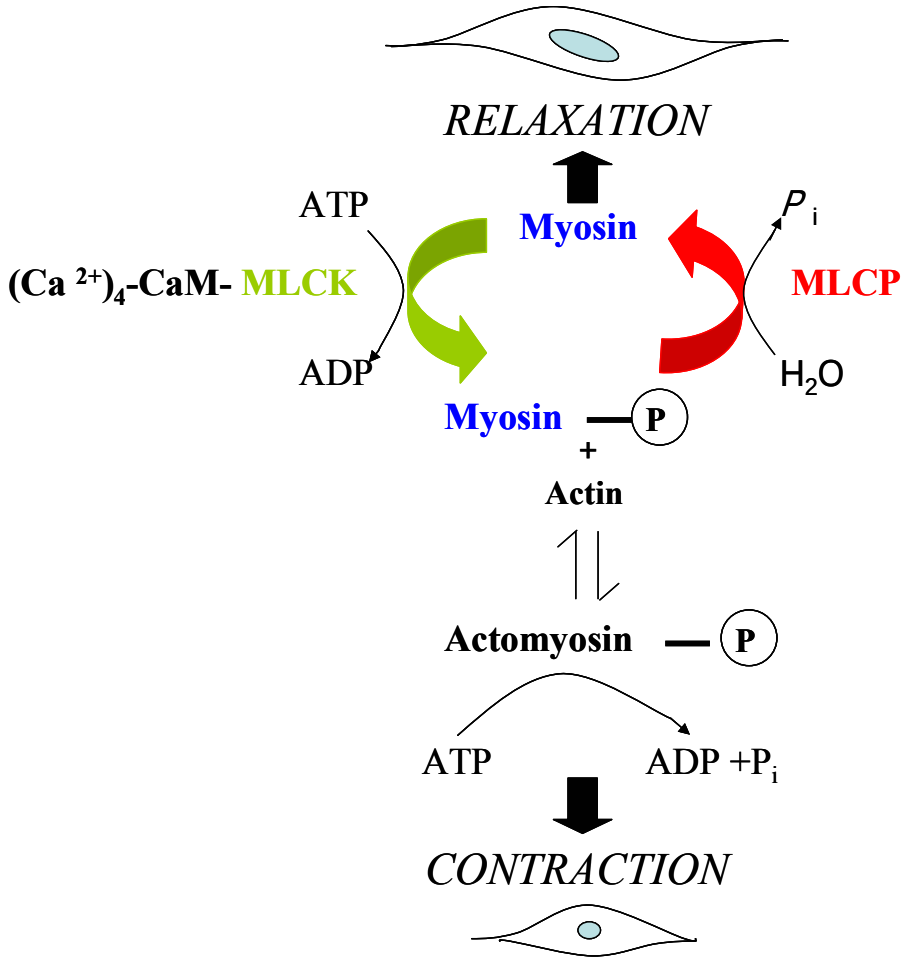

Figure 5. Myosin phosphorylation-dephosphorylation as the primary mechanism of regulation of smooth muscle contraction.

CaM, calmodulin; MLCK, myosin light chain kinase; MLCP, myosin light chain phosphatase; Myosin-P, phosphorylated myosin; Actomyosin-P, phosphorylated actomysin; P_i, inorganic phosphate; ATP, adenosine 5'-triphosphate; ADP, adenosine 5'-diphosphate. Adapted from Kargacin & Walsh, 2001.

1.6 Gastrointestinal inflammation and Inflammatory Bowel Disease

Because the intestinal mucosa is constantly exposed to the external environment and carries an extremely abundant and varied endogenous flora, the gut mucosa is adapted to a permanent antigenic pressure. This pressure elicits a mature and activated population of immunocytes permanently present in the intestine exhibiting a controlled or physiological intestinal inflammation rather than causing injury, protecting the gut and indirectly the rest of the body (Fiocchi, 2003). However, patients with inflammatory bowel disease (IBD) exhibit an inability to down-regulate these inflammatory responses and develop chronic intestinal inflammation (Hanauer, 2006).

IBD is a chronic, uncontrolled, relapsing and remitting inflammation of the intestinal mucosa, which can affect any part of the gastrointestinal tract. IBD encompasses two disorders: ulcerative colitis (UC) and Crohn's disease (CD). Epidemiological and ethnical differences in prevalence of CD and UC have revealed that they are polygenic diseases sharing some susceptibility genes (Ahmad *et al*. 2001). Many susceptibility loci of IBD have been identified with the development of a linkage map of the human genome and microsatellite markers (Weissenbach, 1998). Nine loci, termed IBD 1-9, have been distinguished (McKusick, 2006 & Ahmad *et al*., 2004). Whereas some loci seem to be specific to CD (e.g., IBD1 on 16q-OMIM 266000 (Cavanaugh, 2001) or UC (e.g., IBD2 on 12q-OMiM 601458) (Parkes *et al*., 2000), others seem to confer susceptibility to IBD overall (e.g., IBD 3p-OMIM 604519) (Hampe *et al*., 1999; van Heel *et al*., 2004). These findings have provided new insight into disease pathogenesis and have redirected efforts to

unravel the interactions among genetic factors, bacterial flora, innate immune response and pathogen-associated molecular patterns (Gaya *et al*., 2006).

1.7 Experimental murine models of IBD

IBD involves genetic, immunologic, and environmental factors; however, the precise etiology and initiating events leading to IBD are still unknown. The early inductive phases of these diseases are particularly difficult to study in humans because patients come to clinic after their symptoms are well established. One approach to investigating the mechanisms involved in a complex disease such as IBD is the use of appropriate animal models. No single animal model exactly reproduces human IBD because they do not possess all of the hallmark features of IBD in regards to disease location, histological characteristics, or clinical course of the human condition. Moreover, it is difficult to generate precise models of imprecise, ill-defined diseases. The remarkable value of the animal models is the insight they allow into the complex, multifaceted processes associated with a chronic intestinal inflammation.

The currently available IBD mouse models can be classified according to where the primary disruption in healthy intestine occurs (Byrne & Viney, 2006) (Figure 6).

1.7.1 Disruption of T-cell activation:

This group of animal models, usually mice, is generated by transferring T cells or bone marrow precursors into immunodeficient recipients. Immunological models have helped to identify the pathways of mucosal immune regulation. Two examples are the

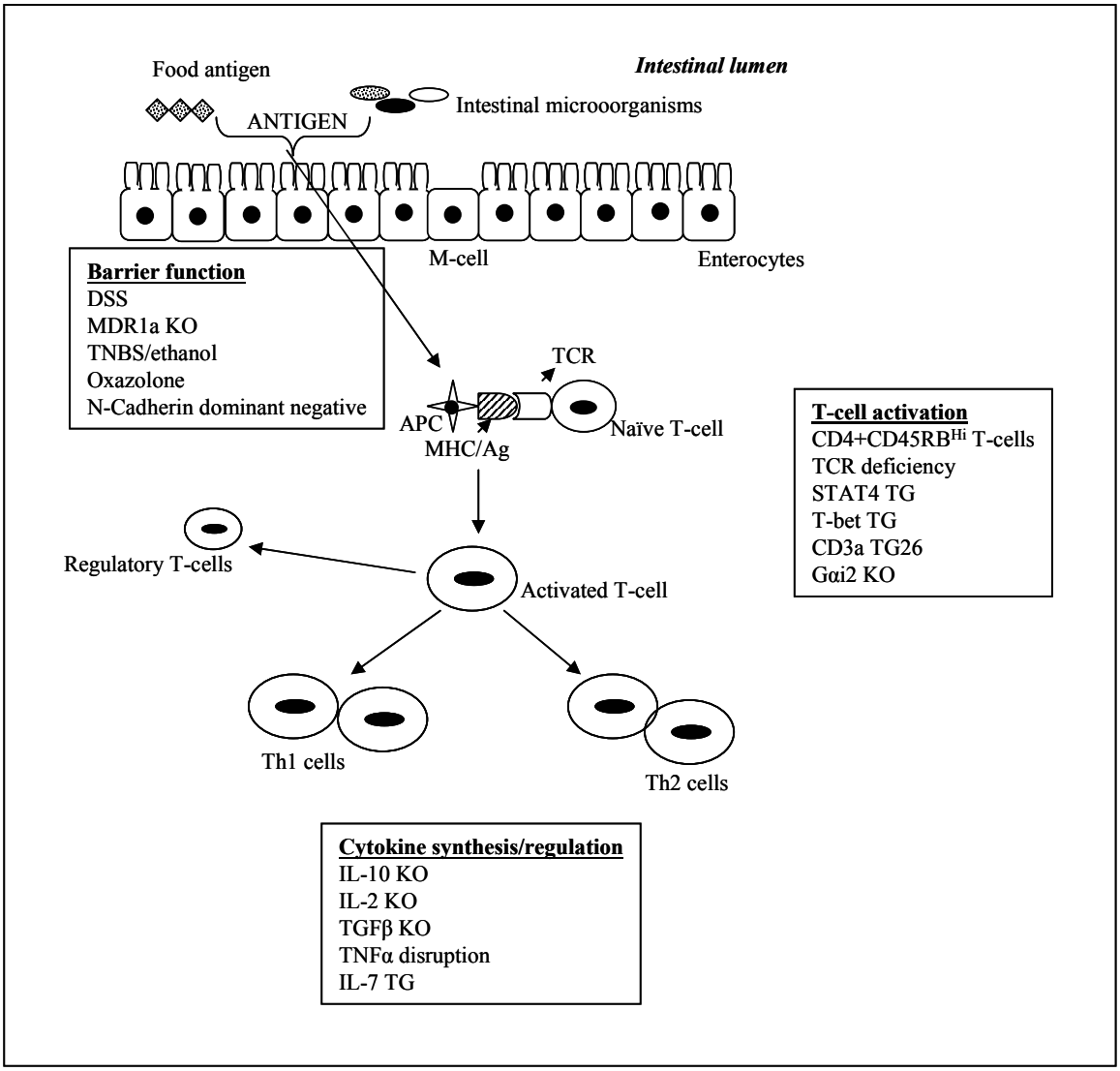

Figure 6. Schematic description of the mouse colitis models according to where the primary disruption in healthy intestine occurs.

APC, antigen presenting cells; IEL, intra-epithelial lymphocyte; IL, interleukin; KO, knockout; LPL, lamina propia lymphocyte; MHC/Ag, major histocompatibility complex antigen; TCR, T-cell receptor; TG, transgenic; TGF, transforming growth factor; TNBS, trinitrobenzene sulfonic acid; TNF, tumor necrosis factor; STAT, signal transducer and activator of transcription. Adapted from Byrne & Viney (2006).

CD45RBhigh transfer model and the T-bet transgenic mice model (Aranda *et al*., 1997; Neurath *et al*., 2002).

1.7.2 Disruption of cytokine synthesis/regulation:

The animal models in this category are produced by transgenic and knockout method. Examples include IL-10, TNF $^{\Delta ARE}$, IL-2, among other models (Kühn *et al*., 1993; Kontoyiannis *et al*., 1999; Barmeyer *et al*., 2004). Interestingly, the generation and use of these cytokine perturbation models have corroborated the idea that different targeted disruptions can, at the end, converge on a common phenotype.

1.7.3 Spontaneous models:

In these models, intestinal inflammation occurs without any apparent exogenous manipulation, a situation that is similar to human IBD. Environmental factors appear to be important in disease expression in that the phenotypic expression of spontaneous inflammation is reduced or eliminated when the mice are housed in specific pathogen-free (SPF) conditions. Three animal models have been investigated and characterized in this category: C3H/HeJBir mice, SAMP1/Yit mice and cotton-top tamarin model (Brandwein *et al*., 1997; Matsumoto *et al*., 2001; Elson *et al*., 1995).

1.7.4 Disruption of barrier function:

The models included in this category are diverse and require the administration of an exogenous chemical agent to induce inflammation. Some are limited to acute tissue injury; in others, the tissue injury is part of a more complex immunologic reactivity.

Examples include the oxazolone/ethanol model of colitis, the 2, 4, 6-trinitrobenzenesulfonic acid (TNBS) model of colitis, and the dextran sodium sulfate (DSS) model (Kojima *et al*., 2004; Appleyard & Wallace, 1995; Okayasu *et al*, 1990).

1.7.4.1 DSS colitis model

Since its development in 1990 by Okayasu and colleagues, the DSS mouse model of intestinal inflammation has been a popular model because of its speed, ease of use, robust nature and reproducibility. DSS-induced experimental colitis is also applicable to hamsters, guinea-pigs and rats (Cooper *et al*., 1993; Okayasu *et al*., 1990). Overall, the model manifests as colonic disease, with the distal colon being the most affected colonic segment (Vowinkel *et al*., 2004). Mice can develop an acute or a chronic inflammation, and there are differences in the genetic susceptibility to DSS-induced colitis among inbred strains of mice (Mähler *et al*., 1998). The acute intestinal inflammation is induced within 6-10 days by addition of 30-50 kDa DSS, a sulphated polysaccharide, to the drinking water at 3-10%. Acute inflammation is manifested by bloody diarrhea, gross rectal bleeding, weight loss, colonic shortening, mucosal ulceration and neutrophilic infiltration. Cycling the DSS administration can induce a chronic colitis characterized by erosions, inactivity areas, crypt distortion, epithelial proliferation and dysplasia (Copper *et al*., 1993). The mechanism by which DSS induces colitis is unclear. A proposed mechanism suggests that DSS generates toxic effects on the epithelium and increased exposure to luminal antigens by destruction of mucin content or altered macrophage function (Ni *et al*., 1996). As the colitis occurs in T- and B-cell deficient mice (i.e., SCID, $Rag1^{-/-}$) fed with DSS, the adaptive immune system is not required (at least in the acute phase) in this model (Dieleman *et al*., 1994). Luminal

microflora may play a role in the pathogenesis of the DSS model since concomitant metronidazole therapy can prevent colitis (Yamada, *et al*., 1992).

Further to the advantages previously mentioned, the use of the DSS mouse model has generated important information on the specific biochemical pathways of inflammation. The reproducibility of lesions that DSS produces has allowed the identification and mapping of genes important in susceptibility to colitis, mainly with mucosal homeostasis (Elson & Weaver, 2003). However, this model presents some limitations. It represents a non-specific injury model that does not require either T cells or B cells; therefore, it is not well-suited for the evaluation of immunologic or therapeutic aspects of the adaptive immune system.

1.8 Hypothesis and specific objectives

Intestinal inflammation is well recognized to alter the motor function of the gastrointestinal tract. The inflammatory events in the intestinal mucosa lead to functional changes in the underlying smooth muscle. Investigators have hypothesized that motility dysfunction can secondarily induce abnormal growth of the intestinal flora, and the resulting disturbance of the flora can further aggravate mucosal inflammation. This, in turn, would exacerbate intestinal dysmotility. Coordinated regulation of contraction is a key property of GI smooth muscle, which when functioning normally, contributes to general health and wellness, but when dysfunctional is associated with morbidity and mortality. Motility disorders that arise in the context of inflammation or immune activation are clinically important as they can lead to systemic disease (Ozaki *et al*., 2005).

Intestinal motility is a complex activity resulting from the interaction of enteric neurons, immunologic response, agonist-stimulated contraction, and activity of the contractile apparatus of smooth muscle. Studies of intestinal inflammation and associated changes in smooth muscle contractile protein expression, specifically myosin isoforms, have not been completed. While there is evidence that correlates inflammation-associated alterations in smooth muscle contractility with changes in contractile protein expression (Gil *et al*., 2006), studies of the myosin isoform content in altered colonic motility during intestinal inflammation have not been completed. This project examines the myosin isoform expression and content in inflamed mouse colon, hypothesising that changes in myosin isoform expression contributes to altered circular colonic smooth muscle contractility that occurs during intestinal inflammation. The specific objectives were to examine the receptor and non-receptor mediated contractility, Ca^{2+} sensitization, Ca^{2+}-force relationships and assess the myosin isoforms expression at the mRNA and protein levels.

2 MATERIALS AND METHODS

2.1 Animals and induction of colitis

Female C57BL/6 mice (18-20 g) were purchased from Charles River Laboratories, Inc. (Wilmington, MA) and were housed under conventional conditions with free access to animal chow and water. Colonic inflammation was induced by administration of 2.5% (w/v) dextran-sodium sulfate (molecular weight, 36000-50000; MP Biomedical, Solon, OH) in drinking water for 7 days (DSS-treated mice). For control mice, drinking water without DSS was supplied for the same period. All animal experiments were carried out with approval of the University of Calgary Animal Care and Use Committee.

2.2 Macroscopic scoring

Animals were weighed and their behavior observed during the duration of DSS-administration. After sacrifice, a macroscopic examination of the colon was completed. The macroscopic scoring for DSS-induced colitis ranged from 0-6 and was based on a scheme described previously by Murthy *et al*. (1993). The range represents the sum of scores for diarrhea, visible fecal blood, appearance of the colon, and locomotion. Colon length was also measured since previous studies have shown colonic shortening is present during colitis (Okayasu, *et al*., 1990). Details of macroscopic assessment and grading are shown in Table 1.

Table 1. Criteria for macroscopic assessment of intestinal damage in DSS-treated mice.

Feature graded	Grade	Description
Diarrhea	0	Normal pellets
	1	Loose feces
	2	Watery diarrhea
Visible fecal blood	0	Normal
	1	Bloody
	2	Gross blood per rectum
Appearance of the colon	0	Normal
	1	Thickened
Locomotion	0	Lively
	1	Languid

2.3 Collection of colonic tissues

After 7 days, control and DSS-treated mice were anesthetized with halothane (0.1 ml: 60 mg/ml; ICN, Aurora, OH) and sacrificed by cervical dislocation. The ceacum and colon were removed by gross dissection. After the evaluation of macroscopic damage, whole tissue samples containing the full colonic thickness (i.e., mucosa, submucosa, muscularis propia and serosa) were removed from the ceacum, proximal colon and distal colon. Tissue samples were cleaned with normal extracellular solution (NES solution) and then snap-frozen in liquid nitrogen and stored at -80 ˚C. In some cases, the circular smooth muscle layer was isolated from the intestine following removal of the mucosal and submucosal layers by sharp dissection under a stereomicroscope. The smooth muscle layer was either snap-frozen in liquid nitrogen for storage at -80 ˚C or utilized immediately for contractile studies.

2.4 Myeloperoxidase Assay

Myeloperoxidase (MPO) is an enzyme found within the azurophilic granules of neutrophils (polymorphonuclear leukocytes) and other cells of myeloid origin, and its activity is widely used as a marker of inflammation (Smith & Castro, 1978). The action of MPO in the utilized assay for its detection is detailed below,

$$H_2O_2 \xrightarrow{MPO} H_2O + O^-$$
$$O^- + AH_2 \longrightarrow H_2O + A$$

MPO can be liberated from tissue samples by homogenization in a buffer containing the ionic detergent hexadecyltrimethylammonium bromide (HTAB) (Sigma Aldrich Co, St Louis, MO). When an aliquot of tissue homogenate is provided with H_2O_2 as substrate,

MPO can generate oxygen radical (O^-) which can then react with *o*-dianisidine dihydrochloride, the hydrogen donor (AH_2), to produce a colored compound (A). Absorbance measurements of the colored compound at 460 nm allow the MPO content of tissue to be quantified (Bradley *et al*., 1982).

Pieces of whole intestinal and dissected circular smooth muscle tissue (100 - 200 mg) from sections of mouse distal and proximal colon as well as ceacum were snap-frozen in liquid nitrogen and stored at -80 ˚C. MPO assays were carried out soon after collecting samples since tissues lose about 15% activity per week. Tissue samples were weighed and then homogenized 1:20 (w/v) with a Polytron tissue disrupter in 50 mM potassium phosphate buffer (pH 6.0) containing 5 mg/ml HTAB. The tissue homogenates were centrifuged at 14,000 rpm for 30 minutes at 4˚C. In a standard 96-well plate, 200 µl of the reaction mixture (containing 16.7 mg of *o*-dianisidine (Sigma Chemical Co.), 90 ml of distilled water, 10 ml of potassium phosphate buffer, and 50 µl of 1% H_2O_2) was added to each well along with 7 µl of tissue homogenate. Using a microtiter plate scanner, three absorbance readings (450 nm) at 30-second intervals were recorded. MPO activity was reported as Units/mg tissue, where one Unit was defined as the conversion of 1 µmol of H_2O_2 per minute at room temperature

2.5 Histological examination

Tissue histology was performed in the laboratory of Dr. Paul Beck (University of Calgary) as described previously (Andres *et al*., 2000). Whole tissue from colonic segments was fixed in 10% neutral formalin solution and embedded in paraffin. Consecutive transverse sections were obtained from each colon and subjected to haematoxylin/eosin

staining. Individual sections were examined under the light microscope to monitor crypt morphology, inflammatory cell infiltration into the mucosa and submucosa, loss of mucosal architecture, muscle thickening, and goblet cell depletion (Berg *et al*., 1996; Appleyard & Wallace, 1995).

2.6 Force measurement of colonic circular smooth muscle

As described previously, distal colon was removed from normal and DSS-treated mice after sacrifice. Mucosa, submucosa, and connective tissue were removed by sharp dissection under a stereomicroscope, and colonic circular smooth muscle sheets were prepared. Small strips (250 μm x 2 mm) of circular muscle were isolated and then tied with monofilament silk to the tips of two fine wires, one of which was connected to a force transducer (SensoNor, AE801). The muscle strip was mounted in a 140 μL 'bubble-well' on a stir-plate to allow rapid solution exchange. A resting tension of 0.19 mN was applied to the muscle strip in the circular axis. Following an initial 30 minute equilibration period in normal extracellular solution (NES) containing: 137.4 mM NaCl, 5.9 mM KCl, 1.2 mM $CaCl_2$, 1.2 mM $MgCl_2$, 11.5 mM glucose, and 11.6 mM 4-(2-hydroxyethyl)-1-piperazine-ethanesulfonic acid (HEPES) (pH 7.3), the contractile response to high potassium (118 mM K^+) extracellular solution (KES), replacement of NaCl in NES solution with equimolar KCl was used as a test of tissue viability. Contractile protocols were completed after stabilization of each muscle strip to three separate KES stimulations. The response to muscarinic receptor agonist, carbachol, was studied in intact colonic strips of the distal colon. The non-cumulative, concentration-dependent response to carbachol was examined with increasing concentrations of carbachol (i.e., 10^{-8} to 10^{-3} M). The contractile response

was allowed to plateau before wash-out and tissue relaxation back to baseline force. Permeabilized smooth muscle strips were used to determine Ca^{2+} sensitization. Muscle was permeabilized by treatment with 10 μg/ml α-toxin (from *Staphylococcus aureus*, List Biological Laboratories Inc., CA) in NES for 60 min. Additional incubations with intracellular solution G1 (30 mM piperazine-1,4-bis(2-ethanesulfonic acid (K_2PIPES), 10 mM creatine phosphate (Na_2CP), 5.16 mM Na_2ATP, 7.31 mM magnesium methanesulfonate ($MgMS_2$), 74.1 mM KMS (potasium methanesulfonate), 1 mM ethylenebis(oxyethylenenitrilo) tetraacetic acid (K_2EGTA)) and with G1 added with 10 μM A23187 were completed to deplete intracellular Ca^{2+} stores. Sub-maximal contractions were generated by addition of pCa 6.3 solution, and Ca^{2+} sensitization was subsequently elicited by addition of 100 μM carbachol. For Ca^{2+} force relationship experiments, smooth muscle strips were exposed to different Ca^{2+} concentrations. The Ca^{2+} concentrations, pCa, were made by mixing the CaG and G10 solutions to achieve the desired Ca-EGTA/EGTA ratio. The composition of CaG solution was: 30 mM K_2PIPES, 10 mM Na_2CP, 5.14 mM Na_2ATP, 7.25 mM $MgMS_2$, 47.1 mM KMS, 10 mM K_2CaEGTA; and G10 solution was: 30 mM K_2PIPES, 10 mM Na_2CP, 5.14 mM Na_2ATP, 7.92 mM $MgMS_2$, 46.6 mM KMS, 10 mM K_2CaEGTA.To assess the viability of muscle strips, maximal contractions were generated with pCa 4.5 solution before and after the protocol in all experiments. The force levels obtained with relaxing solution G1 and pCa 4.5 were designated as 0% and 100%, respectively. At the end of the experiments, colonic strips were weighed to normalize contractile force against muscle mass. All contractile measurements were completed at room temperature (23 ˚C).

2.7 RT-PCR

2.7.1 RT-PCR primer design

RT-PCR was performed to determine the relative amounts of the different variants of the myosin heavy and light chains. Since different myosin isoforms are produced by alternative splicing, RT-PCR primers were designed to flank the unique intervening sequences associated with the different isoforms (Figure 7).

Using this strategy, each set of primer pairs was able to amplify two different myosin isoforms, so that only one primer set was required to amplify SM1 and SM2, one set for SMA and SMB and one set for LC17a and LC17b. The sequences of the genes under investigation were taken from an internet based database (GeneBank www.ncbi.nlm.nih.gov/Genbank/), and primers were designed with Generunner^{TM} software (Hastings Software Inc.). Oligonucleotides were ordered from University Core DNA Services (University of Calgary). The primers used for the individual RT-PCR amplifications are shown in Table 2.

2.7.2 RNA isolation

Total RNA was purified from whole intestinal tissue and isolated circular smooth muscle of ceacum, proximal colon and distal colon using a GenElute^{TM} Mammalian Total RNA Kit (Sigma Aldrich, St. Louis, MO). Total RNA was quantified on an Eppendorf spectrophotometer. Only the total RNA samples with 260 nm/280 nm ratios between 1.8 and 2 were considered acceptable for complementary DNA (cDNA) synthesis.

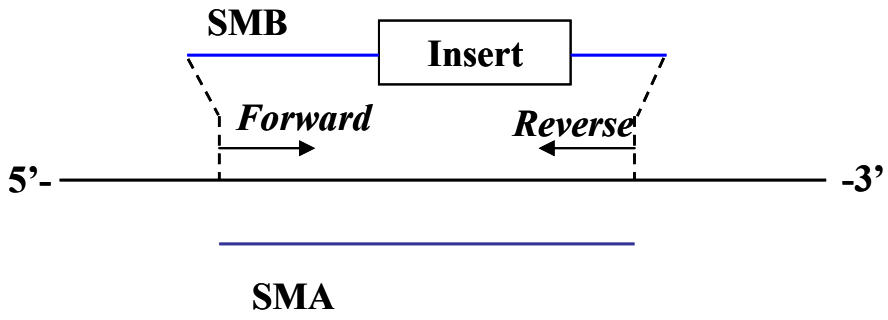

Figure 7. Design strategy for primers to amplify MHC and MLC through RT-PCR. Forward and reverse primers flanked the sequence that differentiates one isoform from the other, producing PCR products of the two isoforms.

2.7.3 cDNA synthesis

Superscript III reverse transcriptase (200 µg/µl; Invitrogen, Burlington, ON) was used to synthesize cDNA from 1 µg of total RNA. The first strand synthesis reaction contained 40 µg oligo dT_{12-18} primer, 5 mM DTT (dithiothreitol), 2 mM dNTPs (deoxyribonucleotides) in 5x First Strand Buffer (Invitrogen, Burlington, ON). The reaction was activated for 5 min at 65 ˚C, followed by elongation of the strands at 50 ˚C for 60 min. Lastly, the synthesis was terminated by inactivating the reverse transcriptase enzyme at 70 ˚C for 15 min.

2.7.4 RT-PCR

The quality of synthesized cDNA was routinely assessed with conventional RT-PCR using Taq polymerase (New England BioLabs, Pickering, ON) and specific primers for the RhoA housekeeping gene (Forward primer: 5'-CGGGATCCCGATGGCTGCCATCGGAAG-3'; reverse primer: 5'-GGAATTCCTCACAAGATGAGGCAA-3'). The RT-PCR products were separated on 1 % agarose gels, visualized by staining with ethidium bromide, and detected using Quantity One software (BioRad, Hercules, CA).

To examine the expression of the distinct myosin heavy chain and myosin light chain isoforms conventional polymerase chain reactions (PCR) were performed with the SM1/SM2, SMA/SMB, and LC17a/LC17b primer sets. The PCR products were separated on 3% agarose gels, stained with ethidium bromide and detected as described previously. The relative proportions of the diverse myosin isoforms were determined by densitometry and expressed as means ± S.E.M.

Table 2. RT-PCR primers for the amplification of murine myosin isoforms (SM1/2, SMA/B, and LC17a/b).

Primer set	Forward 5' – 3'	Reverse 5' – 3'	Amplicon
SM1/2	GAGGCAGAGGAGGAGTCCCAGTGCATC	GGCTTTGGTTCCATTGAAGTCTGAGTCCC	287/247
SMA/B	CGTGAAGACCAGTCCATTCTGTGCACAG	GCCAAAGCGAGAGGAGTTGTCGTTCTTG	245/224
LC17a/b	GACCGTGGCCAAGAACAAGGACCAGGG	GTCCTCAGCCATTCAGCACCATCCGGAC	232/282

2.7.5 Real-time PCR

Real-time PCR was performed on cDNA samples with the iCycler detection system (Bio-Rad, Hercules, CA) and the intercalating dye, SYBRgreen. Methods for total RNA isolation and cDNA synthesis were followed for the real-time PCR experiments. PCR conditions were optimized on the gradient thermal cycler on the iCycler. For each cDNA sample, real-time PCR was conducted in a 25 µl reaction volume containing Quantitect™ SYBRgreen PCR Mastermix (Qiagen, Mississauga, ON). The following time and temperature profile was used for the real-time PCR reactions: 95 ˚C for 5 min; 50 cycles of a series consisting of 15 s at 94 ˚C, 30 s at 52 ˚C, 30 s at 72 ˚C; and a final extension of 5 min at 72 ˚C. The optimal annealing temperatures were determined empirically for each primer set. The specific designed primers are shown in Table 3.

Real-time PCR reactions were performed in triplicate. Each primer set generated only one PCR product, and the identity and integrity of these products were confirmed by electrophoresis on non-denaturating polyacrylamide gels and sequencing of the individual bands. The fluorescent threshold value was calculated using the iCycle iQ System software. The absence of peaks in water controls suggested a lack of primer-dimer formation.

2.7.6 Quantification of gene expression

Two general types of quantification strategies can be performed in quantitative RT-PCR (qRT-PCR). The levels of expressed genes may be measured by an absolute quantification or by a relative qRT-PCR. The absolute quantification approach relates the PCR signal to input copy number using a calibration curve (Pfaffl & Hageleit, 2001).

Table 3. Real-time RT-PCR primer sequences

Primers for amplification of myosin isoforms (SMA/B, SM1/2 and LC17b) and housekeeping genes (MHC invariant, MLC invariant, β-actin, 18S rRNA) from colonic tissue.

Primer set	Forward 5' – 3'	Reverse 5' – 3'	Size amplicon (bp)
SM1	CGAGGCTTCATTTGTTCC	CACTGGCTTTGGTTCC	119
SM2	GCCACAGAGAGCAATGAG	CAATCCTGAATTTACCTGGTGGC	122
SMA	CAGAGAACACACAGAAAGTCATACAG	CTTTTCCAGCTCCCCCG	116
SMB	GTGAGTCTGGAGCCGGAAAG	GTAGGCAAAAGATGGACCTTG	122
LC17b	GATTTCTGTGTGGCTCC	GGAGGGCAAAGAGAGC	107
MHC invariant	GATGGATTCTCAGCCGTG	CAAACCCAGCAATATCCAG	90
MLC invariant	GCCAGAACCCTACCAACG	CAGGAAGTGCTCAAAGTC	95
β-actin	GAGAGGGAAATCGTGC	GCCAATAGTGATGACCTG	141
18S rRNA	CCGATAACGAACGAGACTC	GGACATCTAAGGGCATCAC	141

Relative quantification relates the PCR signal of the target transcript in a treatment group to that of another sample such as an untreated control. Relative quantification of a target gene in relation to another gene (reference gene or housekeeping gene) can be calculated on the basis of *delta delta* C_T values (C_T, called as well C_P, is the cycle number at which the fluorescence generated within a reaction crosses the threshold. C_T reflects the point during the reaction at which a sufficient number of amplicons has accumulated). There are several mathematical models to calculate the relative expression ratio (R), based on the comparison of the diverse cycle differences. Among them are the *delta delta* C_T method (Livak & Schmittgen, 2001) and the efficiency corrected calculation model (Pfaffl, 2006). In these models, the target-gene expression is normalized to the expression of one or more non-regulated housekeeping genes. The choice of an internal control to normalize the expression of the gene of interest is critical to the interpretation of experimental real-time PCR results. The housekeeping gene expression must not be influenced by the applied treatment (Pfaffl, 2006; Schmittgen & Zakrajsek, 2000).

a) *Delta delta* C_T method

$$\Delta\Delta CT = (C_{T,Tag} - C_{T,HKG})_{Treatment} - (C_{T,Tag} - C_{T,HKG})_{Control}$$

$$R = 2^{-\Delta\Delta C_T}$$

Where, *HKG* is the housekeeping gene and *Tag*, the evaluated gene.

b) Efficiency corrected calculation model: takes into account the PCR efficiency in the calculation. Application of this model requires the use of three housekeeping genes as minimal. The geometric mean of the values obtained with these housekeeping genes is

calculated as HKGindex. The formula for multiple samples and multiple housekeeping genes (HKGindex) is:

$$R = \frac{(E_{tag})^{\Delta C_{T_{tag}}(MEANcontrol - MEANsample)}}{(E_{HKGindex})^{\Delta C_{T_{HKGindex}}(MEANcontrol - MEANsample)}}$$

Following the criteria for choosing the reference genes and *delta delta* method, in this study β-actin was selected as reference gene (Appendix A). After normalization, the data for DSS-treated mice were expressed as the fold-change in mRNA expression relative to that obtained for control mice.

In addition, the relative quantification of the expression of the myosin isoform genes of all the samples in this study was calculated following the efficiency corrected calculation model and using three housekeeping genes: β-actin gene, 18S rRNA, MHC invariant/MLC invariant. The description of the design of the MHC invariant and MLC invariant, the calculations, and results following the efficiency corrected calculation method are discussed in Appendix A.

2.8 Western blot analysis

2.8.1 Total protein extract

The SMB, SM2 and LC17a/b myosin isoforms present in the control and DSS-treated mice were determined at the protein level. Mouse intestinal samples, mouse bladders (positive control for SMB and total myosin), mouse aortae (negative control for SMB), and mouse skeletal limb muscles (negative control for total myosin and SMB) were

harvested and stored as previously described. For quantification of MHC isoforms, tissues (0.03-0.06 g) were homogenized in 10 volumes of sodium dodecyl sulfate polyacrylamide gel electrophoresis (SDS-PAGE) sample buffer (30 mM Tris, pH 6.8, 12.5% (vol/vol) glycerol, 1% SDS, and phenylmethylsulfonyl fluoride (PMSF)) by using a glass-glass hand-operated homogenizer. To minimize proteolytic degradation, the homogenization buffer also included protease inhibitors (1 mM PMSF, 1 mM leupeptin, and 1 mM aprotinin, 1 mM pepstatin A). Homogenates were denatured by boiling in Laemmli SDS-polyacrylamide gel electrophoresis (SDS-PAGE) (Laemmli, 1970) and centrifuged at 14,000 rpm. An equivalent amount of protein was loaded on the gel based on assessment by Bradford assay (BioRad, Hercules, CA).

2.8.1.1 Myosin Heavy Chains (SMB and SM2)

Proteins were resolved on SDS-PAGE (7.5%) gels and then electroblotted onto 0.22 μm nitrocellulose (PALL Life Sciences, East Hills, NY) in transfer buffer (25 mM Tris, 192 mM glycine, and 20% (v/v) methanol) at 100 V for 3 hours at 4 ˚C. Non-specific binding sites were blocked by incubating the membranes in TBST Buffer (25 mM Tris, pH 7.4, 150 mM NaCl, 0.05% (v/v) Tween 20) plus 0.5% I-Block (Applied Biosystems, Foster City, CA). The mouse primary antibodies directed against myosin isoforms were used at the following dilutions: 1:400 for anti-SM2 (Yamasa Corporation, Japan) and 1:1000 for anti-SMB (gift from Dr. Michael Walsh, University of Calgary). After washing with TBST, the blots were incubated with horseradish peroxidase-conjugated goat anti-rabbit secondary antibody (Pierce, Rockford, IL) at a dilution of 1:10,000. The membranes were washed thoroughly and then developed with enhanced chemiluminescence (ECL) reagent

(Amersham, Piscataway, NJ) and by exposing the membranes to film (Kodak X-OMAT, XAR-5) for different periods of time. The films were scanned using a densitometer (STORM® system) and analyzed using ImageQuant® Software (GE Healthcare, United Kingdom). Last, the membranes were probed with a mouse anti-actin monoclonal antibody (Chemicon) at a dilution of 1:1000, incubated with horseradish peroxidase-conjugated goat anti-mouse secondary antibody (Pierce, Rockford, IL) at a dilution of 1:1000 and developed as above for detection of actin protein.

2.8.2 Separation of proteins and western blots

2.8.3 Myosin light chains (LC17a and LC17b)

The LC17 isoforms were separated and quantified on urea/glycerol gel electrophoresis following a previously described protocol (Sobieszek & Jertschin, 1986; Weber *et al*., 1999). The separating gel contained 10% (w/v) acrylamide, 0.27% (w/v) *N,N'*-methylene bisacrylamide (Bis), 0.375 M Tris-HCl (pH 8.8), and 40% (v/v) glycerol, and the stacking gel contained 2.25% (w/v) acrylamide, 0.12% (w/v) Bis, 0.12 M Tris-HCl (pH 6.8), and 8.5 M urea (Weber *et al*., 1999). Proteins were transferred to nitrocellulose membrane (Millipore, Bedford, MA) in 10 mM sodium cyclohexylaminopropane sulfonic acid (CAPS), pH 11 at 4˚C. The antibody against LC17a/b was a gift from Dr Robert Adelstein (National Institutes of Health, Bethesda, MD, Kelly *et al*., 1996) and was used at 1:500 dilutions. Also, horseradish peroxidase-conjugated donkey anti-rabbit IgG secondary antibody (GE, Memphis, TN) was used at a dilution of 1:10,000. The membrane was developed with Supersignal West Femto enhanced chemiluminescence (Pierce Chemical, Rockford, IL).

2.9 Statistics

Results of the experiments are expressed as the mean and standard error of the mean (S.E.M). Statistical evaluation of the data was performed by a paired and unpaired Student's t test for comparisons between two groups. Statistical differences with a value of $P < 0.05$ was considered to be statistically significant.

3 RESULTS

3.1 Assessment of colitis in the DSS model

3.1.1 Characterization of DSS-induced inflammation in C57BL/6 mice.

To determine the grade of inflammation induced by 2.5% DSS supplied in the drinking water for 7 days to female C57BL/6 mice, the appearance and body weight of individual mice were tested on a daily basis. Upon sacrifice, a macroscopic evaluation of the intestine was performed, and tissue was removed to assay MPO activity and to perform a histological evaluation. The DSS model of colitis has been characterized in several mouse strains (Okayasu *et al*., 1990; Cooper *et al*., 1993), and the results observed in this study are consistent with previous reports (Axelsson *et al*., 1996; Beck *et al*., 2007).

3.1.2 Macroscopic assessment of colitis

Mice exposed to DSS developed acute inflammation and showed signs of weight loss, gross rectal bleeding, and loose feces. Control mice had a significant gain of weight (1.68%) at the seventh day of evaluation (Figure 8). In contrast, DSS-treated animals exhibited a significant weight loss (6.8%) by the seventh day of treatment. The macroscopic score of DSS-treated mice (4.8 ± 0.2) was significantly increased compared to that of control mice (0 ± 0, $P<0.001$). This was mainly reflected by the occurrence of diarrhea and the presence of blood in the rectum of all the treatment animals. During DSS exposure, a shortening of the colon length was also observed at 7^{th} day (45.8%, $P<0.005$).

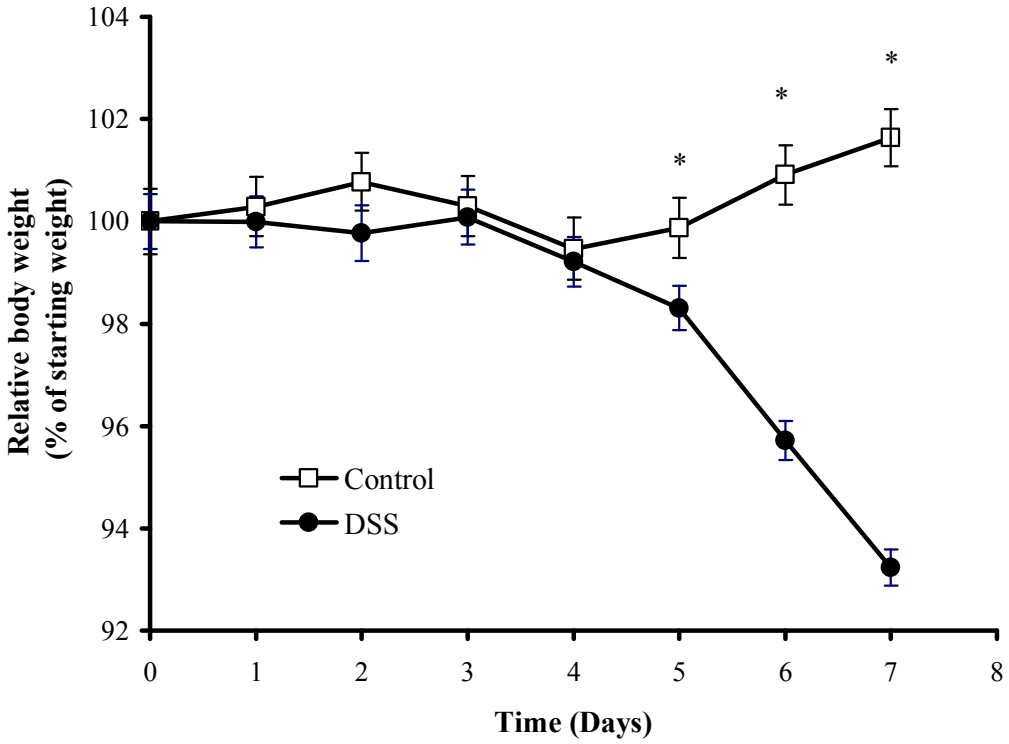

Figure 8. Body weight assessment of control and DSS-treated mice.

Daily body weight of mice is expressed as percentage of starting body weight. Mice received 2.5% DSS in the drinking water for 7 days. Values are means and error bars indicate S.E.M for n = 15-18. *, Significantly different from control mice value (Student's t test, $P<0.05$).

Table 4. Macroscopic score and changes in the length of colon from control and DSS-treated mice.

Mice	Macroscopic score	Colon length (mm)
Control	0	71.5 ± 1.85
Treatment	4.8 ± 0.1	38.8 ± 2.92

3.1.3 MPO activity

The three colonic segments evaluated developed colitis; however, the proximal colon segment registered the highest levels of MPO activity. The maximal MPO activities detected in the proximal colon were 0.94 ± 0.25 U/mg protein (n = 16) for control mice and 5.8 ± 1.0 U/mg protein (n = 18) for DSS-treated animals. The MPO activity was significantly higher in whole tissue of DSS-treated mouse colon when compared to control mice, $P<0.025$ for distal colon and $P<0.005$ for proximal colon and ceacum (Figure 9).

MPO activity was also detected in the smooth muscle layer of the proximal colonic region, both in control (1.7 ± 0.74, n = 3) and DSS-treated animals (7.4 ± 3.1, n = 4). However, the values were not significantly different ($P<0.1$) possibly due to the small number of samples analyzed. Interestingly, the MPO activity values in smooth muscle showed a trend to be higher than those found in whole tissue from proximal colonic segments (Figure 10).

3.1.4 Histology

The main histological changes observed after 7 days of 2.5% DSS exposure were extensive ulceration, loss of epithelium and loss of the normal glandular structure. A profound inflammatory cell infiltrate, predominantly neutrophils, macrophages and lymphocytes, was observed in the lamina propria and submucosa of DSS-treated animals (Figure 11).

Taken together, the findings obtained through the macroscopic assessment, MPO activity assay and histological evaluation indicated that 7 days of DSS treatment elicited

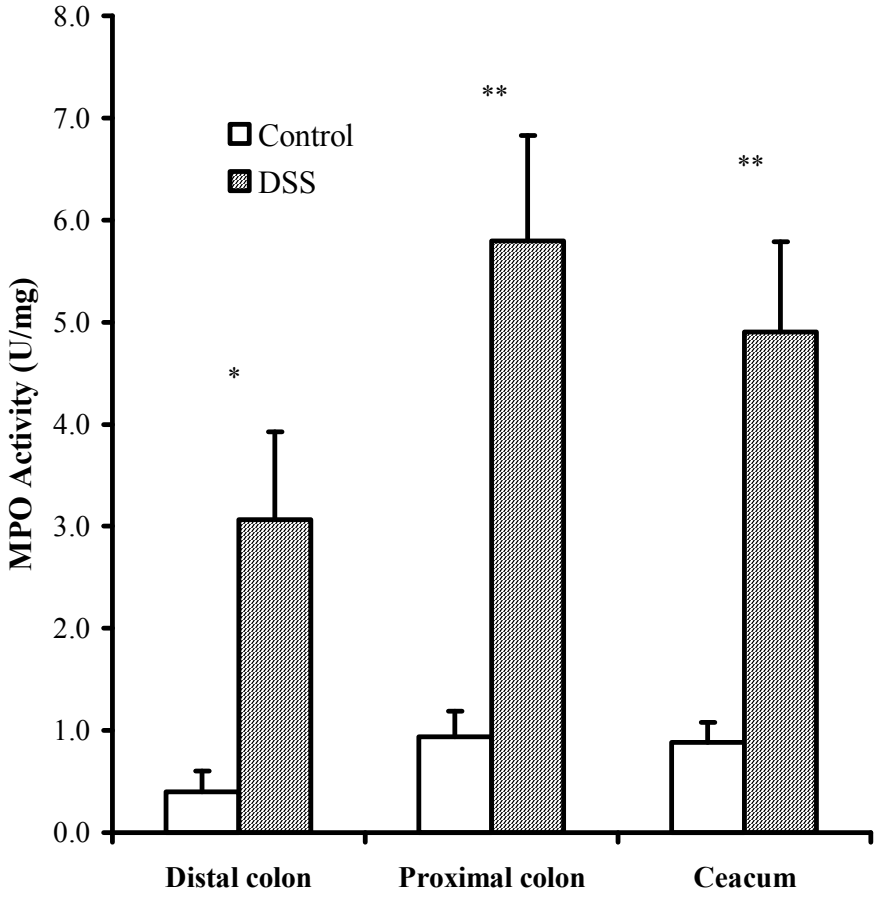

Figure 9. MPO activity of whole tissue from colon of control and DSS-treated mice.

Mice received 2.5% DSS for 7 days in the drinking water. Values are means ± S.E.M for n = 13-18. *, significantly different from control mice value (Student's t test, $P<0.025$); **, significantly different from control mice value (Student's t test, $P<0.005$).

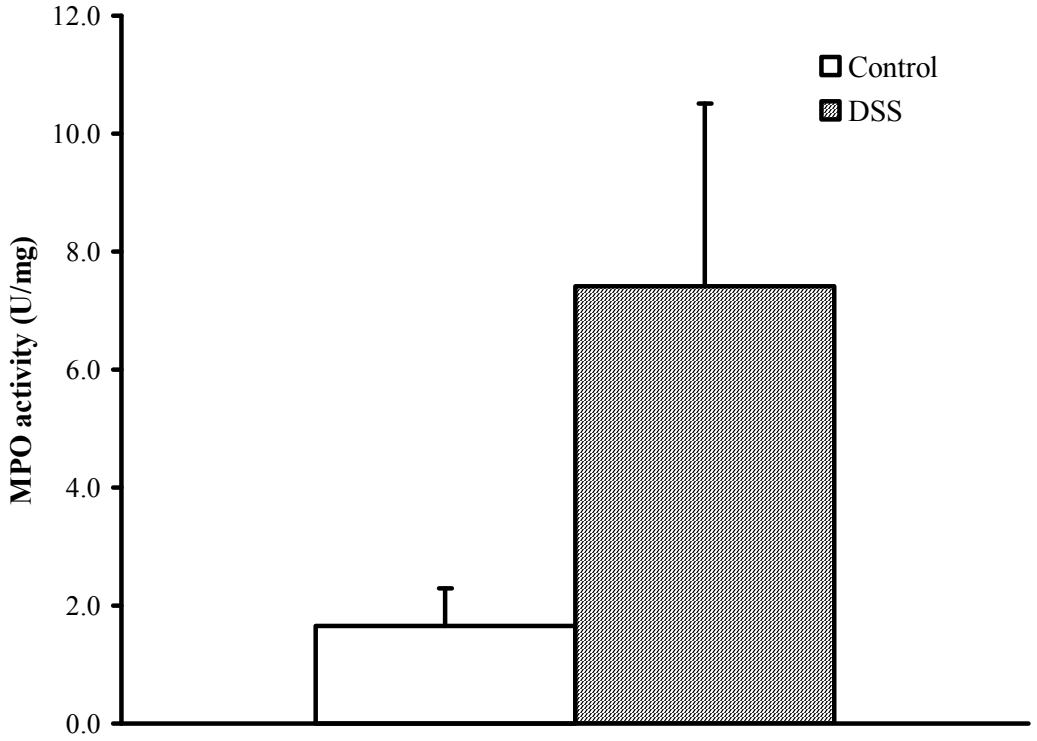

Figure 10. MPO activity in isolated smooth muscle of proximal colon from control and DSS-treated mice.

Mice received 2.5% DSS for 7 days in the drinking water. Values are means ± S.E.M for n = 3 (control) and n = 4 (DSS-treated). Values were not significantly different from one another.

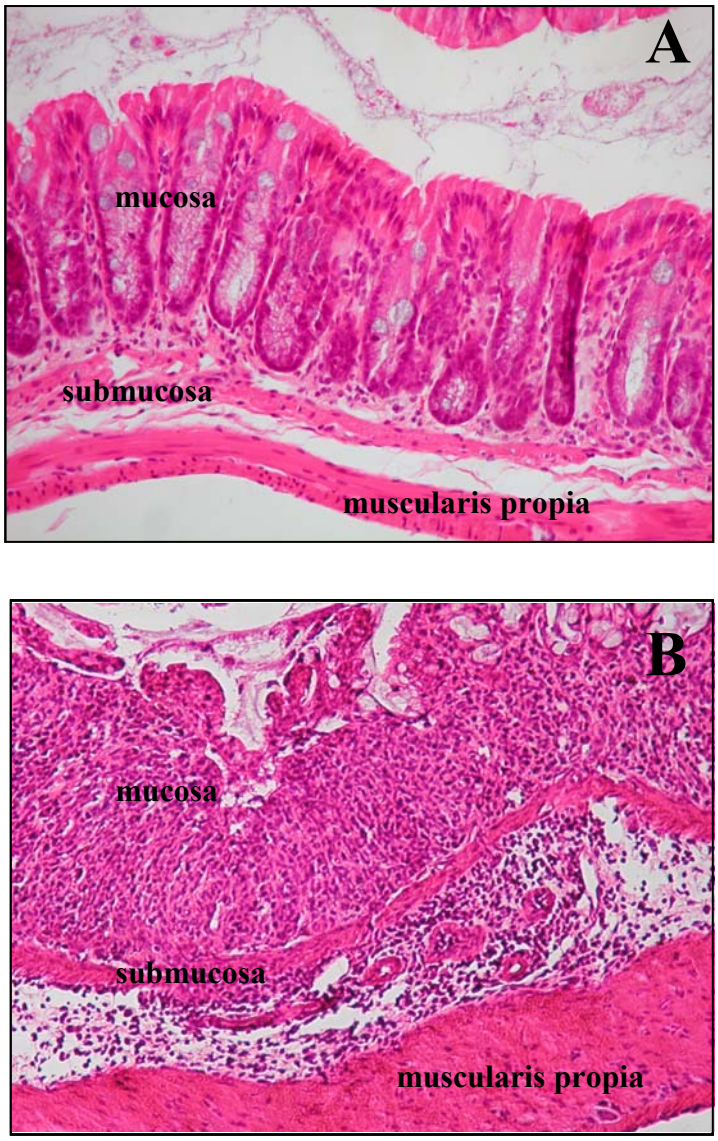

Figure 11. Representative photomicrographs of haematoxylin- and eosin-stained cross sections of mouse colon from control and DSS-treated animals.

A, Control; B, mice treated with 2.5% DSS for 7 days. Histology was completed on mimimun of 7 animals per group. Magnification x200. Provided by Dr. Paul Beck (University of Calgary).

acute intestinal inflammation, as has been reported previously in C57BL/6 mice (Mähler *et al*., 1998; Wirtz *et al.*, 2007).

3.2 Physiological assessment of muscle function

3.2.1 KCl- and carbachol-induced contractions of intact colonic circular smooth muscle strips from control and DSS-treated mice.

Depolarization of the smooth muscle membrane with 118 mM K^+ elicited contractile force in circular colonic smooth muscle strips from both control and DSS-treated mice. Moreover, stimulation of muscarinic receptors by the agonist carbachol (CCh) induced a concentration-dependent increase in tension in colonic circular smooth muscle strips isolated from control and DSS-treated mice. Typical traces of contractile responses induced by K^+ (118 mM) and carbachol (10 nM to 1 mM) in control and DSS-treated muscle strips are shown in Figure 12. K^+- and carbachol-induced contractions were normalized against the wet tissue weight of the circular colonic smooth muscle strips. The tension induced by membrane depolarization with 118 mM K^+ was significantly (P<0.025) higher in colonic circular smooth muscle strips from control mice (2.5 ± 0.3 mN/mg in 16 independent experiments (n = 5), than that calculated in colonic circular smooth muscle strips from DSS-treated mice (1.6 ± 0.2 mN/mg in 22 independent experiments (n = 5), (Figure 13).

Conversely, increasing concentrations (10 nM – 1 mM) of the muscarinic receptor agonist CCh evoked smaller contractile responses in smooth muscle strips isolated from control mice than those from DSS-treated mice (Figure 14). In smooth muscle strips from control mice, the maximum response to CCh was developed at 100 μM (10^{-4} M) and

A. Control

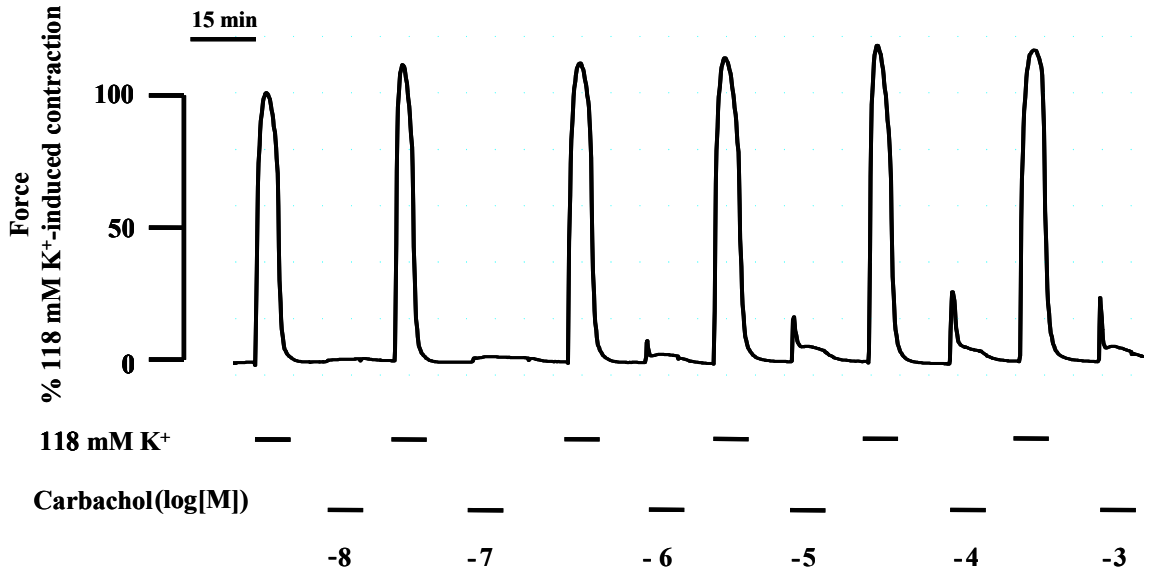

B. DSS

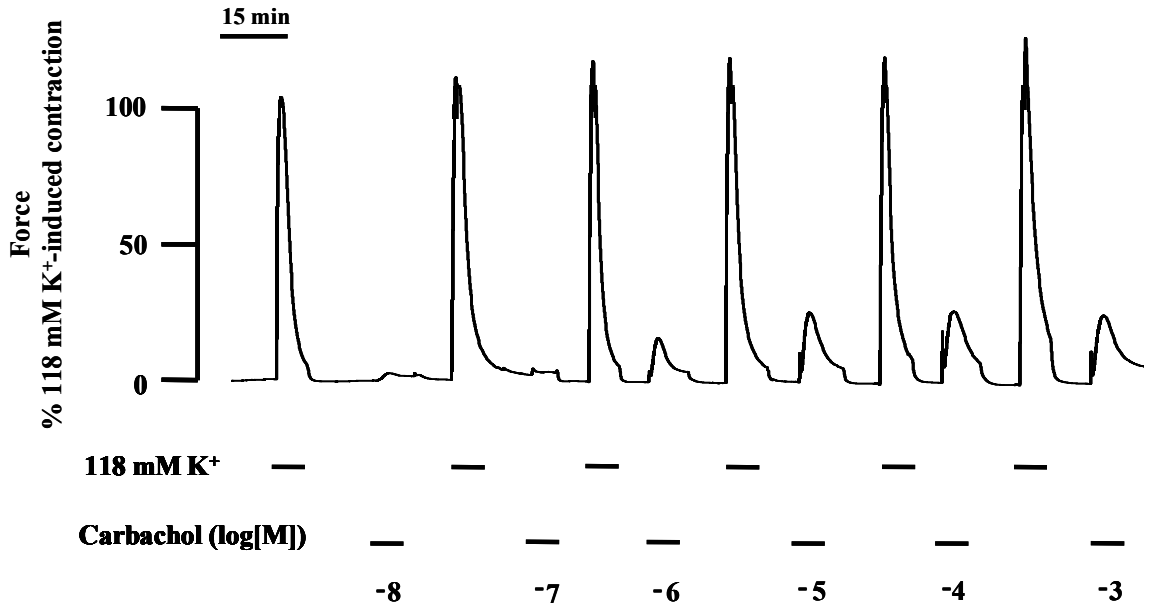

Figure 12. Contractile responses to 118 mM K^+ and carbachol obtained from colonic circular smooth muscle of control and DSS-treated mice.

A, Concentration-dependent responses to carbachol (10 nM – 1 mM) in control mice. B, Concentration-dependent responses to carbachol (10 nM – 1 mM) in DSS-treated mice. The peak force was measured, and data are expressed as a percentage of the 118 mM K^+-induced contraction.

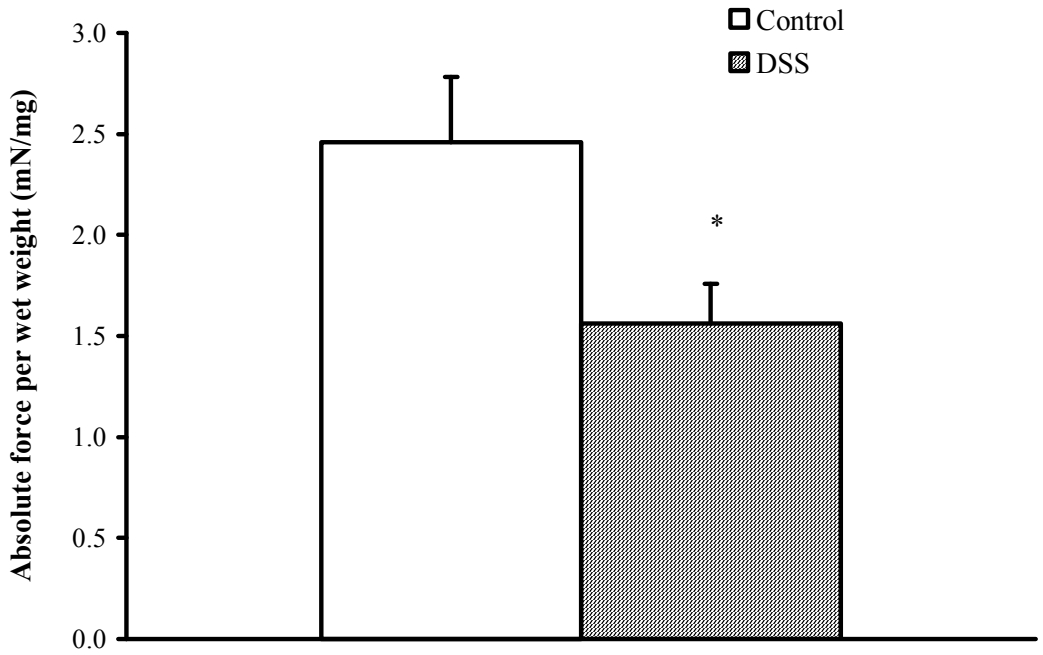

Figure 13. The absolute contractile force induced by 118 mM K^+ in colonic circular smooth muscle isolated from control and DSS-treated mice

The contractile responses of colonic circular smooth muscle isolated from control and DSS-treated mice (day 7) were determined. Force was normalized against the wet weight of the muscle strips. The results are representative of 4 animals per group and from 16 to 22 repetitions of 118 mM K^+. Errors bars indicate S.E.M. *, significantly different from control mice value (Student's t test, $P<0.025$).

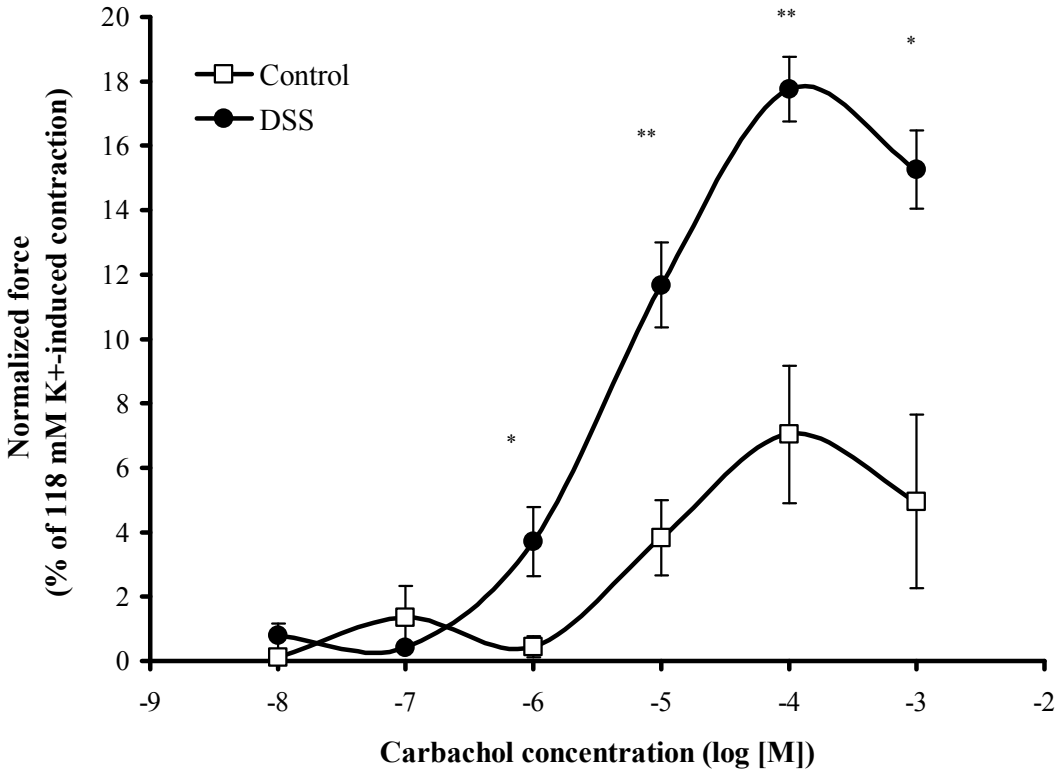

Figure 14. The contractile response to 118 mM K^+ and carbachol observed in colonic circular smooth muscle from normal and DSS-treated mice.

Concentration-dependent responses to carbachol (10 nM – 1 mM) in control and DSS-treated mice strips were determined. The peak force was measured, and data are expressed as percentage of 118 mM K^+-induced contraction. Error bars indicate S.E.M., n = 4. *, significantly different from control mice value (Student's t test, $P<0.005$); **, significantly different from control mice value (Student's t test, $P<0.05$).

increased 319% in DSS-treatment. The tensions measured over a range of CCh concentrations in inflamed colonic circular smooth muscle were significantly (P<0.05) higher that those measured in control colonic circular smooth muscle strips. Moreover, the ED_{50} for CCh was similar for muscle strips from control and inflamed colon (5 μM and 6 μM, respectively), indicating no a real change in sensitivity to CCh..

The absolute forces obtained during CCh (10^{-5}, 10^{-4}, and 10^{-3} M)-induced contractions (0.3 ± 0.07, 0.4 ± 0.07 and 0.3 ± 0.04 mN/mg, respectively; n = 4) were also significantly higher than those measured (0.06 ± 0.02, 0.1 ± 0.03 and 0.1 ± 0.03 mN/mg, respectively; n = 4) for normal colonic circular smooth muscle strips (Figure 15).

3.2.2 CCh-induced Ca^{2+} sensitization in α-toxin permeabilized colonic circular smooth muscle

Ca^{2+} sensitization was investigated following DSS-treatment using α-toxin permeabilized circular colonic smooth muscle strips. Permeabilization of tissue with α-toxin ensures the retention of functional proteins in the cytosol and allows for clamping of internal Ca^{2+} concentrations to evaluate Ca^{2+} sensitivity of the contractile apparatus (Kitazawa *et al*., 1989; Nishimura, *et al*., 1988). The contractile forces obtained during this protocol were measured and calculated with respect to the contractile force generated at pCa 4.5, designated as maximal force (i.e., 100%). A typical contractile response obtained during the evaluation of Ca^{2+} sensitization is shown in Figure 16. There were no differences in the contractile responses to submaximal calcium solution (pCa 6.3) in α-toxin permeabi-

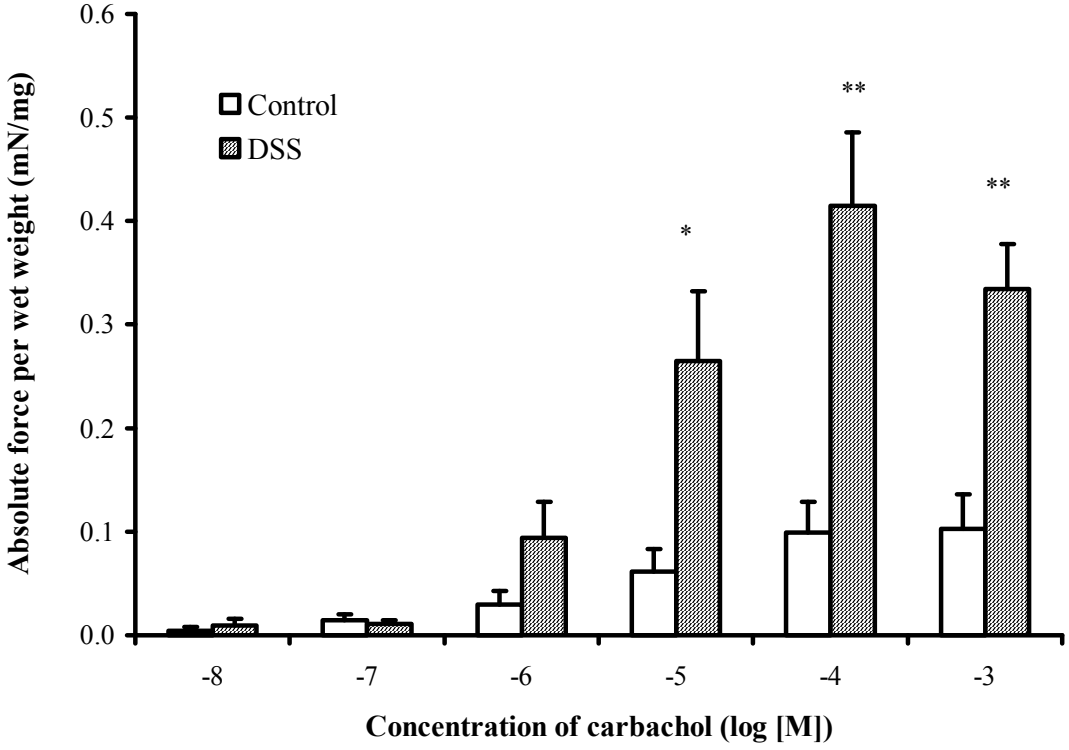

Figure 15. The absolute contractile force induced by carbachol (10 nM – 1 mM) in colonic circular smooth muscle isolated from control and DSS-treated mice

Concentration-dependent responses to carbachol (10 nM – 1 mM) in control and DSS-treated mice strips were determined. The contractile responses are expressed as absolute force which was normalized by wet weight of the samples. Error bars indicate S.E.M., n = 4. *, significantly different from control mice value (Student's t test, $P<0.005$); **, significantly different from control mice value (Student's t test, $P<0.05$).

lized smooth muscle from control and DSS-treated mice. The submaximal forces developed by pCa 6.3 were 47.7 ± 10.6 and 48.2 ± 7.2 % in control and DSS-treated mice, respectively. During the sustained contraction to pCa 6.3, CCh (100 μM) was added to stimulate additional contractile force (Figure 16). This additional force has been defined as CCh-induced Ca^{2+} sensitization. CCh-induced Ca^{2+} sensitization was very similar between control and DSS-treated mice (Figure 17). While colonic circular smooth muscle strips from control mice developed a contractile force of 19.0 ± 4.3%, those from DSS-treated mice generated a contractile force of 18.6 ± 2.3% with respect to the maximal force at pCa 4.5. These values were not significantly different.

3.2.3 Ca^{2+}- force relationships

Ca^{2+}-force relationships were evaluated in β-escin permeabilized strips to further characterize the differences in the contractile responses between circular colonic smooth muscle strips from control and inflamed intestine. A typical contractile response generated during the assessment of the Ca^{2+}-force relationship is shown in Figure 18. The contractile forces developed with increasing $[Ca^{2+}]_i$ were measured and calculated with respect to the tension evoked with pCa 4.5 solution, designated as maximal force (100%). Overall, the contractile forces developed in permeabilized colonic circular smooth muscle strips from control mice could be fit with a sigmoidal curve, which is the typical tendency described by a concentration-response to agonist (De Lean *et al*., 1978). However, the smooth muscle strips from DSS-treated mice did not generate measurable tension with Ca^{2+} concentrations

A. Control

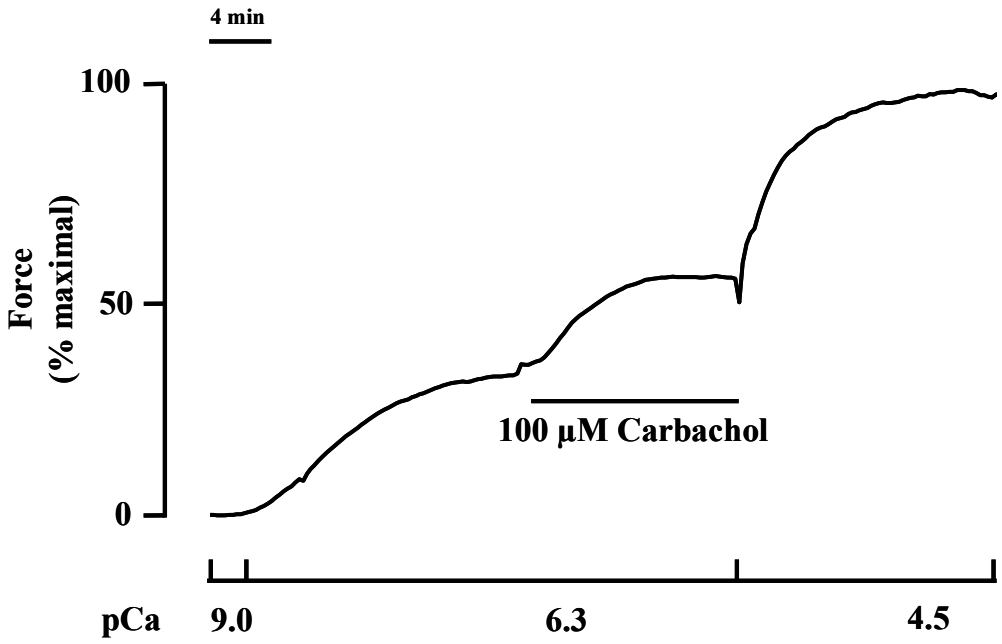

C. DSS

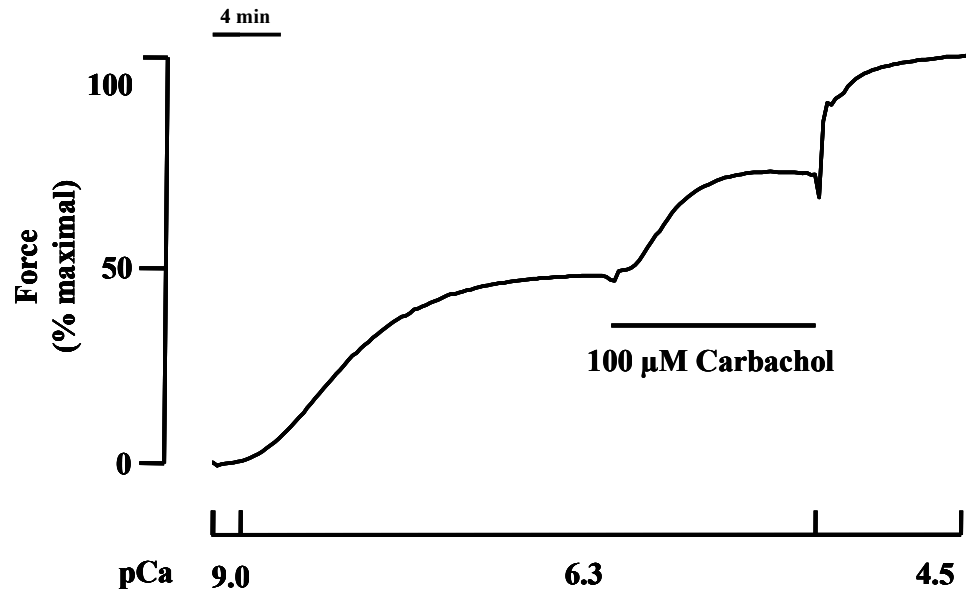

Figure 16. Typical traces of carbachol-induced Ca^{2+} sensitization in α-toxin permeabilized colonic circular smooth muscle strips from control and DSS-treated mice.

Representative recordings of carbachol-induced Ca^{2+} sensitization in control and DSS-treated mice. Carbachol (100 μM) was applied to the strips during the plateau of pCa 6.3 contraction. Forces observed at pCa 9 and pCa 4.5 were designated as 0% and 100%, respectively. The results are representative of n = 3 experiments for CCh-induced Ca^{2+} sensitization.

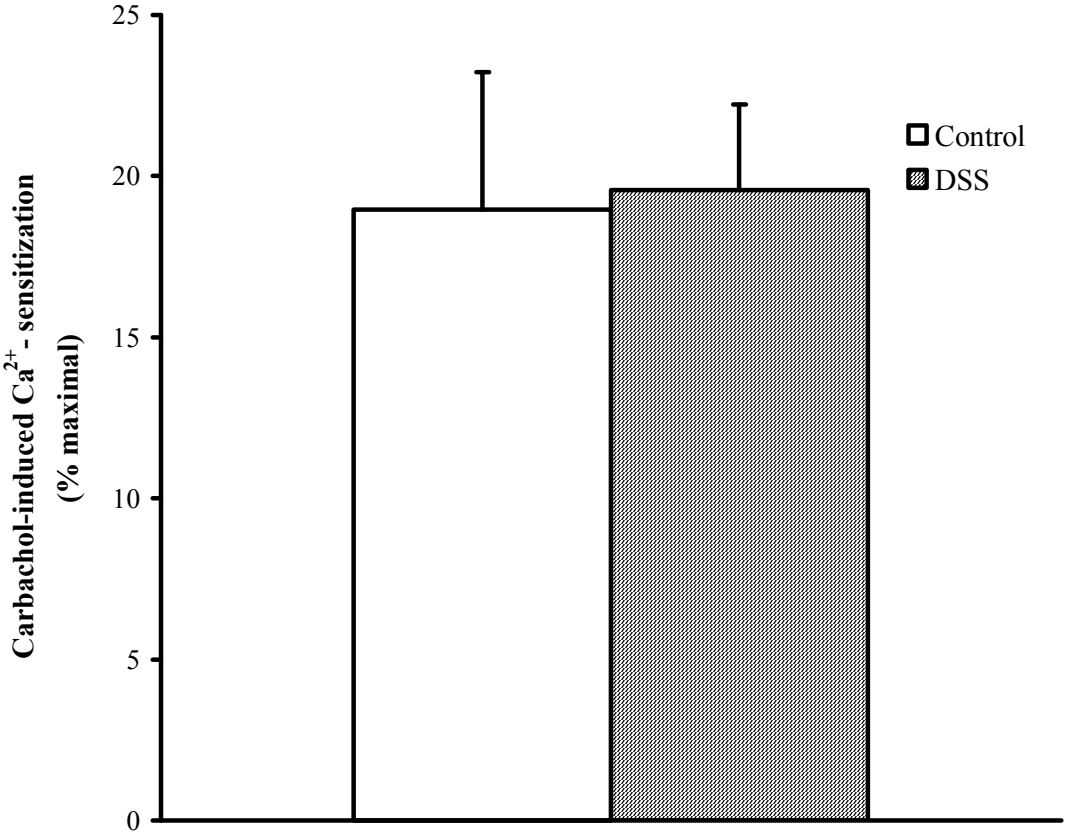

Figure 17. Carbachol-induced Ca^{2+} sensitization of α-toxin permeabilized colonic circular smooth muscle strips from control and DSS-treated mice.

The results are representative of 4 to 5 mice for carbachol-induced Ca^{2+} sensitization in control and DSS-treated mice. Carbachol (100 μM) was applied to the strips during the plateau of pCa 6.3 contraction. Forces observed with pCa 9 and pCa 4.5 were designated as 0% and 100%, respectively. Error bars indicate S.E.M. Values were not significantly different from those measured in control mice (n=3).

A. Control

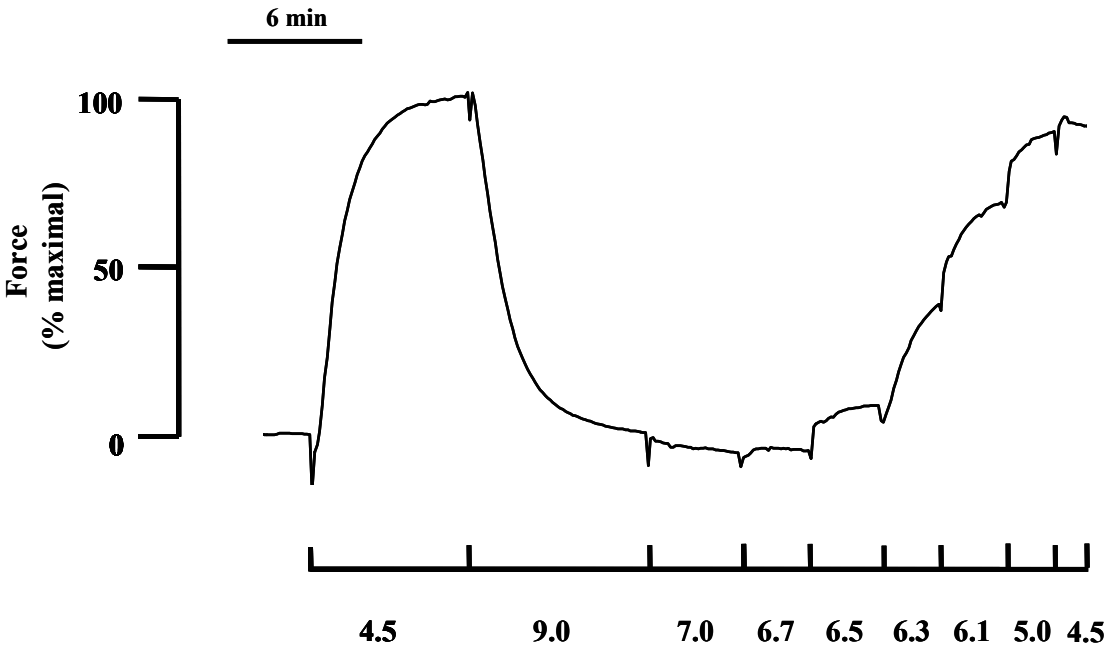

B. DSS

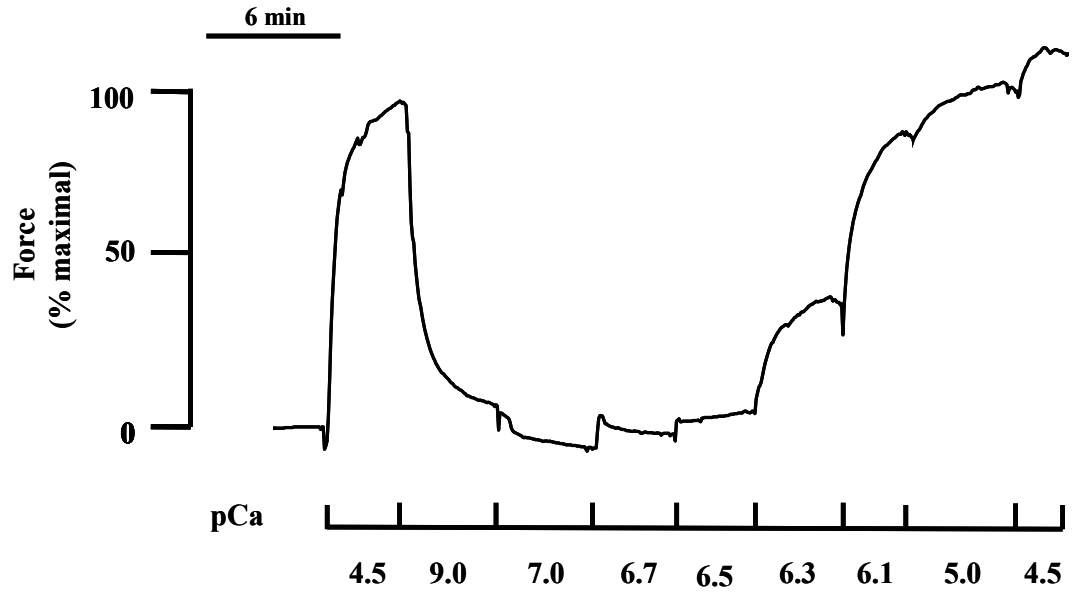

Figure 18. Typical traces of Ca^{2+}-force relationship to different Ca^{2+} concentrations (100 nM – 32 μM) of β-escin permeabilized colonic circular smooth muscle strips from control and DSS-treated mice.

Representative recordings of Ca^{2+}-force relationships of smooth muscle strips from control (A) and DSS-treated (B) mice. Forces observed at pCa 9 and pCa 4.5 were designated as 0% and 100%, respectively. The results are representative of experiments for Ca^{2+}-force relationships (n=3).

lower than 320 nM (pCa 6.5). On the other hand, approximately at Ca^{2+} concentrations between 355 nM (pCa 6.45) and 1260 nM (pCa 5.9) the inflamed strips elicited contractile forces higher than those developed by control strips. The measured forces at pCa 6.5, 6.3, and 6.1 were significantly different between control and DSS-treated strips with $P<0.005$, 0.05, and 0.025, respectively.

While the contractile forces elicited by the control strips at pCa 6.5, 6.3, and 6.1 were 5.68 ± 1.41, 21.26 ± 2.12, and 53.64 ± 3.06% respectively, the evoked contraction by inflamed strips at the same Ca^{2+} concentrations were 0.0 ± 0.0, 31.28 ± 2.61, and 64.33 ± 2.96%, respectively. Moreover, the contractile forces developed at other Ca^{2+} concentrations did not exhibit significant differences. These findings indicate that alterations in the Ca^{2+} sensitivity may be developed in inflamed circular colonic smooth muscle at Ca^{2+} concentrations lower than 1260 nM (pCa 5.9) because of the exposure to 2.5% DSS for 7 days (Figure 19).

3.3 Characterization of contractile protein expression

3.3.1 Molecular level

3.3.1.1 RT-PCR

RT-PCR analysis was used to examine the mRNA levels of myosin isoforms in control and inflamed colon (Figure 20A). Initial experiments demonstrated that the PCR products could be amplified from whole intestinal tissue or isolated smooth muscle layers (Figure 20B).

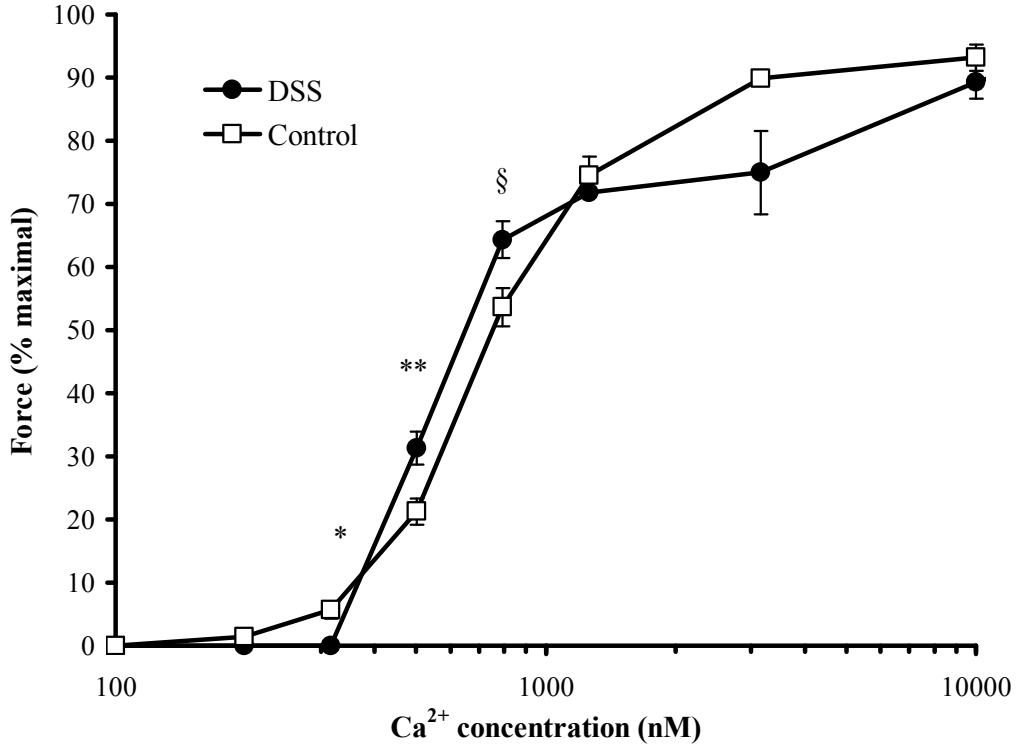

Figure 19. The Ca^{2+}-force relationship of colonic circular smooth muscle from control and DSS-treated mice.

Forces observed at pCa 4.5 were designated as 100%. Error bars indicate S.E.M. *, significantly different from control mice value (Student's t test, $P<0.005$); **, significantly different from control mice value (Student's t test, $P<0.05$); §, significantly different from control mice value (Student's t test, $P<0.025$), n = 3-4.

A.

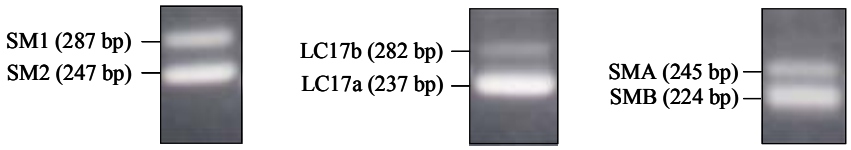

B.

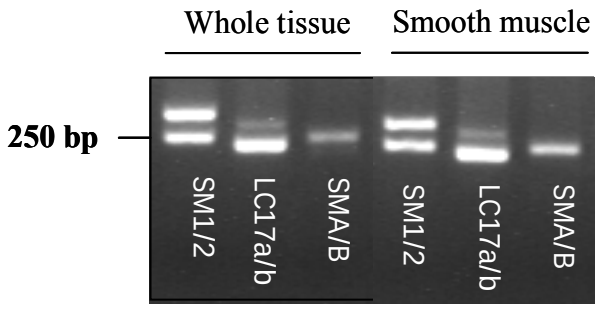

Figure 20. RT-PCR amplification products of myosin isoforms.

A, RT-PCR amplification products for six myosin isoforms. Each set of primers was designed to amplify both isoforms of MHC carboxyl terminal, amino terminal, or MLC, samples obtained from distal colon. B, RT-PCR products from cDNA derived from samples of whole tissue and smooth muscle layer of mouse ceacum.

Densitometric measurements of the RT-PCR products of the various myosin isoforms from three different intestinal segments (distal colon, proximal colon and ceacum) from control and DSS-treated mice are shown in Figure 21. The results obtained with this technique suggested that the mRNA expression of LC17a and LC17b myosin isoforms were different in distal colon of control and DSS-treated mice. It appeared that LC17a was up regulated whereas LC17b was down regulated in inflamed tissue. These findings provided motivation to perform quantitative analysis of the mRNA expression of the myosin isoform with real time RT-PCR.

3.3.1.2 Real time RT-PCR

To determine whether the gene expressions of SM1, SM2, SMA, SMB, and LC17b myosin isoforms were altered by DSS-induced inflammation, the mRNA levels were examined by real-time RT-PCR. In an initial evaluation, the accuracy of the designed primers was evaluated with non-denaturing polyacrylamide gels followed by sequencing of amplicons generated with the primers (Figure 22). Moreover, the formation of primer-dimers and the PCR efficiency of the primer sets were examined. Both the size and the sequence of all real time RT-PCR amplicons were confirmed. Melt curve analyses showed single peaks for control and DSS-treated samples (Figure 23A). The PCR efficiencies were calculated from standard curves (Figure 23B), and the results for each pair of primers are displayed in Table 4. The values of the PCR efficiencies were higher than 90%, and the difference among them was not greater than 5%. These findings validated the design of primers for SM1, SM2, SMA, SMB, and LC17b myosin isoforms and satisfied the

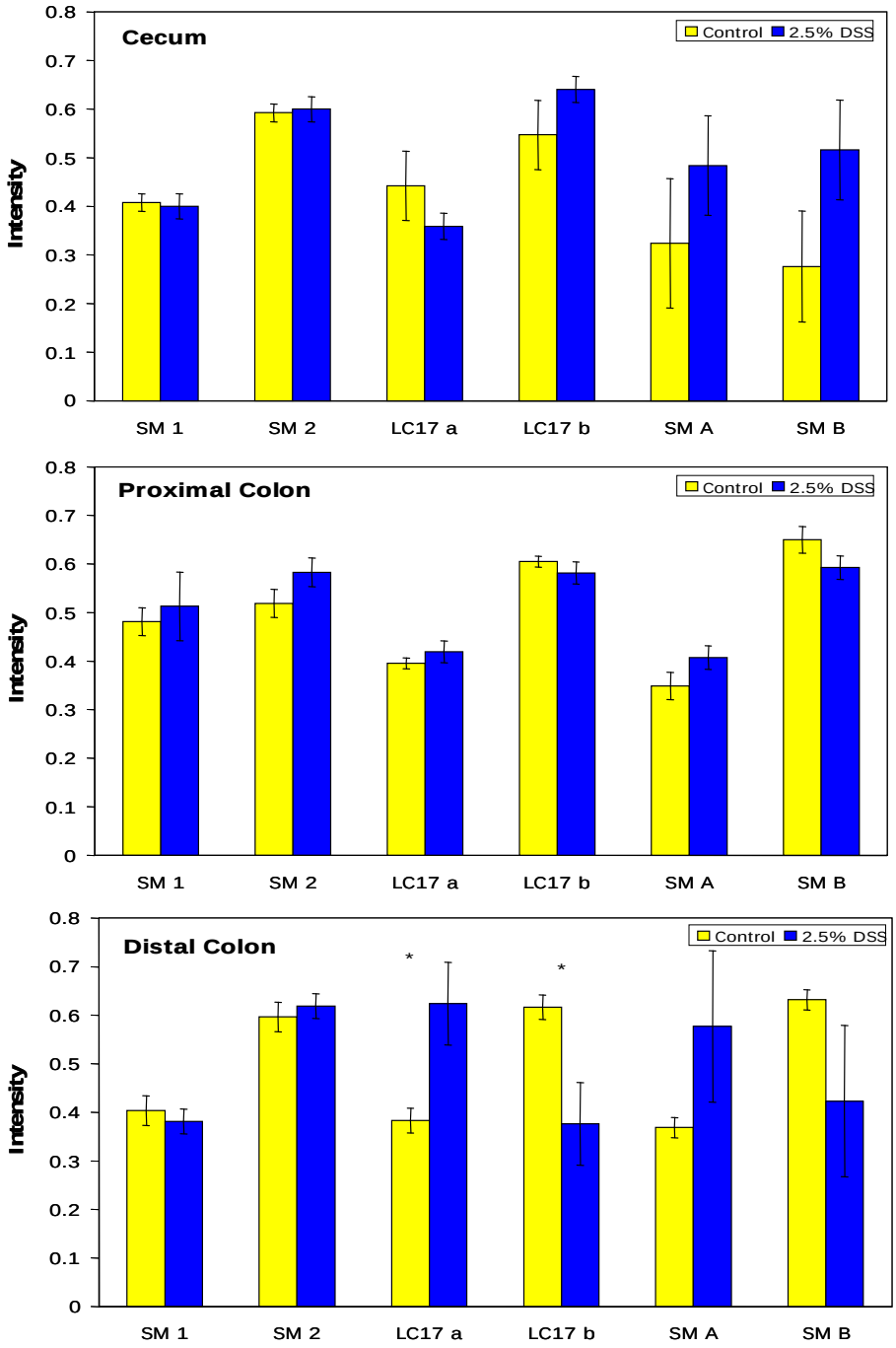

Figure 21. Densitometric measurements of RT-PCR products of myosin isoforms.

Densitometric values of PCR products of the three colonic segments. The values are mean ± S.E.M comparing results of DSS-treated mice against those from control mice. *, significantly different from control mice value (Student's t test, $P<0.05$), n = 5-6.

A.

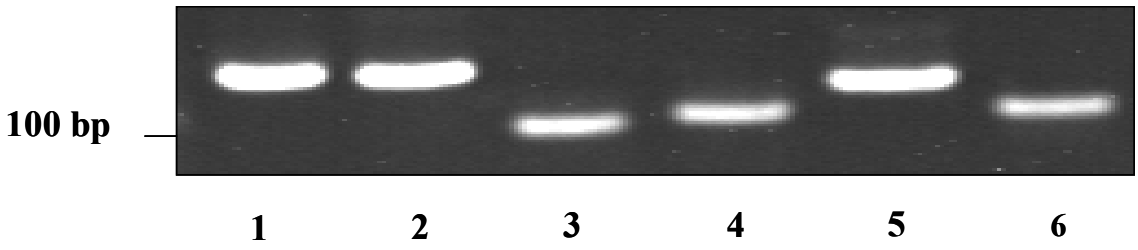

B.

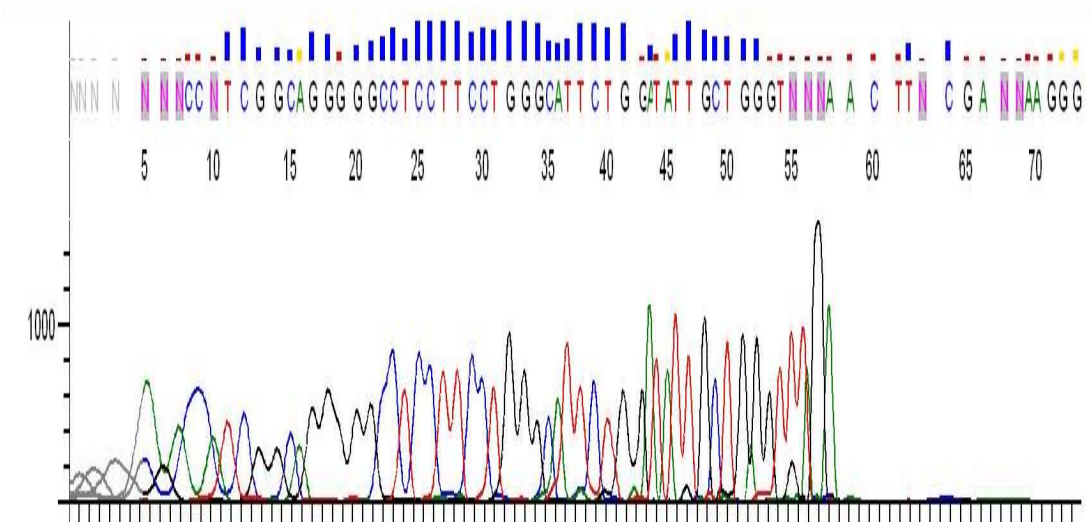

Figure 22. Size and sequence corroboration of real-time PCR amplicons.

A. Real-time PCR products were separated by non-denaturating PAGE (8%). Lane 1, 18S rRNA-141 bp; lane 2, β-actin-141bp; lane 3, MHC invariant-90 bp; lane 4, MLC invariant-95 bp; lane 5, SMB-122 bp; lane 6, SMA-116 bp. B. Results of sequencing of MHC invariant real-time PCR product. A, Adenine (green); C, Cytosine (blue); G, Guanine (black); T, Thymine (red).

A.

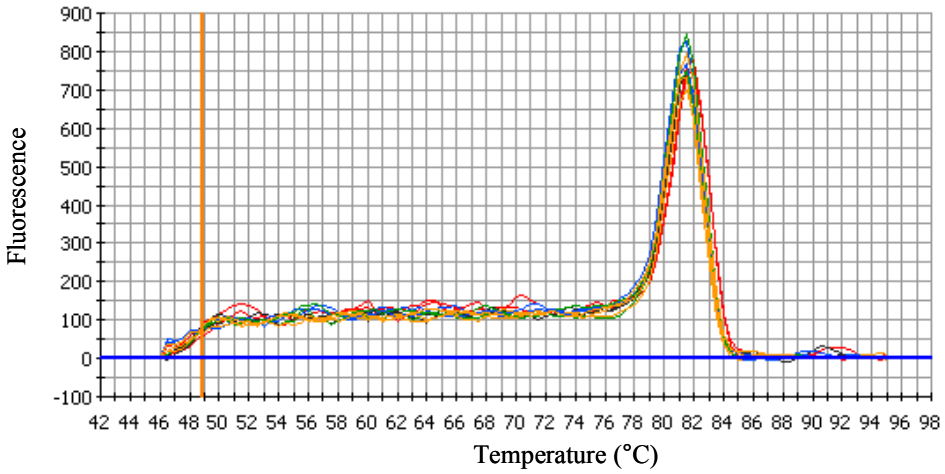

B.

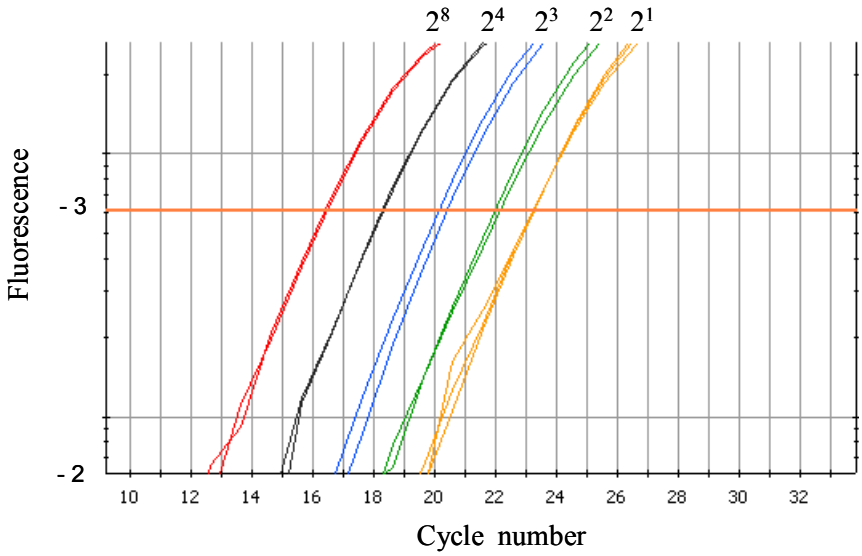

Figure 23. SYBR Green assay melt curve and serial dilutions of standard curve for the MHC invariant primer set.

A. Melting-curve analysis distinguishes between specific and non-specific PCR products. The real-time PCR designed primers amplify the expected amplicons without formation of dimers (n = 9). B, Five 2-fold serial dilutions ($2^1 – 2^8$) of the MHC invariant cDNA used as template are shown.

Table 5. PCR efficiencies of the real-time PCR designed primers.

Primers sets	*Efficiency (%)*
SM-1	94.8
SM-2	97.9
SM-A	94.6
SM-B	98.5
LC17b	99.7
β-actin	96.2
18S	99.8
MHC invariant	96.1
MLC invariant	98.5

requirements for use of the $2^{-\Delta\Delta CT}$ quantification method, described previously in the *Materials and Methods* section.

According to the results obtained from validation of housekeeping genes (Appendix A), β-actin expression was chosen to normalize the expression of the myosin isoforms. The β-actin amplicon was utilized to normalize and calculate the quantitative expression of the diverse myosin isoform genes. Thus, a quantitative comparison between control and inflamed tissue was calculated with the $2^{-\Delta\Delta CT}$ method by normalizing the ΔC_T counts to β-actin expression. The results showed that most of the myosin isoforms were up-regulated in the DSS-treated mice in comparison with their expression in control animals. These increases comprised values between 0.19 ± 0.12 to 0.98 ± 0.26 (n = 9-12) for the three colonic segments evaluated. Of the five myosin isoforms measured, LC17b presented a moderate up-regulation in distal colon (3.45 ± 0.53, n = 9) with respect to expression detected in control mice (Figure 24). Thus, these analyses indicated an up-regulation of mRNA expression of the myosin isoforms in the DSS-treated mice with respect to control animals for the majority of the myosin isoforms (SMA, SMB, SM1, and SM2) evaluated. The highest up-regulation of mRNA expression was detected for the LC17b isoform.

3.3.1.3 Protein levels

To assess the protein levels of various myosin isoforms (SMB, SM2 and LC17a/b) western blot analyses were performed on samples of colon from control and DSS-treated mice with specific anti-SMB, -SM2, and -LC17a/b antibodies. Figure 25 illustrates a typical outcome observed with western blotting for SMB, SM2, and LC17a/b.

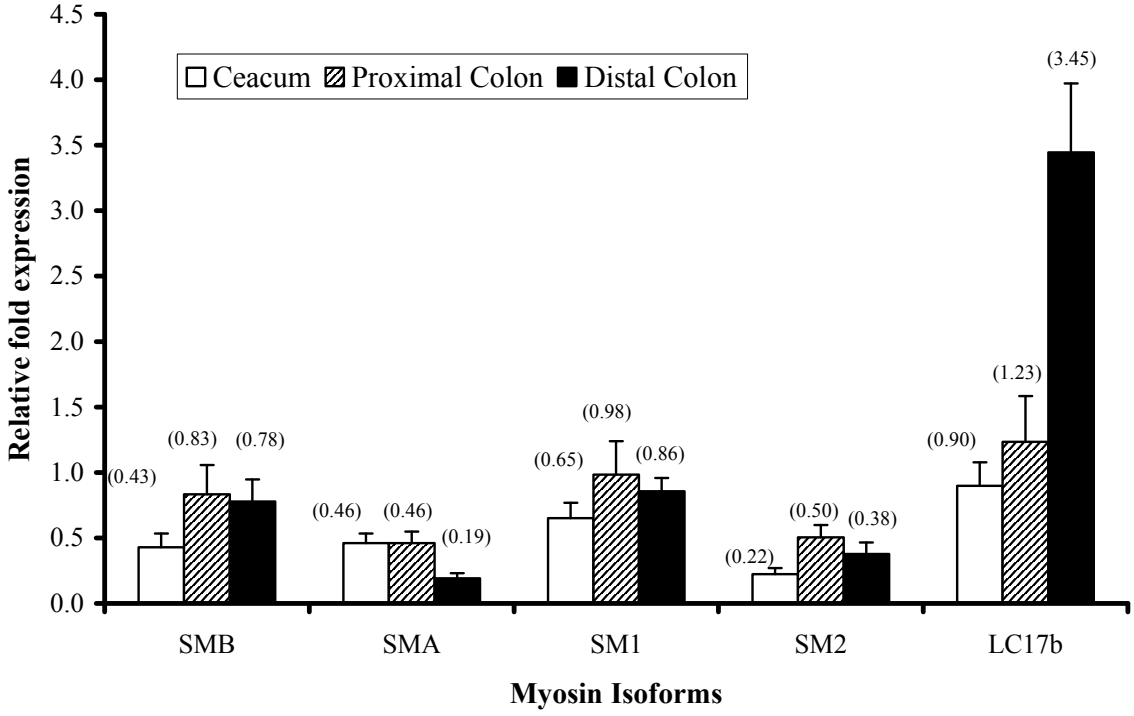

Figure 24. Expression of myosin isoforms in DSS-treated mice with respect to expression detected from control mice.

Reactions were carried out in triplicate with 1.0 μg of total RNA in each 25 μl reaction. Genes analyzed were SMB, SMA, SM1, SM2, and LC17b from three colonic segments, ceacum, proximal colon, and distal colon (n = 9-12). β-actin was used as reference gene in this analysis. Values in brackets represent the fold increase in expression in DSS-treated animals with a value of zero (0) indicating no change.

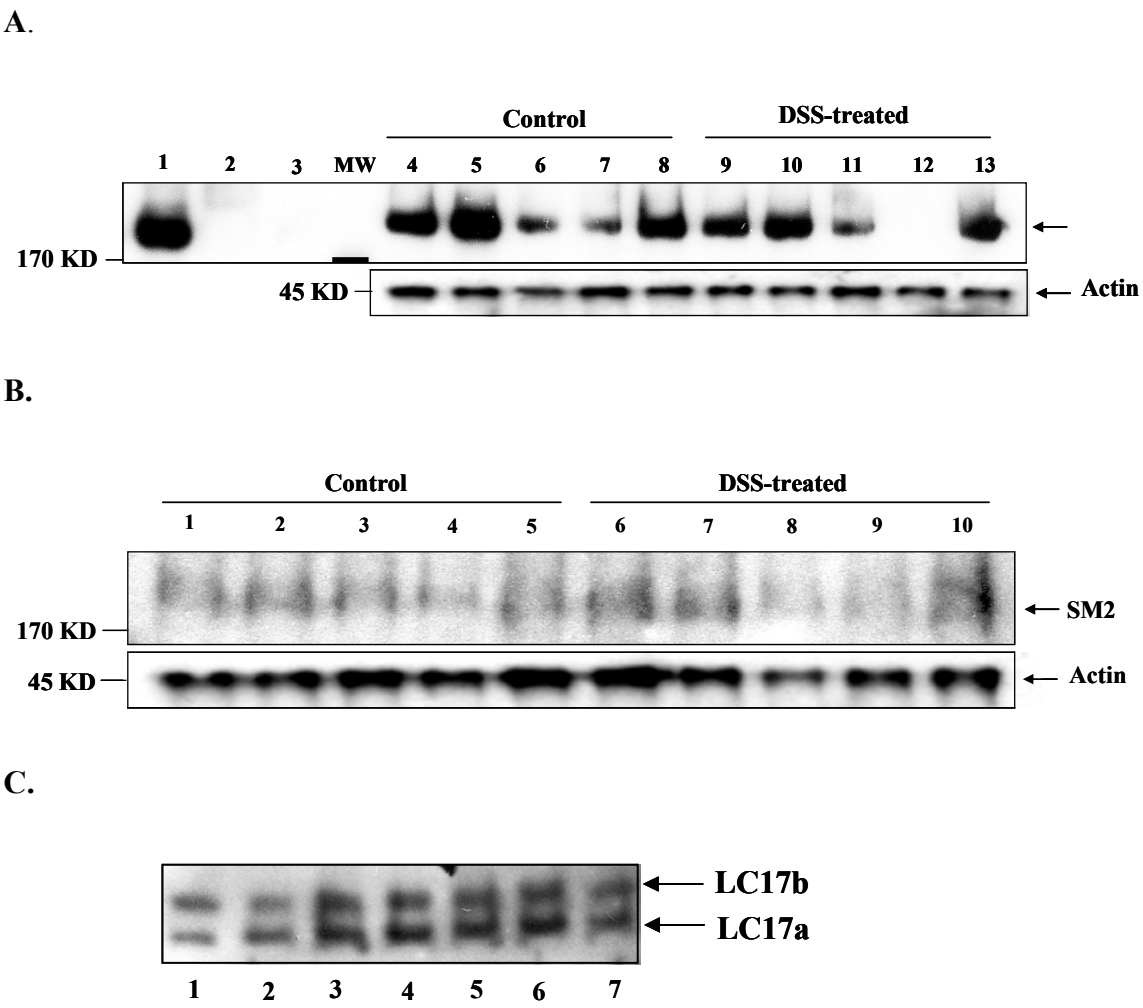

Figure 25. Western blot analysis of SMB, SM2, and LC17a/b from colon of control and DSS-treated mice.

A. Protein expression of SMB in proximal colon. Lane 1, bladder; lane 2, aorta; lane 3, limb skeletal muscle; MW, molecular weight marker 170 kD; lanes 4-8, control mice; lanes 9-13, DSS-treated mice. B. Protein expression of SM2 in distal colon. Lanes 1-5, control mice; lanes 6-10, DSS-treated mice. C. Protein expression of LC17a/b in proximal colon. Lane 1, rat uterus, lane 2-4, DSS-treated mouse; lane 5-7, control mouse.

Densitometric measurements from DSS-treated mice were normalized to densitometric measurements obtained from control mice. Densitometric measurements of SMB in proximal colon showed 1.0 ± 0.23, n = 5 and 0.61 ± 0.18, n = 5 for control and treated mice, respectively. The relative SMB protein expression in distal colon was 1.0 ± 0.28, n = 5 and 1.0 ± 0.23, n = 5 for control and DSS-treated mice, respectively. SMB protein levels in proximal and distal colon were not significantly different between control and DSS-treated mice. The expression of SM2 isoform was also determined both in proximal and distal colon from control and inflamed mice. The levels of SM2 in distal colon for control and treated mice were 1.0 ± 0.2 and 1.1 ± 0.2, respectively (n = 5). Similarly, SM2 expression in proximal colon did not show significant differences between control and inflamed mice (1.0 ± 0.14 and 1.28 ± 0.22, n = 5).

The levels of LC17b in proximal colon for control and DSS-treated mice were 1.0 ± 0.12 and 0.62 ± 0.23, respectively (n = 3-4). The relative LC17a protein expression in proximal colon was 1.0 ± 0.05 and 0.59 ± 0.35 (n = 3-4) for control and DSS-treated mice, respectively. The expression of LC17b in distal colon was determined to be 1.0 ± 0.20 and 1.21 ± 0.3 for control and DSS-treated mice, respectively (n = 3). The expression of LC17a in distal colon was determined to be 1.0 ± 0.15 and 1.18 ± 0.16 for control and DSS-treated mice, respectively (n = 3). No significant differences in the pattern of expression of LC17a and LC17b were observed between control and DSS-treated mice. The data indicated that treatment with 2.5% DSS for 7 days did not cause a significant change in the expression of myosin isoforms (SMB, SM2, LC17a/b) (Figure 26).

A.

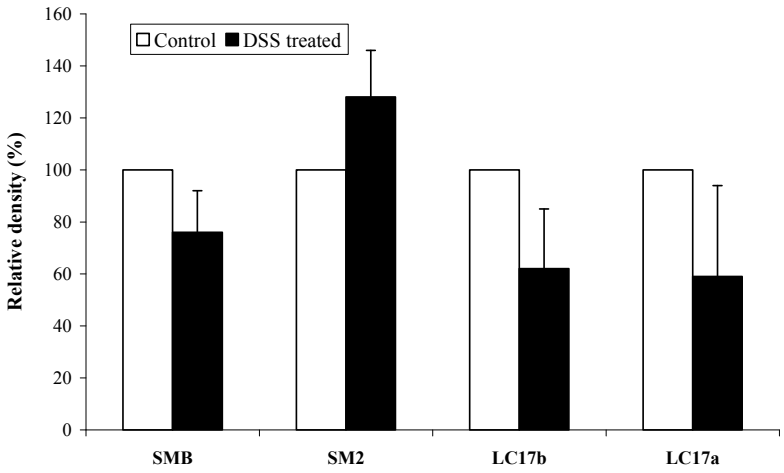

B.

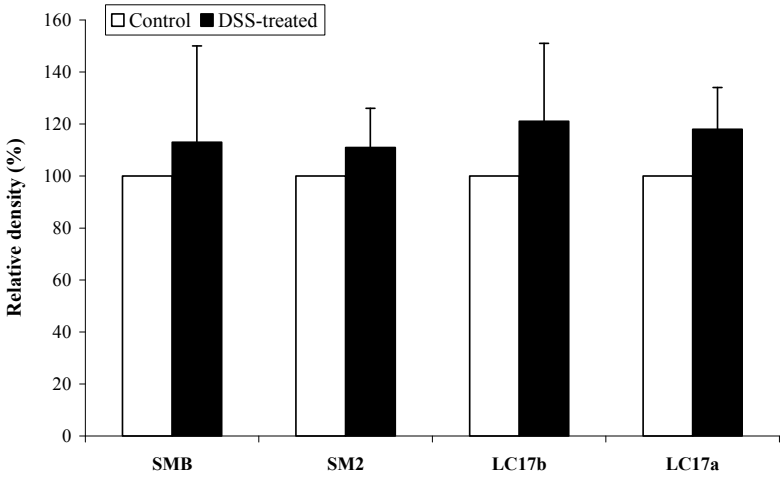

Figure 26. Protein expression of SMB, SM2, and LC17a/b measured using western blot analysis of control and DSS-treated mice from colonic tissues.

Densitometric measurements of SMB, SM2 and LC17a in A, Proximal colon. B, Distal colon. Band densities were normalized to the control. Results are expressed as mean ± S.E.M, n = 3-5. Values from DSS-treated mice were not significantly different from control mice values.

4 DISCUSSION

Conventional research into the pathogenesis and pathophysiology of colonic inflammation (IBD) has been focused on the mucosal compartment. However, the development of strictures and fistulas and the presence of T cells deep in the neuromuscular layer indicate the transmural nature of the inflammatory process. These findings motivated an examination of the functional and structural alterations of the muscularis propia in response to intestinal inflammation during colitis. Colonic motility depends upon the contractile responses of smooth muscle cells. The contractile properties of the intestinal smooth muscle cells can be driven by extrinsic factors, including ICC, transmitters released from enteric nerves, circulating hormones and locally released paracrine substances (Sanders & Smith, 1989). Intrinsic properties of the smooth muscle cells also play an important role in the regulation of mechanical activity. However, these regulators can be influenced by the inflammatory status of the intestine to alter the contractile nature of the colonic smooth muscle layers. For example, it has been reported that the typical enhanced contraction of airway smooth muscle during asthma is dependent upon the intracellular signalling and structural properties of the smooth muscle cells (Gil *et al*., 2006). The present thesis examines the effect of acute colonic inflammation on the intrinsic contractile nature of the smooth muscle. Weight loss, polymorphonuclear leukocyte infiltration (MPO activity assessment) and macroscopic/microscopic characterization of colonic tissue were used to assess the severity of intestinal inflammation induced in C57BL/6 mice following administration of DSS. Specific investigations were carried out to assess the effect of

inflammation on the colonic circular smooth muscle contractility induced by non-receptor and receptor stimulation. Moreover, the expression of myosin isoforms was examined to assess inflammation effects on the smooth muscle contractile machinery.

4.1 Characterization of DSS-induced inflammation in C57BL/6 mice.

The administration of 2.5% (w/v) DSS via the drinking water to C57BL/6 mice for 7 days generated a reproducible colitis. Macroscopic signs of acute inflammation were reflected by diarrhea, presence of rectal blood, loss of body weight and colonic shortening. The observed weight loss (7 ± 0.3%) was less than that reported by other authors (10%, Itoh *et al*. 1999; 12%, Beck *et al*. 2004) for the same conditions, 2.5% DSS for 7 days in C57BL mice. This disparity may be caused by differences in molecular weight of the administered DSS compound. It has been reported that the severity of colitis induced by DSS is dependent upon the molecular weight and degree of sulphation of the DSS compound as well as the dose and duration of DSS compound administration (Axelsson *et al*., 1996; Kitajima *et al*., 2000).

Interestingly, the reduction in colon length assessed in this study (46%) was similar to that reported by Swee and colleagues (2008) (42%) with 2.5% DSS for 7 days. In addition, the MPO activity measurements obtained in this study were higher than those detected by Beck *et al*. (2004) following similar protocols both for inducing colitis (2.5% DSS for 7 days in C57BL/6 mice) and for MPO determination. This variation may be due to the differences of DSS previously mentioned. Besides, studies have reported that the intraluminal microbiological flora play a fundamental role not only in the conservation of the normal intestinal function but also in the induction and maintenance of gastrointestinal

inflammation (Sartor *et al*., 1996). Variations in the microbial composition of the gastrointestinal tract may generate alterations in the inflammatory response (Yamada *et al*., 1992). Thus, a plausible explanation for the differences in the inflammatory response observed between this study and other investigations may be the differences in the bacterial microflora of the evaluated mice. In fact, the bacterial microflora are related to environment and type of food that mice receive in the different animal facilities.

It is worth mentioning that the MPO activity detected in the isolated smooth muscle layer of proximal colon from DSS-treated mice was double that measured in whole tissue sections. This finding may be due to differences in the total protein content and the wet weight of the tissues (i.e., edema content). Whole intestinal sections are expected to possess significant edema in the mucosal and submucosal layers. In contrast, the muscularis layer is comprised of a thin layer of smooth muscle cells and would not be expected to contain as much edema as the mucosal and submucosal layers. Regarding this finding, other possible explanation involves the activation of the resident macrophages of the muscularis propia and the rolling of polymorphonuclear neutrophils (PMN). In rat colon following TNBS-induced colitis, the activation of resident macrophages induces an increase in the secretion of cytokines and chemokines, thereby resulting in an influx of mononuclear cells and neutrophilic granulocytes to the muscularis propia (Kinoshita *et al*., 2007). This augmentation of PMN in the muscularis propia may explain the high MPO activity detected in the colonic smooth muscle layer. However, it is important to consider the nature of the inflammatory stimulus (Ghia *et al*., 2008) since the results just mentioned contrast with those reported in other inflammatory models. Immunohistochemical studies of MPO from muscularis propia of lipopolysaccharide (LPS)-inflamed mouse ileum detected few MPO^{+}

cells (Mikkelsen *et al*., 2008). Interestingly, it has been pointed out that DSS can interfere with the accumulation of PMN cells by reducing PMN rolling in the early stage of PMN adhesion to the blood vessel wall (Fiebig *et al*., 1991). The decrease of PMN in the mucosa may be related to this effect (Axelsson *et al*., 1996).

4.2 KCl- and carbachol-induced contractions of intact colonic circular smooth muscle strips from control and DSS-treated mice.

The tension developed in response to administration of high extracellular [K^+] was significantly decreased in the DSS-treated mice (Figure 13). This result suggested that functional alterations of the smooth muscle cells occur at the post-depolarization level. These alterations may be reflective of changes in the voltage-dependent Ca^{2+} channels which open after membrane depolarization to increase cytosolic [Ca^{2+}] and initiate the signalling cascade that ultimately leads to LC20 phosphorylation and contractile force. The decreased contractility of intestinal circular smooth muscle after membrane depolarization may be attributable to a reduction in the activity of the voltage-dependent Ca^{2+} channels. Studies have demonstrated a reduced activity of L-type Ca^{2+} channel (voltage-dependent Ca^{2+} channel) in both DSS mouse (BALB/c) and TNBS rat colitis models (Akbarali *et al*., 2000; Kinoshita *et al*., 2003).

In contrast, the contraction induced by CCh was enhanced in DSS-treated mice (Figure 15). Agonist-induced smooth muscle contraction is the result of a train of events mediated by muscarinic receptors. Increased expression of muscarinic receptors may explain the enhancement of the smooth muscle contraction. Pharmacological data (Ehlert *et al*., 2003) and data on mutant mice lacking M_3 muscarinic receptors (Matsui *et al*., 2002)

have indicated that M_3 receptors are primarily responsible for mediating the contraction of circular smooth muscle of mouse ileum. Evaluations of the expression of M_3 muscarinic receptors have shown that levels are not altered in animal models of DSS-induced intestinal inflammation (Sato *et al*., 2007). Therefore, the hypercontractility observed in this study is most likely not caused by alterations in the muscaric M_3 receptor expression.

Further, the significantly higher contractile response to CCh did suggest that an important phase in the regulation of the contractile activity in murine colonic smooth muscle is either Ca^{2+} independent (Figure 2) or occurs at a point downstream from changes in $[Ca^{2+}]_i$. Ca^{2+} sensitization experiments were performed and an increase was expected in inflamed circular colonic smooth muscle. However, the Ca^{2+} sensitization measured in inflamed smooth muscle was not significantly different from that found in control tissue. In addition, experiments conducted to assess the contractile force-Ca^{2+} relationships showed interesting alterations in the Ca^{2+} sensitivity of the inflamed colonic circular smooth muscle. A progressive increase of $[Ca^{2+}]$ from 100 nM evoked a steadily increased contraction in colonic smooth muscles strip from control animals (Figure 19). A similar trend has been reported by other authors (Siegman *et al*., 1997). The minimal contractile force elicited was with 100 nM of Ca^{2+} (pCa 6.7), and the maximal contraction was registered at 32 μM of Ca^{2+} (pCa 4.5). These values are consistent with the $[Ca^{2+}]_i$ determinations in native smooth muscle cells where contraction is elicited when the $[Ca^{2+}]_i$ increases from 100 to 700 nM (Yagi *et al*., 1988). However, even though a similar trend is observed, the Ca^{2+} concentrations needed to evoke contractile force in rat small intestine smooth muscle were 10-fold lower that those observed in this study. The difference is possibly due to the loss or rearrangement of contractile proteins during the permeabilization

process. Remarkably, contractile force was not developed at Ca^{2+} concentrations lower than 320 nM (pCa 6.5) in smooth muscle strips of DSS-inflamed animals, even with an exogenous supply of calmodulin (CaM, 0.3 mg/ml). The threshold for force development in control smooth muscle strips was approximately 150 nM, just slightly greater than the $[Ca^{2+}]_i$ of the resting smooth muscle cell. The decrease in contractile activity associated with $[Ca^{2+}]_i$ lower than 320 nM may reside with alterations in the Ca^{2+} sensitivity of LC20 phosphorylation. Furthermore, Ca^{2+} concentrations between 355 nM (pCa 6.45) and 1260 nM (pCa 5.9) elicited greater contractile force in smooth muscle isolated from inflamed intestine. Thus, the Ca^{2+} sensitivity of inflamed colonic smooth tissue is altered in the range of Ca^{2+} concentrations from 320 nM to 900 nM. The alterations in contractility observed in this study for $[Ca^{2+}]_i$ higher than 700 nM may not have functional repercussions *in vivo* because concentrations of cytosolic Ca^{2+} exceeding 700 nM generate a steady-state contractile force response (Yagi *et al*., 1988). Taken together, the decreased force level elicited by membrane depolarization in this study may be a result of reduced Ca^{2+} influx and decreased sensitivity to $[Ca^{2+}]_i$ (Figure 13).

4.3 Characterization of myosin isoform expression

There is evidence showing that alterations in the relative content of myosin isoforms affect the contractile function of smooth muscle in distinct pathological conditions, including bladder outlet obstruction (DiSanto *et al*., 2003), megacolon (Siegman *et al*., 1997), erectile dysfunction (Koi *et al*., 2006), pulmonary hypertension (Mitani *et al*., 2001) and hypercontractility in airway hyperresponsiveness (Gil *et al*., 2006). To my knowledge, this is the first study to assess the expression of distinct myosin

isoforms in intestinal colonic smooth muscle under inflammatory conditions. One of the most interesting findings in this study was that the expression of all the myosin mRNA isoforms was slightly increased in the DSS-treated mice. Notably, initial studies with RT-PCR suggested increased expression of LC17 isoforms in distal colonic smooth muscle. Further experiments with real-time PCR revealed alterations in the LC17b isoform expression. However, the protein expression of both LC17 and the other of myosin isoforms evaluated by western blotting showed that protein content was not altered in DSS-inflamed colonic smooth muscle. Interestingly, some of the pathologies previously mentioned (e.g., hypertrophied small intestinal smooth muscle, hypertrophied rat urethra and hypertrophied detrusor smooth muscle following bladder outlet obstruction), along with other animal models of hypertrophic intestinal smooth muscle (Löfgren *et al*., 2002), encompass hypertrophic growth as one of the histological features (an increase of the size of an organ or an area of tissue due to enhanced size of the cells) and an overexpression of LC17b myosin isoform. Although the DSS administration in the present study was thought to generate an acute bout of intestinal inflammation, another report has demonstrated that a chronic and progressive colitis can be induced by a single exposure of C57BL/6 to DSS (Melgar *et al*., 2005). Interestingly, prominent hypertrophy of mucosa was detected in C57BL/6J mice in a DSS chronic colitis model (Nakanishi *et al*., 2007). The data presented in this study and current information suggest that myosin isoform transcripts, specifically LC17, are tightly regulated in colonic smooth muscle or the alteration of myosin isoforms may be more probable in the chronic colitis model. The up-regulation of protein synthesis and structural remodelling (hypertrophy) observed in chronic colitis models may be more likely to generate alterations at the protein level. The increase of LC17b mRNA levels in

the present study indicated that myosin isoform translation is tightly regulated as this has been reported for myosin heavy chains, SM1 and SM2 (Martin *et al*., 2007).

A specific function for the different LC17 isoforms in smooth muscle contractility has not been determined. Immunohistochemical studies have shown distinct cellular locations and different assemblies (e.g., as homodimers and heterodimers) of the LC17 isoforms (Takeuchi *et al*., 1999). Both regulatory and essential light chains are bound to myosin heavy chain; this complex constitutes a regulatory domain (Houdusse & Cohen, 1996) and is thought to act as a lever arm during force production (Highsmith, 1999). Matthew *et al*. (1998) suggested that LC17 stiffens the lever arm of myosin. On the other hand, it has been proposed that the LC17a/LC17b isoform composition may determine the tonicity of smooth muscle since a greater amount of LC17b relative to LC17a is found in tonic muscles, such as aorta, than in more phasic muscles, such as bladder. However, there is still controversy surrounding this hypothesis. When Somlyo *et al*. (1968) replaced the LC17a isoform with LC17b, the cycling cross-bridge diminished. Conversely, studies that performed myosin isoform exchange, i.e., replacing LC17a and LC17b from turkey aortas for equal amounts of LC17a from gizzard, did not affect the average velocity of actin filament movement in a motility assay (Kelley *at al*., 1993). Moreover, some researchers have documented an inverse correlation between the LC17b content and the maximal shortening velocity (Malmqvist & Arner, 1991). It has also been proposed that LC17b increases the affinity of the myosin head for actin while suppressing actomyosin ATPase activity (Hasegawa *et al*., 1992; Helper *et al*., 1988). There are distinct correlations of SMA/SMB and LC17a/17b co-expression in different smooth muscle beds. SMB and LC17a are the predominant species in phasic smooth muscles, whereas SMA and LC17b

are expressed mainly in tonic smooth muscles. So it may be the dual expression of these myosin isoforms that dictates the tonicity of the smooth muscle.

Evidence indicates that changes in the proportion of the SMB isoform have the greatest effect on the contractile nature of the smooth muscle. The additional 7 amino acids in the SMB isoform near the ATP binding site not only alter the length and flexibility of the myosin head but also the enzyme kinetics of the actin-myosin interaction that occurs in this region (Sweeney *et al*., 1998). The insert may influence smooth muscle kinetics by influencing the cross-bridge cycle. The actomyosin ATPase activity and the motile velocity are doubled in the SMB isoform when compared to the SMA isoform (Kelly *et al*., 1993; Rovner *et al*., 1997, Babu *et al*., 2004).

4.4 Possible reasons that influence the hypercontractility in colonic smooth muscle

The findings of this thesis indicate that the changes in contractile activity in acutely inflamed colonic smooth muscle are not associated with altered expression of myosin isoforms. Numerous inflammatory mediators participate in the complex inflammatory process. Solid evidence indicates the important role of cytokines as key factors in the regulation of the intestinal immune response and mediation of tissue damage in IBD (Sartor, 1994; Vrees *et al*., 2002). It has been characterized that in DSS-induced acute colitis, massive infiltrates appear in the inflammatory lesions, consisting particularly of T and B lymphocytes, macrophages and neutrophils, which produce diverse pro-inflammatory cytokines, including tumor necrosis factor (TNF)-α, interleukin (IL)-6, IL-8, IL-12, IL-17 and interferon (IFN)-γ (Egger *et al*, 2000; Melgar *et al*., 2005). A marked

enhancement of pro-inflammatory cytokines (tumor necrosis factor (TNF)-α, interleukin (IL)-1, IL-6, and IL-8) have been detected in patients with ulcerative colitis and Crohn's disease (Isaacs *et al*., 1992). Specifically, elevated levels of the pro-inflammatory cytokine IL-1β has been detected in the mucosa and the muscle layer during acute and chronic inflammation. Additionally, IL-1β can inhibit smooth muscle contractility by modulating the release of ACh, norepinephrine, and substance P. On the other hand, exogenous administration of two anti-inflammatory cytokines, IL-4 and IL-13, to mice induced hypercontractility in longitudinal smooth muscle (Zhao *et al*., 2003). Likewise, Akiko *et al*. (2005) showed that stimulation of cultured smooth muscle cells with IL-4 and IL-13 induced a hypercontractile response to the cholinergic agonist CCh. In short, changes in intestinal muscle contraction have been found in human disease and animal models and are associated with alterations in the smooth muscle response to neurotransmitters and inflammatory mediators.

Interestingly, Itoh and colleagues (2006) recently found an important up-regulation of IFN-γ in the DSS-induced mouse model of colitis (e.g., 2.5% DSS for 7 days in C57BL/6 mice). Furthermore, they demonstrated a direct relationship between the development of colitis and the presence of this cytokine, since knockout IFN-γ-/- mice did not display progressive colitis. Additionally, stimulation of cultured intestinal cells with IFN-γ and TNF-α generates an up-regulation of MLCK (Wang *et al*., 2005). Studies have shown that increased MLCK activity can enhance smooth muscle contractile activity. The acute inflammation generated under the conditions of our study may have induced production of these pro-inflammatory cytokines which in turn might have potentiated contractions in inflamed colonic smooth muscle via an enhancement of MLCK expression.

In contrast, Ohama *et al*. (2007), Kinoshita *et al*., (2006) found that intestinal inflammation decreased smooth muscle contractility, and this decrease in contractility was associated with TNF-α. Although, in this thesis the data shown no changes in the sensitivity to CCh by muscarinic receptors during inflammation, it has been reported that muscarinic receptors can be influenced by the cytokines IFN-γ and TNF-α and these cytokines have opposing effects on the contractile force of colonic longitudinal smooth muscle (Akiho *et al*., 2007).

It is important to highlight that the DSS mouse model provides valuable information during the early stages of colonic inflammation, a period which is difficult to study in patients with IBD. Also, there is evidence that human colonic circular smooth muscle cells secrete pro-inflammatory and anti-inflammatory cytokines during different stages of the inflammation. Shi and Sarna (2005) reported that pro-inflammatory mediators such as IL-6 were expressed early, whereas the anti-inflammatory cytokine IL-11 was expressed later. Remarkably, in DSS murine models of chronic colitis, both cytokine profiles (pro-inflammatory and anti-inflammatory) are present (Dieleman *et al*., 1998). Therefore, smooth muscle contractility may be tightly associated with the specific types of cytokines (i.e., pro-inflammatory or anti-inflammatory) and with the stage of the inflammation progression. Thus, it is recommended to evaluate the cytokine profiles and the MLCK activity in future experiments.

4.5 Conclusions and future directions

In summary, the main conclusions of this study were: (i) DSS treatment induced intestinal inflammation in C57BL/6 mice; (ii) the non-receptor mediated contraction evoked by depolarization with high K^+ concentrations was higher in control mice than in DSS-treated mice; (iii) receptor mediated contraction induced by carbachol was higher in DSS-treated mice than in control mice; (iv) Ca^{2+} sensitivity was altered in DSS-treated mice in comparison with that of control mice; (v) there was a general increased expression of myosin isoforms in DSS-treated mice; (vi) the LC17b myosin isoform exhibited the highest change in expression in DSS-treated mice; and (vii) inflammation in C57BL/6 did not evoke changes in the myosin isoforms at the protein level.

Since hypocontractility was measured during membrane depolarization with high K^+ and previous studies (Akbarali *et al*., 2000; Kinoshita *et al*., 2003) reported a decrease in the activity of L-type Ca^{2+} channels with inflammation, a characterization of Ca^{2+}-channel activity may be pertinent. Patch-clamp recordings of Ca^{2+}–channel currents may be performed on smooth muscle from DSS-treated animals.

The expression of myosin isoforms might show more significant alterations with chronic inflammation. Cycling the supply of DSS with periods of water can induce a state of chronic colitis in mice (Cooper *et al*., 1993). Interestingly, the increased expressions of LC17b at the mRNA level have been reported with hypertrophied growth of smooth muscle. An assessment of smooth muscle hypertrophy by measuring the changes in the size of smooth muscle cells or the smooth muscle layer would be important.

In addition, inflammatory mediators have been reported to influence smooth muscle contractility (Kinoshita *et al*., 2006). A description of the cytokine profile might provide

useful information about the mechanism modulating the contractile activity of colonic circular smooth muscle. Tissue homogenates of DSS-treated and control colon could be used to measure the levels of cytokines (i.e., TNF-α, IFN-γ and IL-1β) with an enzyme-linked immunosorbent assay (ELISA) kit.

Alterations of Ca^{2+}-sensitivity detected in this study suggest that alterations in the expression and/or in the activity of Ca^{2+} -dependent kinases (e.g. MLCK or CaMKII) may be responsible for the changes detected. An evaluation of the expression and activity of MLCK in DSS-treated mice is recommended. The design of specific primers for MLCK and completion of quantitative PCR analysis (e.g., real-time PCR) will indicate if changes in the expression of MLCK occur at the mRNA level. Furthermore, western blots for MLCK would allow quantification of the any alterations at the protein level.

Evaluations of myosin diphosphorylation would reveal the involvement of Ca^{2+} independent kinases during the inflammatory process. It is known that diphosphorylation of myosin is present in certain pathologies and may lead to hypercontraction. The level of myosin phosphorylation could be addressed by separation and staining of the phosphoproteins with Phos-Tag^{TM} SDS-PAGE.

An evaluation of colitis-dependent changes in Ca^{2+} handling during smooth muscle contraction would be appropriate. The most common method for Ca^{2+} monitoring is the use of fluorescent Ca^{2+} indicators, such as Fura-2, Indo-1 or Fluo-3. Such studies would increase our understanding of Ca^{2+} handling during inflammation with possible variations expected in Ca^{2+}influx, re-uptake by intracellular stores and Ca^{2+} efflux.

This project analyzed for the first time the alterations of myosin isoforms in colonic smooth muscle during acute inflammation. The data gathered could be used toward an

assessment of alterations in myosin isoform expression in chronic colitis. Moreover, the finding of altered Ca^{2+}-sensitivity suggests an influence of inflammation on Ca^{2+} handling during colonic inflammation. An understanding of the molecular and physiologic changes in the smooth muscle cells during intestinal inflammation is important for a definitive understanding of inflammatory bowel disease.

REFERENCES

Adelstein, R., Eisenberg, E. (1980). Regulation and kinetics of the actin-myosin-ATP interaction. *Annu Rev Biochem.* 49:921-956.

Ahmad, T., Tamboli, C., Jewell, D., Colombel, J. (2004). Clinical relevance of advances in genetics and pharmacogenetics of IBD. *Gastroenterology.* 126:1533–1549.

Ahmad, T., Satsangi, J., McGovern, D., Bunce, M., Jewell, D. (2001). Review article: the genetics of inflammatory bowel disease. *Aliment Pharmacol Ther.* 15: 731–48.

Akbarali, H., Pothoulakis, C., & Castagliuolo, I. (2000). Altered ion channel activity in murine colonic smooth muscle myocytes in an experimental colitis model *Biochem Biophys Res Commun*. 275**:**637–642.

Akiho, H., Khan, W., Al-Kaabi, A., Blennerhassett, P., Deng, Y., Collins, S. (2007). Cytokine modulation of muscarinic receptors in the murine intestine. *Am J Physiol Gastrointest Liver Physiol.* 293:G250-G255.

Akiho, H., Lovato, P., Deng, Y., Ceponis, P., Blennerhassett, P., Collins, S. (2005). Interleukin-4- and -13-induced hypercontractility of human intestinal muscle cells-implications for motility changes in Crohn's disease. *Am J Physiol Gastrointest Liver Physiol*. 288:G609-G615.

Andres, P., Beck, P., Mizoguchi, E., Mizoguchi, A., Bhan, A., Dawson, T., Kuziel, W., Maeda, N., MacDermott, R., Podolsky, D., Reinecker, H. (2000). Mice with a selective deletion of the CC chemokine receptors 5 or 2 are protected from dextran sodium sulphate-mediated colitis: Lack of CC chemokine receptor 5 expression results in a $NK1.1^{+}$ lymphocyte-associated Th2-type immune response in the intestine. *J Immunol*. 164:6303-6312.

Annese, V., Bassotti, G., Napolitano, G., Usai, P., Andriulli, A., Vantrappen, G. (1997). Gastrointestinal motility disorders in patients with inactive Crohn's disease. *Scand J Gastroenterol*. 32:1107-1117.

Appleyard, C., Wallace, J. (1995). Reactivation of hapten-induced colitis and its prevention by anti-inflammation drugs. *Gatrointest Liver Physiol.* 32:G119-G125.

Aranda, R., Sydora, B., McAllister, P., Binder, S., Yang, H., Targan, S., Kronenberg, M. (1997). Analysis of intestinal lymphocytes in mouse colitis mediated by transfer of CD4+, CD45RBhigh T cells to SCID recipients. *J Immunol.* 158:3464-3473.

Axelsson, L., Landström, E., Goldschmidt, T., Grönberg, A., Bylund-Fellenius, A. (1996). Dextran sulphate sodium (DSS) induced experimental colitis in immunodeficient mice: Effects in CD4+-cell depleted, athymic and NK-cell depleted SCID mice. *Inflamm Res*. 45:181-191.

Babij, P., Periasamy, M. (1989). Myosin heavy chain isoform diversity in smooth muscle is produced by differential RNA processing. *J Mol Biol*. 210:673-679.

Babu, G., Pyne, G., Zhou, Y., Okwuchukuasanya, C., Brayden, J., Osol, G., Paul., R., Low, R., Periasamy, M. (2004). Isoform switching from SM-B to SM-A myosin results in decreased contractility and altered expression of thin filament regulatory proteins. *Am J Physiol Cell Physiol*. 287:C723-C729.

Babu, G., Loukianov, E., Loukianova, T., Pyne, G., Huke, S., Osol, G., Low, R., Paul, R., Periasamy, M. (2001). Loss of SM-B myosin affects muscle shortening velocity and maximal force development. *Nat Cell Biol*. 3:1025-1029.

Babu, G., Warshaw, D., Periasamy, M. (2000). Smooth muscle myosin heavy chain isoforms and their role in muscle physiology. *Microsc Res Tech*. 50:532-540.

Bárány, M. (1967). ATPase activity of myosin correlated with speed of muscle shortening. *J Gen Physiol*. 50:197-218.

Barmeyer, C., Harren, M., Schmitz, H., Heinzel-Pleines, U., Mankertz, J., Seidler, U., Horak, I., Wiedenmann, B., Fromm, M., Schulzke, J. (2004). Mechanisms of diarrhea in the interleukin-2-deficient mouse model of colonic inflammation. *Am J Physiol Gastrointest Liver Physiol.* 286:G244-G252.

Beck, P., Wong, Y., Chen, C., Keenen, C., Sharkey, K., & McCafferty, D. (2007). Inducible nitric oxide synthase from bone marrow-derived cells plays a critical role in regulating colonic inflammation. *Gastroenterology*. 132:1778-1790.

Beck, P., Xavier, J., Wong, I., Ezedi, H., Mashimo, A., Mizoguchi, E., Mizoguchi, A., Bhan, K., Podolsky, D. (2004). Paradoxical roles of different nitric oxide synthase isoforms in colonic injury. *Am J Physiol Gastrointest Liver Physiol* 286:G137–G147.

Berg, D., Davidson, N., Kuhn, R., Muller, W., Menon, S., Holland, G., Thompson-Snipes, L., Leach, M., Rennick, D. (1996). Enterocolitis and colon cancer in interleukin-10-deficient mice are associated with aberrant cytokine production and CD4(+) TH1-like responses. *J Clin Invest*. 98:1010-1020.

Bitar, K. (2003). Function of gastrointestinal smooth muscle: from signaling to contractile proteins. *Am J Med*. 115:15S-23S.

Bradley, P., Priebat, D., Christensen, R., Rothstein, G. (1982). Measurement of cutaneous inflammation: Estimation of neutrophil content with an enzyme marker. *J Invest Dermatol*. 78:206-209.

Brandwein, S., McCabe, R., Cong, Y., Waites, K., Ridwan, B., Dean, P., Ohkusa, T., Birkenmeier, E., Sundberg, J., Elson, C. (1997). Spontaneously colitic C3H/HeJBir mice demonstrate selective antibody reactivity to antigens of the enteric bacterial flora. *J Immunol.* 159:44-52.

Byrne, F., Viney, J. (2006). Mouse models of inflammatory bowel disease. *Curr Opin Drug Discov Devel.* 9:207-217.

Bywater, R., Spencer, N., Fida, R., Taylor, G. (1998). Second-, minute- and hour-metronomes of intestinal pacemakers. *Clin Exp Pharmacol Physiol*. 25:857-861.

Cavanaugh J. (2001). International collaboration provides convincing linkage replication in complex disease through analysis of a large pooled data set: Crohn disease and chromosome 16. *Am J Hum Genet.* 68:1165–1171.

Cooper, H., Murthy, S., Shah, R., Sedergran, D. (1993). Clinicopathologic study of dextran sulphate sodium experimental murine colitis. *Laboratory Investigation*. 69:238-249.

De Lean, A., Munson, P., Rodbard, D. (1978). Simultaneous analysis of families of sigmoidal curves : Application to bioassay, radioligand assay, and physiological dose-response curves. *Am J Physiol*. 235:E97-E102.

Dieleman, L., Palmen, M., Akol, H., Bloemena, E., Peña, A., Meuwissen, S., Van Rees, E. (1998). Chronic experimental colitis induced by dextran sulphate sodium (DSS) is characterized by Th1 and Th2 cytokines. *Clin Exp Immunol.* 114:385-391.

Dieleman, L., Ridwan, B., Tennyson, G., Beagley, K., Bucy, R., Elson, C. (1994). Dextran sulfate sodium-induced colitis occurs in severe combined immunodeficient mice. *Gastroenterology.* 107:1643-1652.

DiSanto, M., Stein, R., Chang, S., Hypolite, J., Zheng, Y., Zderic, S., Wein, A., Chacko, S. (2003). Alteration in expression of myosin isoforms in detrusor smooth muscle following bladder outlet obstruction. *Am J Physiol Cell Physiol.* 285:C1397-410.

DiSanto, M., Cox, R., Wang, Z., Chacko, S. (1997). NH_2-terminal-inserted myosin II heavy chain is expressed in smooth muscle of small muscular arteries. *Am J Physiol Cell Physiol*. 272:C1532-C1542.

Egger, B., Bajaj-Elliott, M., MacDonald, T., Inglin, R., Eysselein, V., Büchler, M. (2000). Characterisation of acute murine dextran sodium sulphate colitis: cytokine profile and dose dependency. *Digestion*. 62:240-248.

Ehlert, F. (2003). Pharmacological analysis of the contractile role of M2 and M3 muscarinic receptors in smooth muscle. *Receptors Channels*. 9:261-277.

Elson, C., Weaver, C. (2003). Experimental mouse models of inflammatory bowel disease: New insights into pathogenic mechanisms. In S. Targan, F. Shanahan, & L. Karp (Ed.), Inflammatory bowel disease. From bench to bedside (pp. 67-99). Dordrecht NL:Kluwer Academic Publishers.

Elson, C., Sartor, R., Tennyson, G., Riddell, R. (1995). Experimental models of inflammatory bowel disease. *Gastroenterology.* 109:1344-1367.

Faussone, M., Cortesini, C., Romagnoli, P. (1977). Ultrastructure of the tunica muscularis of the cardial portion of the human esophagus and stomach, with special reference to the so-called Cajal's interstitial cells. *Arch Ital Anat Embriol*. 82:157-177.

Fiocchi, C. (2003). More answers and more questions in inflammatory bowel disease. *Curr Opin Gastroenterol*. 19:325-326.

Foebig, E., Ley, K., Arfors, K. (1991). Rapid leukocyte accumulation by "spontaneous" rolling and adhesion in the exteriorized rabbit mesentery. *Int J Microcirc Clin Exp.* 10:127-144.

Furness, J., Johnson, P., Pompolo, S., Bornstein, J. (1995). Evidence that enteric motility reflexes can be initiated through entirely intrinsic mechanisms in the guinea-pig small intestine. *Neurogastroenterol Motil*. 7:89-96.

Gaya, D., Russell, R., Nimmo, E., Satsangi, J. (2006). New genes in inflammatory bowel disease: lessons for complex diseases. *Lancet*. 367:1271-1284.

Generunner software by Michael Spruyt and Frank Buquicchio. www.generunner.com

Ghia, J., Galeazzi, F., Ford, D., Hogaboam, C., Vallance, B., Collins, S. (2008). Role of M-CSF-dependent macrophages in colitis is driven by the nature of the inflammatory stimulus. *Am J Physiol Gastrointest Liver Physiol* 294: G770–G777.

Gil, F., Zitouni, N., Azoulay, E., Maghni, K., Lauzon, A. (2006). Smooth muscle myosin isoform expression and LC20 phosphorylation in innate rat airway hyperresponsiveness. *Am J Physiol Lung Cell Mol Physiol.* 291:L932-L940.

Girardin, S., Boneca, I., Viala, J., Chamaillard, M., Labigne, A., Thomas, G., Philpott, D., Sansonetti, P. (2003). *NOD2* is a general sensor of peptidoglycan through muramyl dipeptide (MDP) detection. *J Biol Chem.* 278: 8869–8872.

Grossi, L., McHugh, K., Collins,S. (1993) On the specificity of altered muscle function in experimental colitis in rats. *Gastroenterology*. 104:47-56.

Hamada, Y., Yanagisawa, M., Katsuragawa, Y., Coleman, J., Nagata, S., Matsuda, G., Masaki, T. (1990). Distinct vascular and intestinal smooth muscle myosin heavy chain mRNAs are encoded by a single-copy gene in the chicken. *Biochem Biophys Res Commun.* 170:53-58.

Hampe, J., Cuthbert, A., Croucher, P., Mirza, M., Mascheretti, S., Fisher, S., Frenzel, H., King, K., Hasselmeyer, A., MacPherson, A., Bridger, S., van Deventer, S., Forbes, A., Nikolaus, S., Lennard-Jones, J., Foelsch, U., Krawczak, M., Lewis, C., Schreiber, S., Mathew, C. (2001). Association between insertion mutation in *NOD2* gene and Crohn's disease in German and British populations. *Lancet.* 357:1925–1928.

Hampe, J., Shaw, S., Saiz, R., Leysens, N., Lantermann, A., Mascheretti, S., Lynch, N., MacPherson, A., Bridger, S., van Deventer, S., Stokkers, P., Morin, P., Mirza, M., Forbes, A., Lennard-Jones, J., Mathew, C., Curran, M., Schreiber, S. (1999). Linkage of inflammatory bowel disease to human chromosome 6p. *Am J Hum Genet.* 65:1647–1655.

Hanauer, S. (2003). Inflammatory bowel disease: epidemiology, pathogenesis, and therapeutic opportunities. *Inflamm Bowel Dis*. 1:S3-9.

Hasegawa, Y., Morita, F. (1992). Role of 17-kDa essential light chain isoforms of aorta smooth muscle myosin. *J Biochem (Tokyo).* 111:804-809.

Helper, D., Lash, J., Hathway, D. (1988). Distribution of isoelectric variants of 17,000-dalton myosin light chain in mammalian smooth muscle. *J Biol Chem*. 263:15748-15753.

Hewett, T., Martin, A., Paul, R. (1993). Correlations between myosin heavy chain isoforms and mechanical parameters in rat myometrium. *J Physiol (Lond)*. 460:351–364.

Highsmith, S. (1999). Lever arm model of force generation by actin-myosin-ATP. *Biochemistry*. 38:9791-9797.

Hosgor, M., Karaca, I., Ulukus, C., Ozer, E., Ozkara, E., Sam, B., Ucan, B., Kurtulus, S., Karkiner, A., Temir, G. (2005). Structural changes of smooth muscle in congenital ureteropelvic junction obstruction. *Pediatr Surg*. 40:1632-1636.

Hosseini, J., Goldhill, J., Bossone, C., Piñero, V., Donohue, S. (1999). Progressive alterations in circular smooth muscle contractility in TNBS-induced colitis in rats. *Neurogastroenterol. Mot*. 11:347-356.

Houdusse, A., Cohen, C. (1996). Structure of the regulatory domain of scallop myosin at 2 Å resolution: implications for regulation. *Structure.* 15:21-32.

Hugot, J., Chamaillard, M., Zouali, H., Lesage, S., Cézard, J., Belaiche, J., Almer, S., Tysk, C., O'Morain, C., Gassull, M., Binder, V., Finkel, Y., Cortot, A., Modigliani, R., Laurent-Puig, P., Gower-Rousseau, C., Macry, J., Colombel, J., Sahbatou, M., Thomas, G. (2001). Association of *NOD2* leucine-rich repeat variants with susceptibility to Crohn's disease. *Nature.* 411:599–603.

Ihara, E., Beck, P., Medlicott, S., MacDonald, J. Protein kinase signalling pathways responsible for hypercontractility and increased calcium sensitization in a TH2 murine model of colitis. (*in progress*).

Isaacs, K., Sartor, R., Haskill., S. (1992). Cytokine messenger RNA profiles in inflammatory bowel disease mucosa detected by polymerase chain reaction amplification. *Gastroenterology*. 103:1587-1895.

Itoh, R., Shin-Ya, M., Kishida, T., Urano, A., Takada, R., Sakagami, J., Imanishi, J., Kita, M., Ueda, Y., Iwakura, Y., Kataoka, K., Okanoue, T., Mazda, O. (2006). Interferon-gamma is causatively involved in experimental inflammatory bowel disease in mice. *Clin Exp Immunol.* 146:330–338

Kargacin, G., Walsh, M. 2001. Vascular smooth muscle contraction. In N. Sperelakis (Ed.), Heart physiology and pathophysiology (pp. 527-539). London:Academic Press.

Kelly, C., Takahashi, M., Yu, J., Adelstein, R. (1993). An insert of seven amino acids confers functional differences between smooth muscle myosins from the intestines and vasculature. *J Biol Chem*. 17:12848-12854.

Kern, F., Almy, T., Abbot, F., Bogdonoff, M. (1951). The motility of the distal colon in nonspecific ulcerative colitis. *Gastroenterology*. 19:492-503.

King, B., Szurszewski, J. (1989). Peripheral reflex pathways involving abdominal viscera: transmission of impulses through prevertebral ganglia. *Am J Physiol Gastrointest Liver Physiol*. 256:G581-G588.

Kinoshita, K., Horiguchi, K., Fujisawa, M., Kobirumaki, F., Yamato, S., Hori, M., Ozaki, H. (2006). Possible involvement of muscularis resident macrophages in impairment of interstitial cells of Cajal and myenteric nerve systems in rat models of TNBS-induced colitis. *Histochem Cell Biol*. 127:41-57.

Kinoshita, K., Sato, K., Hori, M, Ozaki, H., Karaki, H. (2003). Decrease in activity of smooth muscle L-type Ca^{2+} channels and its reversal by NF-κB inhibitors in Crohn's colitis model. *Am J Physiol Gastrointest Liver Physiol*. 285:G483-G493.

Kitajima, S., Takuma, S., Morimoto, M. (2000). Histological analysis of murine colitis induced by dextran sulfate sodium of different molecular weights. *Exp Anim.* 49:9-15.

Kitazawa, T., Kobayashi, S., Horiuti, K., Somlyo, A., Somlyo, A. (1989). Receptor-coupled, permeabilized smooth muscle. Role of the phosphatidylinositol cascade, G-proteins, and modulation of the contractile response to Ca^{2+}. *J Biol Chem*. 264:5339-5342.

Kiyosue, M., Fijisawa, M., Kinoshita, K., Hori, M. & Ozaki, H. (2006). Different susceptibilities of spontaneous rhythmicity and myogenic contractility to intestinal muscularis. *Neurogastroenterol Motil*. 18:1019-1030.

Koi, P., Milhoua, M., Monrose, V., Melman, A., DiSanto, M. (2006). Expression of myosin isoforms in the smooth muscle of human corpus cavernosum. *Int J Impot Res.* 19:62-68.

Kojima, R., Kuroda, S., Ohkishi, T., Nakamaru, K., Hatakeyama, S. (2004). Oxazolone-induced colitis in BALB/C mice: a new method to evaluate the efficacy of therapeutic agents for ulcerative colitis. *J Pharmacol Sci.* 96:307-313.

Kontoyiannis, D., Pasparakis, M., Pizarro, T., Cominelli, F., Kollias, G. (1999). Impaired on/off regulation of TNF biosynthesis in mice lacking TNF AU-rich elements: implications for joint and gut-associated immunopathologies. *Immunity*. 10:387-398.

Kühn, R., Löhler, J., Rennick, D., Rajewsky, K., Müller, W. (1993). Interleukin-10-deficient mice develop chronic enterocolitis. *Cell*. 75:263-274

Laemmli, U. (1970). Cleavage of structural proteins during the assembly of the head of bacterophage T4. *Nature* (London). 227:680-685.

Langton, P., Ward, S., Carl, A., Norell, M., Sanders, K. (1989) Spontaneous electrical activity of interstitial cell of Cajal isolated from canine proximal colon. *Proc Natl Acad Sci USA*. 86:7280-7284

Lauzon,, A., Tyska, M., Rovner, A., Freyzon, Y., Warshaw, D., Trybus, K. (1998). A 7-amino-acid insert in the heavy chain nucleotide binding loop alters the kinetics of smooth muscle myosin in the laser trap. *Muscle Res Cell Motil*. 19:825-837.

Léguillette, R., Gil, F., Zitouni, N., Lajoie-Kadoch, S., Sobieszek, A., Lauzon, A. (2005). (+)Insert smooth muscle myosin heavy chain (SM-B) isoform expression in human tissues. *Am J Physiol Cell Physiol.* 289:C1277-C1285.

Lenz, S., Lohse, P., Seidel, U., Arnold, H. (1989). The alkali light chains of human smooth and nonmuscle myosins are encoded by a single gene. Tissue-specific expression by alternative splicing pathways. *J Biol Chem.* 264:9009-9015.

Li, L., Eto, M., Lee, M., Morita, F., Yazawa, M., Kitazawa, T. (1998). Possible involvement of the novel CPI-17 protein in protein kinase C signal transduction of rabbit arterial smooth muscle. *J Physiol*. 508:871-881.

Livak, K., Schmittgen, T. (2001). Analysis of relative gene expression data using real-time quantitative PCR and the 2(-Delta Delta C(T)) Method. *Methods.* 25:402-408.

Löfgren, M., Fagher, K., Wede, OK., Arner, A. (2002). Decreased shortening velocity and altered myosin isoforms in guinea-pig hypertrophic intestinal smooth muscle. *J Physiol*. 544:707-714.

Mähler, M., Bristol, I., Leiter, E., Workman, A., Birkenmeier, E., Elson, C., Sundberg, J. (1998). Differential susceptibility of inbred mouse strains to dextran sulfate sodium-induced colitis. *Am J Physiol Gastrointest Liver Physiol*. 274:G544-G551.

Malmqvist, U., Arner, A. (1991). Correlation between isoform composition of the 17 kDa myosin light chain and maximal shortening velocity in smooth muscle. *Eur J Biochem*. 418:523-530.

Martin, A., Bhatti, S., Pyne-Geithman, G., Farjah, M., Manaves, V., Walker, L., Franks, R., Strauch, A., Paul, R. (2007). Expression and function of COOH-terminal myosin heavy chain isoforms in mouse smooth muscle. *Am J Physiol Cell Physiol*. 293:C238-C245.

Matsui, M., Motomura, D., Fujikawa, T., Jiang, J., Takahashi, S., Manabe, T., Taketo, M. (2002). Mice lacking M2 and M3 muscarinic acetylcholine receptors are devoid of cholinergic smooth muscle contractions but still viable. *J Neurosci.* 22:10627-10632.

Matsumoto, S., Okabe, Y., Setoyama, H., Takayama, K., Ohtsuka, J., Funahashi, H., Imaoka, A., Okada, Y., Umesaki, Y. (1998). Inflammatory bowel disease-like enteritis and caecitis in a senescence accelerated mouse P1/Yit strain. *Gut.* 43:71-78.

Matthew, J., Khromov, A., Trybus, K., Somlyo, A., Somlyo, A. (1998). Myosin essential light chain isoforms modulate the velocity of shortening propelled by nonphosphorylated cross-bridges. *J Biol Chem*. 273:31289-31296.

McKusick-Nathans Institute for Genetic Medicine, Johns Hopkins University Baltimore MD and National Center for Biotechnology Information National Library of Medicine Bethesda MD. Online Mendelian Inheritance in Man. http://www.ncbi.nlm.nih. gov/entrez/query.fcgi?db=OMIM (accessed Jan 1, 2006).

Melgar, S., Karlsson, A., Michaëlsson, E. (2005). Acute colitis induced by dextran sulfate sodium progresses to chronicity in C57BL/6 but not in BALB/c mice: correlation between symptoms and inflammation. *Am J Physiol Gastrointest Liver Physiol.* 288:G1328-G1338.

Mikkelsen, H., Larsen, J., Hadberg, H. (2008). The macrophage system in the intestinal muscularis externa during inflammation: an immunohistochemical and quantitative study of osteopetrotic mice. *Histochem Cell Biol.* [Epub ahead of print]

Mitani, Y., Ueda, M., Komatsu, R., Maruyama, K., Nagai, R., Matsumura, M., Sakurai, M. (2001). Vascular smooth muscle cell phenotypes in primary pulmonary hypertension. *Eur Respir J.* 17:316-320.

Murthy, K. (2006) Signaling contraction and relaxation in smooth muscle of the gut. *Annu Rev Physiol*. 68:345-374.

Murthy, S., Cooper, H., Shim, H., Shab, R., Ibrahim, S., Sedergran, D. (1993). Treatment of dextran sulfate sodium-induced murine colitis by intracolonic cyclosporine. *Dig Dis Sci*. 38:1722-1734.

Nabeshima, Y., Nabeshima, Y., Nonomura, Y., Fujii-Kuriyama, Y. (1987). Nonmuscle and smooth muscle myosin light chain mRNAs are generated from a single gene by the tissue-specific alternative RNA splicing. *J Biol Chem*. 262:10608-10612.

Nagai, R., Kuro-o, M., Babij, P., Periasamy, M. (1989). Identification of two types of smooth muscle myosin heavy chain isoforms by cDNA cloning and immunoblot analysis. *J Biol Chem.* 264:9734-9737.

Nakanishi, M., Tazawa, H., Tsuchiya, N., Sugimura, T., Tanaka, T., Nakagama, H. (2007). Mouse strain differences in inflammatory responses of colonic mucosa induced by dextran sulfate sodium cause differential susceptibility to PhIP-induced large bowel carcinogenesis. *Cancer Sci.* 98:1157-1163.

Neurath, M., Weigmann, B., Finotto, S., Glickman, J., Nieuwenhuis, E., Iijima, H., Mizoguchi, A., Mizoguchi, E., Mudter, J., Galle, P., Bhan, A., Autschbach, F., Sullivan, B., Szabo, S., Glimcher, L., Blumberg, R. (2002). The transcription factor T-bet regulates mucosal T cell activation in experimental colitis and Crohn's disease. *J Exp Med*. 195:1129-1143. Erratum in: *J Exp Med* 2002 Jun 3;195:1513.

Ni, J., Chen, S., Hollander, D. (1996). Effects of dextran sulphate sodium on intestinal epithelial cells and intestinal lymphocytes. *Gut.* 39:234-241.

Nishimura, J. Kolber, M., van Breemen, C. (1988). Norepinephrine and GTP-gamma-S increase myofilament Ca^{2+} sensitivity in alpha-toxin permeabilized arterial smooth muscle *Biochem Biophys Res Commun*. 157, 677-683.

Ogura, Y., Bonen, D., Inohara, N., Nicolae, D., Chen, F., Ramos, R., Britton, H., Moran, T., Karaliuskas, R., Duerr, R., Achkar, J., Brant, S., Bayless, T., Kirschner, B., Hanauer, S., Nuñez, G., Cho, J. (2001). A frameshift mutation in *NOD2* associated with susceptibility to Crohn's disease. *Nature.* 411: 603–606.

Ohama, T., Hori, M., Momotani, E., Iwakura, Y., Guo, F., Kishi, H., Kobayashi, S., Ozaki, H. (2007). Intestinal inflammation downregulates smooth muscle CPI-17 through induction

of TNF-α and causes motility disorders. *Am J Physiol Gastrointest Liver Physiol*. 292:G1429-G1438.

Okayasu, I, Hatakeyama, S., Yamada, M., Ohkusa, T., Inagaki, Y., Nakaya, R. (1990). A novel method in induction of reliable experimental acute and chronic colitis in mice. *Gastroenterology*. 98: 694-702.

Pfaffl, M. (2006). Relative quantification. In T Dorak (Ed.), Real-time PCR (pp 63-82). New York, USA:Taylor & Francis.

Pfaffl, M., Hageleit, M. (2001). Validities of mRNA quantification using recombinant RNA and recombinant DNA external calibration curves in real-time RT-PCR. *Biotechn Lett*. 23:275-282.

Parkes, M., Barmada, M., Satsangi, J., Weeks, D., Jewell, D., Duerr, R. (2000). The IBD2 locus shows linkage heterogeneity between ulcerative colitis and Crohn disease. *Am J Hum Genet*. 67:1605-1610.

Reddy, S., Bazzocchi, G., Chan, S., Akashi, K., Villaneuva, J., Yanni, G. (1991). Colonic motility and transit in health and ulcerative colitis. *Gastroenterology*. 101:1289-1297.

Rogers, D., Burnstock, G. (1966). The interstitial cell and its place in the concept of the autosomic ground plexus. *J Comp Neurol*. 126:255-284.

Rovner, A., Freyzon, Y., Trybus, K. (1997). An insert in the motor domain determines the functional properties of expressed smooth muscle myosin isoforms. *J Muscle Res Cell Motil.* 18:103-110.

Sanders, K., Koh, D., Ward, S. (2006). Organization and electrophysiology of interstitial cells of Cajal and smooth muscle cells in the gastrointestinal tract. In L. R. Johnson (Ed*.).* Physiology of the gastrointestinal tract (pp. 533-548). Burlington MA : Elsevier Academic Press.

Sanders K. (1996). A case for interstitial cells of Cajal as pace markers and mediators of neurotransmission in the gastrointestinal tract. *Gastroenterology*. 111:492-515.

Sarna, S. (1991). Physiology and pathophysiology of colonic motor activity. *Dig Dis Sci*. 36:827-862.

Sarna, S. & Shi, S. (2006). Function and regulation of colonic contractions in health and disease. In L. Johnson (Ed.), Physiology of the gastrointestinal tract (pp.965-994). Burlington, MA:Elsevier Academic Press.

Sato, K., Ohkura, S., Kitahara, Y., Ohama, T., Hori, M., Sato, M., Kobayashi, S., Sasaki, Y., Hayashi, T., Nasu, T., Ozaki, H. (2007). Involvement of CPI-17 downregulation in the

dysmotility of the colon from dextran sodium sulphate-induced experimental colitis in mouse model. *Neurogastroenterol Motil*. 19:504-514.

Sartor, R. (2008). Microbial influences in inflammatory bowel diseases. *Gastroenterology*.134:577–594.

Sartor, R. (1994). Cytokines in intestinal inflammation: Pathophysiological and clinical considerations. *Gastroenterology*. 106:533-539.

Schmittgen, T., Zakrajsek, B.(2000). Effect of experimental treatment on housekeeping gene expression: validation by real-time, quantitative RT-PCR. *J Biochem Biophys Methods*. 46:69-81.

Serio, R., Barajas, C., Daniel, E., Berezin, I., Huizinga, J. (1991). Slow-wave activity in colon: role of network of submucosal intestitial cells of Cajal. *Am J Physiol Gastrointest Liver Physiol*. 260:G636-G645.

Shi, X., Sarna, S. (2005). Transcriptional regulation of inflammatory mediators secreted by human colonic circular smooth muscle cells. *Am J Physiol Gastrointest Liver Physiol.* 289:G274-G284.

Shi, X. & Sarna, S. (2004). G protein–mediated dysfunction of excitation-contraction coupling in ileal inflammation. *Am J Physiol Gastrointest Liver Physio*l. 286:899-905.

Shi, X., Lindholm, P., Sarna, S. (2003). NF-κB activation by oxidative stress and inflammation suppresses contractility in colonic circular smooth muscle cells. *Gastroenterology*. 124:1369-1380.

Siegman, M., Butler, T., Mooers, S., Trinkle-Mulcahy, L., Narayan, S., Adam, L., Chacko, S., Haase, H., Morano, I. (1997). Hypertrophy of colonic smooth muscle: contractile proteins, shortening velocity, and regulation. *Am J Physiol Gastrointest Liver Physiol.* 272:G1571-G1580.

Smith, J., Castro, G. (1978). Relation of peroxidase activity in gut mucosa to inflammation. *Am J Physiol Regul Integr Physiol.* 234:R72-R79.

Smith, T., Reed, J., Sanders, K. (1989). Electrical pacemakers of canine proximal colon are functionally innervated by inhibitory motor neurons. *Am J Physiol Cell Physiol.* 256:C466-C477.

Smith, J., Castro, G. (1978). Relation of peroxidase activity in gut mucosa to inflammation. *Am J Physio Regul Integr Physiol*. 235, R72-R79.

Snape, W., Williams, R., Hyman, P. (1991). Defect in colonic smooth muscle contraction in patients with ulcerative colitis. *Am J Physiol Gastrointest Liver Physiol*. 261:G987-G991.

Sobieszek, A. & Jertschin, P. (1986). Urea-glycerol-acrylamide gel eletrophoresis of acidic low molecvular weight muscle proteins: Rapid determination of myosin light chain phosphorylation in myosin, actomyosin and whole muscle samples. *Electrophoresis*. 7:417-425.

Somlyo, A., Somlyo, A. (1968). Vascular smooth muscle. I. Normal structure, pathology, biochemistry, and biophysics. *Pharmacol Rev*. 20:197-272.

Sparrow, M., Mohammad, M., Arner, A., Hellstrand, P., Ruegg, J. (1988). Myosin composition and functional properties of smooth muscle from the uterus of pregnant and non-pregnant rats. *Pflügers Arch*. 412:624–633.

Standring, S. (2004). Gray's anatomy (39th ed.). UK:Elsevier Churchill Livingstone.

Swee, M., Wilson, C., Wang, Y., McGuire, J., Parks, W. (2008). Matrix metalloproteinase-7 (matrilysin) controls neutrophil egress by generating chemokine gradients *J Leukoc Biol.* 83:1-10.

Sweeney, H., Rosenfeld, S., Brown, F., Faust, L., Smith, J., Xing, J., Stein, L., Sellers, J.. (1998). Kinetic tuning of myosin via a flexible loop adjacent to the nucleotide binding pocket. *J Biol Chem.* 273:6262-6270

Takeuchi, K., Senba, S., Furukawa, K., Eto, M., Morita, F. (1998). Localization of 17-kDa myosin light chain isoforms in cultured aortic smooth muscle cells. *J Biochem (Tokyo)*. 125:334-342.

Tanabe, T., Chamaillard, M., Ogura, Y., Zhu, L., Qiu, S., Masumoto, J., Ghosh, P., Moran, A., Predergast, M., Tromp, G., Williams, C., Inohara, N., Núñez, G. (2004). Regulatory regions and critical residues of *NOD2* involved in muramyl dipeptide recognition. *EMBO J.* 23:1587–1597.

Tanaka, T., Kohno, H., Suzuki, R., Yamada, Y., Sugie, S., Mori, H. (2003). A novel inflammation-related mouse colon carcinogenesis model induced by azoxymethane and dextran sodium sulfate. *Cancer Sci.* 94:931-1020.

Thomson, A., Shaffer, E. (1992). First principles in gastroenterology. Toronto: University of Toronto.

Trinkle-Mulcahy, L., Ichikawa, K., Hartshorne, D., Siegman, M., Butler, T. (1995). Thiophosphorylation of the 130-kDa subunit is associated with a decreased activity of

myosin light chain phosphatase in alpha-toxin-permeabilized smooth muscle. *J Biol Chem*. 270:18191-18194.

Van Dijk, A., Keuskamp, Z., Wilson, J., Zijlstra, F. (1995). Sequential release of cytokines, lipid mediators and nitric oxide in experimental colitis. *Mediators Inflamm*. 4:186-190.

Van Heel, D., Fisher, S., Kirby, A., Daly, M., Rioux, J., Lewis, C. (2004). Inflammatory bowel disease susceptibility loci defined by genome scan meta-analysis of 1952 affected relative pairs. *Hum Mol Genet.* 13: 763–770.

Venkova, K., Greenwood, B., Krier, J. (2002). Neural control of the large intestine. In S. Brookes & M. Costa (Ed.), Innervation of the gastrointestinal tract (pp.171-188). London UK:Taylor & Francis.

Vermillion, D., Huizinga, J., Riddell, R., Collins, S. (1993). *Gastroenterology*. 104:1692-16990.

Vowinkel, T., Kalogeris, T., Mori, M., Krieglstein, C., Granger, D. (2004). Impact of dextran sulfate sodium load on the severity of inflammation in experimental colitis. *Dig Dis Sci*. 49:556-564.

Vrees, M., Pricolo, V., Potenti, F., Cao, W. (2002). Abnormal motility in patients with ulcerative colitis: role of inflammatory cytokines. *Arch Surg*. 137:439-445.

Wang, F., Graham, W., Wang, Y., Witkowski, E., Schwarz, B., Turner, J. (2005). Interferon-gamma and tumor necrosis factor-alpha synergize to induce intestinal epithelial barrier dysfunction by up-regulating myosin light chain kinase expression. *Am J Pathol*. 166:409-419.

Weber, L., Van Lierop, J., Walsh, M. (1999). Ca^{2+}-independent phosphorylation of myosin in rat caudal artery and chicken gizzard myofilaments. *J Physiol*. 516:805-824.

Weissenbach J. (1998). The human genome project: from mapping to sequencing. *Clin Chem Lab Med.* 36: 511–514.

Wells, R., Blennerhasset, M. (2004). Persistent and selective effects of inflammation on smooth muscle cell contractility in rats colitis. *Pflugers Arch Eur J Physiol*. 448:515-524.

White, S., Martin, A., Periasamy, M. (1993). Identification of a novel smooth muscle myosin heavy chain cDNA: isoform diversity in the S1 head region. *Am J Physiol Cell Physiol.* 264:C1252-C1258.

Wilson, T., Aziz, K., Vazques, D., Wuermser, L., Lin, V., Lemack, G. (2005). Changes in detrusor smooth muscle myosin heavy chain mRNA expression following spinal cord injury in the mouse. *Neurourol Urodyn*. 24:89-95.

Wirtz, S., Neufert, C., Weigmann, B., Neurath, M. (2007). Chemically induced mouse models of intestinal inflammation. *Nat Protoc.* 2:541-546.

Yagi, S., Becker, P., Fay, F. (1988). Relationship between force and Ca^{2+} concentration in smooth muscle as revealed by measurements on single cells. *Proc Natl Acad Sci USA*. 85:4109-4113.

Yamada, A., Ohya, S., Hirano, M., Watanabe, M., Walsh, M., Imaizumi, Y. 2003. Ca^{2+} sensitization of smooth muscle contractility induced by ruthenium red. *Am J Physiol Cell Physiol.* 276:566-575.

Yamada, M., Ohkusa, T., Okayasu, I. (1992). Occurrence of dysplasia and adenocarcinoma after experimental chronic ulcerative colitis in hamsters induced by dextran sulphate sodium. *Gut*. 33:1521-1527.

Yamada, T. (2003). Texbook of gastroenterology. New York:Lippincott Williams & Wilkins.

Zhao, A., McDermott, J., Urban, J., Gause, W., Madden, K., Yeung, K., Morris, S., Finkelman, F., Shea-Donohue, T. (2003). Dependence of IL-4, Il-13, and nematode-induced alterations in murinbe small intestinal smooth muscle contractility on Stat6 and enteric nerves. *J Immunol*. 171:948-954.

APPENDIX A

The design of the housekeeping gene followed the same guidelines as those used to design the primers sets for the myosin isoforms. Figure A1 shows the position and strategy of design of MHC invariant (D85). The same strategy was used to design the MLC invariant (NM).

The following results were obtained with BestKeeper (Pfaffl *et al*., 2004) and REST (Relative expression software tool) (Pfaffl *et al*., 2002) software tools. The BestKeeper software determined the best suited housekeeping genes of three candidates (β-actin, 18S rRNA and MHC/MLC invariant), and combined them into an index. The index was compared with five additional target genes using the REST software tool, which determined the expression ratio results of the five investigated transcripts testing them for significance by a randomisation test.

The output from the BestKeeper software tool indicated that the three housekeeping gene candidates were suitable for the analysis (Figures A2, A3).

The output of REST software tool showed no significant differences in the expression of the myosin isoforms both in the proximal and distal colon (Figures A4, A5, A6).

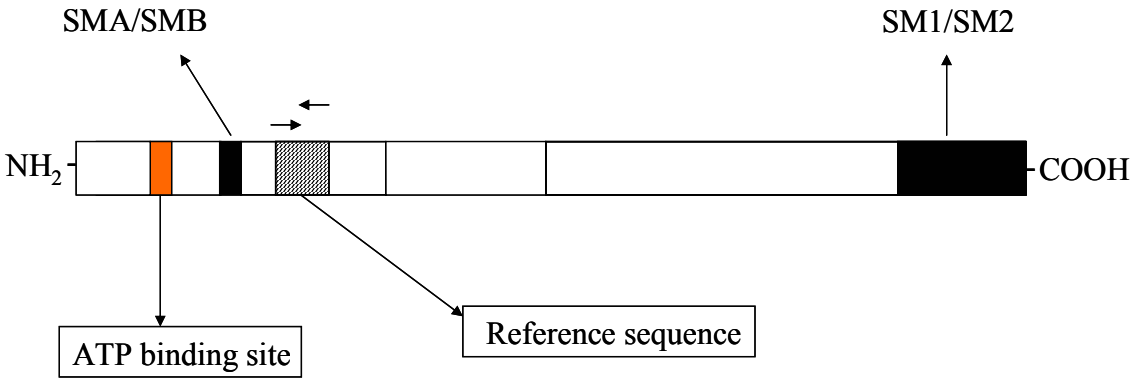

Figure A1. Diagram showing the design strategy for real-time PCR primers of reference sequence.

MHC invariant (D85).

Result - Genes: Repeated Pair-wise Correlation Analysis & Regression Analysis of ***BestKeeper*** **vs. Housekeeping Genes**

print result pages

CP data of housekeeping Genes:

	D85 HKG 1	Beta HKG 2	18S HKG 3	HKG 4	HKG 5	HKG 6	HKG 7	HKG 8
n	90	88	90	0	0	0	0	0
geo Mean [CP]	25.91	18.88	13.29					
ar Mean [CP]	26.06	18.99	13.37					
min [CP]	21.05	15.70	9.63					
max [CP]	31.60	25.00	21.15					
std dev [± CP]	2.38	1.67	1.04					
CV [% CP]	9.14	8.80	7.75					
min [x-fold]	-24.31	-7.95	-12.61					
max [x-fold]	41.89	54.21	232.37					
std dev [± x-fold]	4.78	3.00	1.97					

Pearson correlation coefficient (r)

vs.	HKG 1	HKG 2	HKG 3	HKG 4	HKG 5	HKG 6	HKG 7	HKG 8
HKG 2	0.188	-	-	-	-	-	-	-
p-value	0.080	-	-	-	-	-	-	-
HKG 3	0.751	0.046	-	-	-	-	-	-
p-value	0.001	0.668	-	-	-	-	-	-
HKG 4				-	-	-	-	-
p-value				-	-	-	-	-
HKG 5					-	-	-	-
p-value					-	-	-	-
HKG 6						-	-	-
p-value						-	-	-
HKG 7							-	-
p-value							-	-
HKG 8								-
p-value								-
HKG 9								
p-value								
HKG 10								
p-value								

BestKeeper vs.	HKG 1	HKG 2	HKG 3	HKG 4	HKG 5	HKG 6	HKG 7	HKG 8
coeff. of corr. [r]	0.872	0.559	0.799					
p-value	0.001	0.001	0.001					

Regression Analysis: ***HKG vs. BestKeeper***

	D85 HKG 1 vs. BK	Beta HKG 2 vs. BK	18S HKG 3 vs. BK	HKG 4 vs. BK	HKG 5 vs. BK	HKG 6 vs. BK	HKG 7 vs. BK	HKG 8 vs. BK
coeff. of corr. [r]	0.87	0.56	0.80					
coeff. of det. [r^2]	0.76	0.31	0.64					
intercept [CP]	-3.99	4.37	-1.45					
slope [CP]	1.60	0.78	0.79					
SE [CP]	±1.377	±1.758	±0.91					
p-value	0.001	0.001	0.001					
Power of HKG [x-fold]	2.87	1.67	1.73					

Figure A2. Output BestKeeper software tool of the samples from distal colon.

Descriptive statistics of the housekeeping genes, the Pearson correlation n coefficient, and regression analysis of the three housekeeping gene candidates with the calculated BestKeeper index. The Pearson correlation coefficient estimates inter-gene relations of all possible housekeeping genes. The three genes are analysed based on their CP values.

Result - Genes: Repeated Pair-wise Correlation Analysis & Regression Analysis of ***BestKeeper*** **vs. Housekeeping Genes**

print result pages

CP data of housekeeping Genes:

	D85 HKG 1	Beta HKG 2	18S HKG 3	HKG 4	HKG 5	HKG 6	HKG 7	HKG 8
n	82	82	82	0	0	0	0	0
geo Mean [CP]	22.62	18.52	12.05					
ar Mean [CP]	22.99	18.67	12.25					
min [CP]	9.90	15.70	9.50					
max [CP]	34.87	32.57	22.47					
std dev [± CP]	2.52	1.78	1.73					
CV [% CP]	10.98	9.51	14.14					
min [x-fold]	-4222.30	-6.30	-5.87					
max [x-fold]	3109.01	9534.76	1363.42					
std dev [± x-fold]	5.24	3.21	3.12					

Pearson correlation coefficient (r)

vs.	HKG 1	HKG 2	HKG 3	HKG 4	HKG 5	HKG 6	HKG 7	HKG 8
HKG 2	0.308	-	-	-	-	-	-	-
p-value	0.005	-	-	-	-	-	-	-
HKG 3	0.293	0.795	-	-	-	-	-	-
p-value	0.008	0.001	-	-	-	-	-	-
HKG 4				-	-	-	-	-
p-value				-	-	-	-	-
HKG 5					-	-	-	-
p-value					-	-	-	-
HKG 6						-	-	-
p-value						-	-	-
HKG 7							-	-
p-value							-	-
HKG 8								-
p-value								-
HKG 9								
p-value								
HKG 10								
p-value								

BestKeeper vs.	HKG 1	HKG 2	HKG 3	HKG 4	HKG 5	HKG 6	HKG 7	HKG 8
coeff. of corr. [r]	0.712	0.832	0.854					
p-value	0.001	0.001	0.001					

Regression Analysis: ***HKG vs. BestKeeper***

	D85 HKG 1 vs. BK	Beta HKG 2 vs. BK	18S HKG 3 vs. BK	HKG 4 vs. BK	HKG 5 vs. BK	HKG 6 vs. BK	HKG 7 vs. BK	HKG 8 vs. BK
coeff. of corr. [r]	0.71	0.83	0.85					
coeff. of det. [r^2]	0.51	0.69	0.73					
intercept [CP]	2.92	2.62	-2.71					
slope [CP]	1.16	0.93	0.87					
SE [CP]	±2.689	±1.454	±1.24					
p-value	0.001	0.001	0.001					
Power of HKG [x-fold]	2.14	1.83	1.82					

Figure A3. Output BestKeeper software tool of the samples from proximal colon.

Descriptive statistics of the housekeeping genes, the Pearson correlation n coefficient, and regression analysis of the three housekeeping gene candidates with the calculated BestKeeper index. The Pearson correlation coefficient estimates inter-gene relations of all possible housekeeping genes. The three genes are analysed based on their CP values.

Relative Expression Report

Assay Parameters

Parameter	Value
Iterations	50000
Normalisation Factor	0.45

Results

Gene	Type	Reaction Efficiency	Expression	Std. Error	95% C.I.	P(H1)	Result
D85	REF	0.961	0.398	0.087 - 2.552	0.000 - 304.461	0.414	
Beta	REF	0.962	1.755	0.327 - 9.501	0.060 - 23.599	0.812	
18S	REF	0.998	1.432	0.321 - 7.490	0.059 - 20.434	0.954	
SMB	TRG	0.985	2.457	0.194 - 37.114	0.035 - 9,085.877	0.523	
SM1	TRG	0.948	0.921	0.424 - 2.591	0.035 - 7.039	0.963	
SM2	TRG	0.979	4.318	0.758 - 35.188	0.433 - 405.000	0.159	
SMA	TRG	0.946	1.320	0.143 - 9.335	0.027 - 170.785	0.827	

Legend:
P(H1) - Probability of alternate hypothesis that difference between sample and control groups is due only to chance.
TRG - Target
REF - Reference

Interpretation

D85 sample group is not different to control group. P(H1)=0.414

Beta sample group is not different to control group. P(H1)=0.812

18S sample group is not different to control group. P(H1)=0.954

SMB sample group is not different to control group. P(H1)=0.523

SM1 sample group is not different to control group. P(H1)=0.963

SM2 sample group is not different to control group. P(H1)=0.159

SMA sample group is not different to control group. P(H1)=0.827

Figure A4. Relative expression obtained through REST software: MHC from proximal colon

The mathematical model of the software for the relative expression in real-time PCR is based on the PCR efficiencies and the mean crossing point deviation between the treated and control. Analysis of myosin heavy chains (SMB, SM1, SM2, SMA) from proximal colon.

Relative Expression Report

Assay Parameters

Parameter	Value
Iterations	50000
Normalisation Factor	0.38

Results

Gene	Type	Reaction Efficiency	Expression	Std. Error	95% C.I.	P(H1)	Result
beta	REF	0.962	0.922	0.252 - 3.126	0.087 - 10.067	0.974	
18s	REF	0.998	1.149	0.596 - 2.125	0.365 - 3.245	0.998	
nm	REF	0.985	0.944	0.157 - 4.893	0.064 - 10.441	0.971	
lc17b	TRG	0.997	2.143	1.145 - 4.438	0.644 - 7.367	0.795	

Legend:
P(H1) - Probability of alternate hypothesis that difference between sample and control groups is due only to chance.
TRG - Target
REF - Reference

Interpretation

beta sample group is not different to control group. P(H1)=0.974

18s sample group is not different to control group. P(H1)=0.998

nm sample group is not different to control group. P(H1)=0.971

lc17b sample group is not different to control group. P(H1)=0.795

Figure A5. Relative expression obtained through REST software: LC17b from distal colon

The mathematical model of the software for the relative expression in real-time PCR is based on the PCR efficiencies and the mean crossing point deviation between the treated and control. Analysis of myosin light chain (LC17b) from distal colon.

Relative Expression Report

Assay Parameters

Parameter	Value
Iterations	50000
Normalisation Factor	0.45

Results

Gene	Type	Reaction Efficiency	Expression	Std. Error	95% C.I.	P(H1)	Result
beta	REF	0.962	0.813	0.150 - 4.471	0.061 - 11.335	0.883	
18s	REF	0.998	0.924	0.235 - 3.007	0.140 - 12.281	0.967	
nm	REF	0.985	1.331	0.499 - 3.354	0.243 - 13.982	0.902	
lc17b	TRG	0.997	0.840	0.127 - 2.686	0.015 - 4.078	0.859	

Legend:
P(H1) - Probability of alternate hypothesis that difference between sample and control groups is due only to chance.
TRG - Target
REF - Reference

Interpretation

beta sample group is not different to control group. P(H1)=0.883

18s sample group is not different to control group. P(H1)=0.967

nm sample group is not different to control group. P(H1)=0.902

lc17b sample group is not different to control group. P(H1)=0.859

Figure A6. Relative expression obtained through REST software: LC17b from proximal colon

The mathematical model of the software for the relative expression in real-time PCR is based on the PCR efficiencies and the mean crossing point deviation between the treated and control. Analysis of myosin light chain (LC17b) from proximal distal colon.